

Survival Kernets: Scalable and Interpretable Deep Kernel Survival Analysis with an Accuracy Guarantee

George H. Chen
Heinz College of Information Systems and Public Policy
Carnegie Mellon University
georgechen@cmu.edu

Abstract

Kernel survival analysis models estimate individual survival distributions with the help of a kernel function, which measures the similarity between any two data points. Such a kernel function can be learned using deep kernel survival models. In this paper, we present a new deep kernel survival model called a *survival kernet*, which scales to large datasets in a manner that is amenable to model interpretation and also theoretical analysis. Specifically, the training data are partitioned into clusters based on a recently developed training set compression scheme for classification and regression called *kernel netting* that we extend to the survival analysis setting. At test-time, each data point is represented as a weighted combination of these clusters, and each such cluster can be visualized. For a special case of survival kernets, we establish a finite-sample error bound on predicted survival distributions that is, up to a log factor, optimal. Whereas scalability at test time is achieved using the aforementioned kernel netting compression strategy, scalability during training is achieved by a warm-start procedure based on tree ensembles such as XGBOOST and a heuristic approach to accelerating neural architecture search. On three standard survival analysis datasets of varying sizes (up to roughly 3 million data points), we show that survival kernets are highly competitive with the best of baselines tested in terms of concordance index. Our code is available at: <https://github.com/georgehc/survival-kernets>

1 Introduction

Survival analysis is about modeling the amount of time that will elapse before a critical event of interest happens. Examples of such critical events include death, hospital readmission, disease relapse, device failure, or a convicted criminal reoffending. A key technical challenge in survival analysis is that typically when collecting training data, we cannot wait until the critical event happens for every training data point, such as waiting for everyone in a clinical study to be deceased. Thus, in our training data, we observe the time duration we aim to predict for only some but not all of the data points. This is in contrast to standard classification and regression problem settings in which the target label to be predicted is observed across all training data. Importantly, the data points that do not encounter the critical event could still provide valuable information and should not simply be discarded from the data analysis. For instance, they may have specific characteristics that significantly delay when the critical event will happen.

In the last few decades, survival analysis datasets have dramatically grown in size, from hundreds of data points (e.g., the German Breast Cancer Study Group dataset [Schumacher et al., 1994]) to now millions (e.g., customer churn data from the music streaming service KKBOX¹). We anticipate that in the years to come, survival analysis datasets larger than ones typically encountered today will become the norm. Meanwhile, we remark that many survival analysis problems are in high-stakes application domains such as healthcare. For such applications, it can be helpful for the

¹<https://www.kaggle.com/c/kkbox-churn-prediction-challenge>

survival analysis models used to be interpretable. With these large-scale high-stakes applications in mind, in this paper, we propose a new deep survival analysis model called a *survival kernel* that has all of the following properties:

- highly accurate (achieves concordance indices nearly as high as or higher than the best of the baselines tested in our experimental results)
- scalable (uses a compression technique to construct a test-time predictor that can handle large datasets such as the KKBOX dataset)
- interpretable (any data point is represented by a weighted combination of a few clusters, each of which can be visualized—this is somewhat like how topic modeling for text describes each text document in terms of a few topics, each of which can be visualized)
- for a special case of the model, comes with a theoretical guarantee on prediction accuracy (a finite-sample error bound for predicted survival distributions)

In contrast, existing deep survival analysis models that have been developed typically are not easily interpretable (e.g., Ranganath et al. 2016, Fotso 2018, Chapfuwa et al. 2018, Giunchiglia et al. 2018, Katzman et al. 2018, Lee et al. 2018, Kvamme et al. 2019, Chen 2020, Nagpal et al. 2021, Wu et al. 2021, Zhong et al. 2021). Instead, to get a deep survival analysis model to be interpretable, Zhong et al. [2022], for instance, model a subset of features by a linear model (that is straightforward to interpret) and then model the rest of the features by an arbitrarily complex neural net that they do not aim to interpret or explain. While this sort of interpretability could be valuable, it does not resolve the difficulty of interpreting the part of the model that actually uses the neural net. Meanwhile, we are aware of only two existing deep survival analysis models that have accuracy guarantees [Zhong et al., 2021, 2022], both of which have only been tested on small datasets (the largest real dataset these authors consider has about two thousand data points).

Our work builds on an existing model called deep kernel survival analysis [Chen, 2020]. Unlike non-kernel-based deep survival models that have been developed, deep kernel survival analysis and a Bayesian variant by Wu et al. [2021] learn a kernel function that measures how similar any two data points are. To predict the survival distribution of a specific test point, these kernel-based methods use information from training points most similar to the test point according to the learned kernel function. The learned kernel function can help us probe a resulting survival model. For instance, these kernel functions can provide forecast evidence in terms of which training points contribute to a test point’s prediction. As pointed out by Chen [2020], the kernel functions can also be used to construct statistically valid prediction intervals that are *relative* (e.g., the hospital length of stay of patients *similar to Alice* are within the interval [0.5, 2.5] days with probability at least 80%). Separate from these practical advantages, a kernel-based approach is also amenable to theoretical analysis, where we import proof techniques by Chen [2019] to analyze survival kernels.

A key obstacle to using kernel survival models in practice is that at test time, these models in principle depend on knowing the similarity between a test point and every training point. The computation involved in a naive implementation becomes impractical when the training dataset size grows large. In the Bayesian setting, this scalability problem has been addressed but without guarantees in the survival analysis setting and also thus far without experiments on datasets with censoring [Wu et al., 2021].

Our main technical contribution in this paper is to show how to scale deep kernel survival analysis at test time to large datasets in a manner that not only yields an interpretable model but also achieves a finite-sample accuracy guarantee on predicted survival distributions. The resulting model is what we call a *survival kernel*. We achieve this test-time scalability by extending an existing data compression scheme (*kernel netting* by Kpotufe and Verma [2017] developed for classification and regression) to the survival analysis setting (“survival kernel” combines “survival analysis” and “kernel netting” into a short phrase). Kernel netting could be viewed as partitioning the training data into clusters and then representing any data point as a weighted combination of a few clusters. We show how to visualize such clusters. We remark that Kpotufe and Verma did not consider interpretability or how to visualize clusters in their original kernel netting paper.

We next turn to training scalability. Here, minibatch gradient descent readily enables fitting a deep kernel survival model to large datasets for a specific neural net architecture. The challenge

is that there could be many neural net architectures to try, making the overall training procedure computationally expensive. Our second contribution is in proposing a warm-start approach to deep kernel survival model training that drastically reduces the amount of computation needed when sweeping over neural net architecture choices. Our proposed warm-start strategy first learns a kernel function using a scalable tree ensemble such as XGBOOST [Chen and Guestrin, 2016]. We then fit a neural net (trying different neural net architectures) to this learned tree ensemble kernel function before fine tuning using survival kernel training (at which point the neural net architecture is fixed). We call our warm-start approach TUNA (*Tree ensemble Under a Neural Approximation*). We remark that Chen [2020] had come up with an earlier tree ensemble initialization strategy but it does not scale to large datasets.

We demonstrate survival kernels with and without TUNA on three standard survival analysis datasets, two of which are healthcare-related on predicting time until death (with number of data points ranging from thousands to tens of thousands), and the third is the KKBOX dataset (millions of data points). Survival kernels with TUNA achieve accuracy scores nearly as high or higher than the best performing baseline that we tested, DEEPHIT [Lee et al., 2018]. Meanwhile, using TUNA to accelerate training consistently results in higher accuracy models than not using TUNA and reduces overall training times by 62%–86% in our experiments. We show how to interpret survival kernel models trained on all three datasets we consider.

2 Background

We first review the standard right-censored survival analysis setup (model and prediction task) and deep kernel survival analysis [Chen, 2020]. For the latter, we do not address the Bayesian formulation (e.g., Wu et al. 2021) as the machinery involved is a bit different and our theoretical analysis later is frequentist. For ease of exposition, we phrase terminology in terms of predicting time until death although in general, the critical event of interest need not be death.

Model Let $(X_1, Y_1, D_1), \dots, (X_n, Y_n, D_n)$ denote the training data, where the i -th training point has feature vector $X_i \in \mathcal{X}$, observed nonnegative time duration $Y_i \geq 0$, and event indicator $D_i \in \{0, 1\}$; if $D_i = 1$, then Y_i is a time until death whereas if $D_i = 0$, then Y_i is a time until censoring (i.e., the i -th point's true time until death is at least Y_i). Each point (X_i, Y_i, D_i) is assumed to be generated i.i.d.:

1. Sample feature vector $X_i \sim \mathbb{P}_X$.
2. Sample nonnegative survival time $T_i \sim \mathbb{P}_{T|X=X_i}$.
3. Sample nonnegative censoring time $C_i \sim \mathbb{P}_{C|X=X_i}$.
4. If $T_i \leq C_i$ (death happens before censoring): set $Y_i = T_i$ and $D_i = 1$.
Otherwise (death happens after censoring): set $Y_i = C_i$ and $D_i = 0$.

Distributions \mathbb{P}_X , $\mathbb{P}_{T|X}$, and $\mathbb{P}_{C|X}$ are unknown to the learning method. We assume that the distribution $\mathbb{P}_{T|X=x}$ is for a continuous random variable with CDF $F_{T|X}(t|x)$ and PDF $f_{T|X}(t|x) = \frac{\partial}{\partial t} F_{T|X}(t|x)$.

Prediction task A standard prediction task is to estimate, for a test feature vector x , the conditional survival function

$$S(t|x) := \mathbb{P}(\text{time until death} > t | \text{feature vector} = x) = 1 - F_{T|X}(t|x),$$

which is defined for all $t \geq 0$. A closely related problem is to estimate the so-called hazard function

$$h(t|x) := -\frac{\partial}{\partial t} \log S(t|x) = -\frac{\frac{\partial}{\partial t} S(t|x)}{S(t|x)} = -\frac{\frac{\partial}{\partial t} [1 - F_{T|X}(t|x)]}{S(t|x)} = \frac{f_{T|X}(t|x)}{S(t|x)}, \quad (2.1)$$

which is (from the final expression) the instantaneous rate of death at time t given survival at least through time t for feature vector x . By how the hazard function is defined, $S(t|x) = \exp(-\int_0^t h(s|x)ds)$, so estimating $h(\cdot|x)$ yields an estimate of $S(\cdot|x)$.

Kernel estimators Let $\mathbb{K} : \mathcal{X} \times \mathcal{X} \rightarrow [0, \infty)$ denote a kernel function that measures how similar any two feature vectors are (a higher value means more similar). We explain how this function can be learned shortly in a neural net framework. For now, consider it to be pre-specified. Then we can estimate the hazard function as follows.

Hazard function estimator. Let $t_1 < t_2 < \dots < t_m$ denote the unique times of death in the training data, and define $t_0 := 0$. Then a kernel predictor for a discretized version of the hazard function is, for time indices $\ell = 1, 2, \dots, m$ and feature vector $x \in \mathcal{X}$,

$$\hat{h}(\ell|x) := \frac{\sum_{j=1}^n \mathbb{K}(x, X_j) D_j \mathbb{1}\{Y_j = t_\ell\}}{\sum_{j=1}^n \mathbb{K}(x, X_j) \mathbb{1}\{Y_j > t_{\ell-1}\}}, \quad (2.2)$$

where $\mathbb{1}\{\cdot\}$ is the indicator function that is 1 when its argument is true and 0 otherwise. Note that $\hat{h}(\ell|x)$ estimates the probability of dying at time t_ℓ conditioned on surviving beyond time $t_{\ell-1}$ for feature vector x . To see this, consider when $\mathbb{K}(x, X_j) = 1$ for all j , in which case the numerator counts the total number of deaths at time t_ℓ , and the denominator counts the total number of data points that survived beyond time $t_{\ell-1}$; adding kernel weights that are not necessarily always 1 weights the contribution of the j -th training point depending on how similar test feature vector x is to X_j . As a corner case, in evaluating equation (2.2), if the numerator and denominator are both 0, we use the convention that $0/0 = 0$.

Survival function estimator. The hazard estimate $\hat{h}(\cdot|x)$ can be used to estimate the conditional survival function $S(\cdot|x)$ by taking products of empirical probabilities of surviving from time 0 to t_1 , t_1 to t_2 , and so forth up to time t :

$$\hat{S}(t|x) := \prod_{\ell=1}^m (1 - \hat{h}(\ell|x))^{\mathbb{1}\{t_\ell \leq t\}}. \quad (2.3)$$

This kernel predictor is called the *conditional Kaplan-Meier estimator* [Beran, 1981] and has known finite-sample error bounds [Chen, 2019]. For equation (2.3), the special case where $\mathbb{K}(x, x') = 1$ for all $x, x' \in \mathcal{X}$ yields the classical Kaplan-Meier estimator [Kaplan and Meier, 1958] that does not depend on feature vectors and is a population-level survival curve estimate:

$$\hat{S}^{\text{KM}}(t) := \prod_{\ell=1}^m \left(1 - \frac{\sum_{j=1}^n D_j \mathbb{1}\{Y_j = t_\ell\}}{\sum_{j=1}^n \mathbb{1}\{Y_j > t_{\ell-1}\}}\right)^{\mathbb{1}\{t_\ell \leq t\}}. \quad (2.4)$$

Deep kernel survival analysis To automatically learn the kernel function \mathbb{K} , deep kernel survival analysis [Chen, 2020] parameterizes \mathbb{K} in terms of a base neural net $\phi : \mathcal{X} \rightarrow \tilde{\mathcal{X}}$ that maps a raw feature vector x to an embedding $\tilde{x} = \phi(x) \in \tilde{\mathcal{X}}$; throughout this paper we denote embeddings with tildes. We always assume that the embedding space $\tilde{\mathcal{X}}$ is a subset of \mathbb{R}^d and that kernel function \mathbb{K} is of the form

$$\mathbb{K}(x, x'; \phi) = K(\rho(x, x'; \phi)), \quad \rho(x, x'; \phi) = \|\phi(x) - \phi(x')\|_2, \quad (2.5)$$

where $K : [0, \infty) \rightarrow [0, \infty)$ is a nonincreasing function, and $\|\cdot\|_2$ denotes Euclidean distance. For example, a common choice is the Gaussian kernel $K(u) = \exp(-\frac{u^2}{2\sigma^2})$ where σ^2 is the user-specified variance hyperparameter. Learning \mathbb{K} or distance function ρ amount to learning the base neural net ϕ . The architecture of ϕ is left for the user to specify, where standard strategies can be used. For example, when working with images, we can choose ϕ to be a convolutional neural net and when working with time series, ϕ can be a recurrent neural net.

To prevent overfitting during training, we replace the hazard estimate $\hat{h}(\ell|x)$ in equation (2.2) with a “leave-one-out” training version, and in terms of notation, we now also emphasize the dependence on the base neural net ϕ :

$$\hat{h}_{\text{train}}(\ell|i;\phi) := \frac{\sum_{j=1}^n \text{s.t. } j \neq i \mathbb{K}(X_i, X_j; \phi) D_j \mathbb{1}\{Y_j = t_\ell\}}{\sum_{j=1}^n \text{s.t. } j \neq i \mathbb{K}(X_i, X_j; \phi) \mathbb{1}\{Y_j > t_{\ell-1}\}}. \quad (2.6)$$

In particular, the prediction for the i -th training point does not depend on the i -th training point’s observed outcomes Y_i and D_i . Similarly, we can define a leave-one-out version $\hat{S}^{\text{train}}(t|x;\phi)$ of the survival function estimate $\hat{S}(t|x)$ given in equation (2.3).

As for what loss function to minimize to learn the base neural net ϕ (and thus the kernel function \mathbb{K} for use with the hazard or survival function estimators), one possibility is the negative log likelihood loss by Brown [1975]:

$$L_{\text{NLL}}(\phi) := \frac{1}{n} \sum_{i=1}^n \left(L_{\text{BCE}}(i;\phi) + \underbrace{\sum_{\substack{\ell=1 \\ \text{s.t. } t_\ell < Y_i}}^m \log \frac{1}{1 - \hat{h}_{\text{train}}(\ell|i;\phi)}}_{i\text{-th individual survives at times before } Y_i} \right),$$

where $L_{\text{BCE}}(i;\phi)$ is the binary cross-entropy loss

$$L_{\text{BCE}}(i;\phi) := D_i \log \frac{1}{\hat{h}_{\text{train}}(\kappa(Y_i)|i;\phi)} + (1 - D_i) \log \frac{1}{1 - \hat{h}_{\text{train}}(\kappa(Y_i)|i;\phi)},$$

and $\kappa(Y_i)$ denotes the sorted time index (from $1, 2, \dots, m$) that time Y_i corresponds to. Minimizing L_{NLL} via minibatch gradient descent yields the deep kernel survival analysis approach by Chen [2020].

Chen also discussed how to incorporate the DEEPHIT ranking loss term [Lee et al., 2018], which could be written

$$L_{\text{rank}}(\phi) := \frac{1}{n^2} \sum_{\substack{i=1 \\ \text{s.t. } D_i=1}}^n \sum_{\substack{j \neq i \\ \text{s.t. } Y_j > Y_i}} \exp \left(\frac{\hat{S}_{\text{train}}(Y_i|X_i;\phi) - \hat{S}_{\text{train}}(Y_i|X_j;\phi)}{\sigma_{\text{rank}}} \right),$$

where $\sigma_{\text{rank}} > 0$ is a hyperparameter; for simplicity, we use a normalization factor of $1/n^2$, which is the same normalization factor used in the DEEPHIT implementation that is part of the now standard PYCOX software package [Kvamme et al., 2019]. Our experiments later use the following overall deep kernel survival analysis (DKSA) loss term that trades off between Brown’s loss L_{NLL} and the ranking loss L_{rank} :

$$L_{\text{DKSA}}(\phi) := \eta L_{\text{NLL}}(\phi) + (1 - \eta) L_{\text{rank}}(\phi), \quad (2.7)$$

where $\eta \in [0, 1]$ is another hyperparameter.

Implementation remarks. As stated, the hazard estimator (2.2) as well as the conditional Kaplan-Meier estimator (2.3) are defined in terms of the unique observed times of death. In practice, Chen [2020] observed that discretizing time into time steps of equal size can sometimes yield more accurate survival predictions. This discretization acts as a form of regularization since we are essentially smoothing the resulting estimated hazard and conditional survival functions. Furthermore, note that the conditional Kaplan-Meier estimator is defined to be piecewise constant. However, in practice, interpolation improves test-time prediction accuracy. Chen’s implementation of deep kernel survival analysis uses the constant density interpolation strategy by Kvamme and Borgan [2021].

Separately, during training, using an infinite-support kernel function such as a Gaussian kernel works well in practice with neural net frameworks to prevent vanishing gradients. If we use a kernel function with finite support (such as the box, triangle, or Epanechnikov kernels), and we initialize ϕ such that for each training point, no other training point is found to be similar enough as to have a nonzero kernel weight, then we would struggle to learn an improved embedding

representation. As a concrete example, suppose that we use the box kernel $K(u) = \mathbb{1}\{u \leq 1\}$, and the base neural net is simply $\phi(x) = wx$ for some scalar weight $w \in \mathbb{R}$ (i.e., w is the only neural net parameter in this case). Then if during neural net training, w becomes too large in absolute value (namely, $|w| > \frac{1}{\min_{i \neq j} \|X_i - X_j\|_2}$), then for all $i \neq j$,

$$\begin{aligned} \mathbb{K}(X_i, X_j; \phi) &= K(\rho(X_i, X_j; \phi)) \\ &= \mathbb{1}\{\|\phi(X_i) - \phi(X_j)\|_2 \leq 1\} \\ &= \mathbb{1}\{\|wX_i - wX_j\|_2 \leq 1\} \\ &= \mathbb{1}\{|w|\|X_i - X_j\|_2 \leq 1\} \\ &= 0. \end{aligned}$$

When this happens, the numerator and denominator of the leave-one-out training hazard estimator (2.6) are both 0, so by the earlier stated convention that $0/0 = 0$, the overall predicted hazard is 0 for all time. This will mean that the loss does not depend on the neural net parameter w at all, so the gradient of the loss with respect to w is 0. By simply using an infinite-support kernel function during training, we avoid having to deal with these zero kernel weight issues.

3 Scalable and Interpretable Test-Time Prediction with an Accuracy Guarantee

To make a prediction for test feature vector x , we would in principle have to compute the similarity between x and every training feature vector, which is computationally expensive for large training datasets. To address this problem, we apply *kernel netting* [Kpotufe and Verma, 2017] to deep kernel survival analysis, obtaining a model we call a *survival kernel*. Kernel netting constructs a compressed version of the training data for use at test time using the standard notion of ε -nets (e.g., see the textbook by Vershynin [2018]). As a technical remark, kernel netting was originally developed for classification and regression; extending the proof ideas to survival analysis is nontrivial, requiring careful stitching of proof ideas by Kpotufe and Verma [2017] and Chen [2019]. Separately, Kpotufe and Verma did not consider interpretability in their original kernel netting paper.

Sample splitting For our theoretical guarantee on test time prediction error later, we assume that the base neural net ϕ has already been trained on “pre-training” data $(X_1^\circ, Y_1^\circ, D_1^\circ), \dots, (X_{n_o}^\circ, Y_{n_o}^\circ, D_{n_o}^\circ)$ that are independent of training data $(X_1, Y_1, D_1), \dots, (X_n, Y_n, D_n)$. As shorthand notation, we use $X_{1:n_o}^\circ := (X_1^\circ, \dots, X_{n_o}^\circ) \in \mathcal{X}^{n_o}$, and similarly define $Y_{1:n_o}^\circ, D_{1:n_o}^\circ, X_{1:n}, Y_{1:n}$, and $D_{1:n}$. The pre-training data $(X_{1:n_o}^\circ, Y_{1:n_o}^\circ, D_{1:n_o}^\circ)$ need not be sampled in the same manner as the “proper” training data $(X_{1:n}, Y_{1:n}, D_{1:n})$. In practice, one could for example take a complete training dataset and randomly split it into two portions, the first portion to treat as the pre-training data, and the second portion to treat as the proper training data. After training ϕ on pre-training data, we refer to the learned neural net as $\hat{\phi}$. Our theory treats how $\hat{\phi}$ is learned as a black box, but requires that the output space of $\hat{\phi}$ (the embedding space $\tilde{\mathcal{X}}$) satisfy some regularity conditions. Later in our experiments, we also intentionally try setting the pre-training and training datasets to be the same although our theory does not cover this scenario.

Survival kernels We now state how to train and make predictions with a survival kernel. At test time, for a test feature vector x , we only consider using training data within a threshold distance τ from x , where distances are computed via the learned distance $\rho(x, x'; \phi) = \|\phi(x) - \phi(x')\|_2$ with pre-trained neural net $\hat{\phi}$. In particular, at test time, we replace the function \mathbb{K} from equation (2.5) with the “truncated” version

$$\hat{\mathbb{K}}(x, x'; \hat{\phi}) = K(\rho(x, x'; \hat{\phi})) \mathbb{1}\{\rho(x, x'; \hat{\phi}) \leq \tau\}. \quad (3.1)$$

From a computational viewpoint, we can take advantage of recent advances in (approximate) nearest neighbor search data structures for Euclidean distance to find neighbors of x that are within distance τ (e.g., Andoni et al. 2015, Andoni and Razenshteyn 2015, Malkov and Yashunin 2018, Prokhorenkova and Shekhovtsov 2020).

Training. The training procedure for a survival kernel works as follows, for a user-specified (approximate) Euclidean distance nearest neighbor data structure:

1. Learn base neural net ϕ with pre-training data $(X_{1:n_o}^\circ, Y_{1:n_o}^\circ, D_{1:n_o}^\circ)$ by minimizing the deep kernel survival analysis loss L_{DKSA} given in equation (2.7) with minibatch gradient descent, *without truncating the kernel function*. Denote the learned neural net as $\hat{\phi}$.
2. For the training (and not pre-training) feature vectors $X_{1:n}$, compute the embeddings $\tilde{X}_1 = \hat{\phi}(X_1), \tilde{X}_2 = \hat{\phi}(X_2), \dots, \tilde{X}_n = \hat{\phi}(X_n)$, and construct a Euclidean-distance-based nearest neighbor data structure using training embeddings $\tilde{X}_{1:n} := (\tilde{X}_1, \tilde{X}_2, \dots, \tilde{X}_n)$.
3. With the help of the nearest neighbor data structure, compute a subsample of $\tilde{X}_{1:n}$ that we denote as $\tilde{Q}_\varepsilon \subseteq \tilde{X}_{1:n}$, where $\varepsilon > 0$ is an approximation parameter (as $\varepsilon \rightarrow 0$, no subsampling is done, i.e., \tilde{Q}_ε becomes $\tilde{X}_{1:n}$). Specifically, \tilde{Q}_ε is an ε -net; \tilde{Q}_ε can be computed efficiently with the help of a nearest neighbor data structure as follows:
 - (a) Initialize \tilde{Q}_ε to be the empty set.
 - (b) For $i \in \{1, 2, \dots, n\}$: if \tilde{X}_i 's nearest neighbor in \tilde{Q}_ε is not within Euclidean distance ε , add \tilde{X}_i to \tilde{Q}_ε .
4. For each training embedding \tilde{X}_i , assign it to a single closest exemplar point in \tilde{Q}_ε (break ties arbitrarily). After this assignment, each exemplar point $\tilde{q} \in \tilde{Q}_\varepsilon$ is assigned to a subset $\mathcal{I}_{\tilde{q}} \subseteq \{1, 2, \dots, n\}$ of training points. This could be viewed as a clustering assignment, where the training points of each cluster is represented by an exemplar.
5. For each exemplar point $\tilde{q} \in \tilde{Q}_\varepsilon$, recalling that $t_1 < \dots < t_m$ are the unique times of death in the training data, compute the following summary functions for $\ell = 1, \dots, m$:

$$\mathbf{D}_{\tilde{q}}(\ell) := \sum_{j \in \mathcal{I}_{\tilde{q}}} D_j \mathbb{1}\{Y_j = t_\ell\}, \quad \mathbf{R}_{\tilde{q}}^+(\ell) := \sum_{j \in \mathcal{I}_{\tilde{q}}} \mathbb{1}\{Y_j \geq t_\ell\}. \quad (3.2)$$

Note that $\mathbf{D}_{\tilde{q}}(t)$ is the number of deaths at time t across training points assigned to exemplar \tilde{q} , and $\mathbf{R}_{\tilde{q}}^+(t)$ is the number of these training points that are “at risk” (could possibly die) at time t .

Prediction. After training a survival kernel, prediction works as follows:

For test feature vector x , first compute the embedding $\tilde{x} = \hat{\phi}(x)$. Then form the hazard estimate

$$\tilde{h}_{\tilde{Q}_\varepsilon}(\ell|\tilde{x}) := \frac{\sum_{\tilde{q} \in \tilde{Q}_\varepsilon} \tilde{\mathbb{K}}(\tilde{x}, \tilde{q}) \mathbf{D}_{\tilde{q}}(\ell)}{\sum_{\tilde{q} \in \tilde{Q}_\varepsilon} \tilde{\mathbb{K}}(\tilde{x}, \tilde{q}) \mathbf{R}_{\tilde{q}}^+(\ell)} \quad \text{for } \ell = 1, 2, \dots, m, \quad (3.3)$$

where $\tilde{\mathbb{K}}(\tilde{x}, \tilde{q}) := K(\|\tilde{x} - \tilde{q}\|_2) \mathbb{1}\{\|\tilde{x} - \tilde{q}\|_2 \leq \tau\}$; as a reminder, $K : [0, \infty) \rightarrow [0, \infty)$ is a non-increasing function (e.g., $K(u) = \exp(-u^2)$). Note that the nearest neighbor data structure constructed in step 2 of the training procedure can be used to find all exemplars in \tilde{Q}_ε within distance τ of \tilde{x} (this is needed to compute $\tilde{\mathbb{K}}$). The conditional survival function can be estimated by computing

$$\tilde{S}_{\tilde{Q}_\varepsilon}(t|\tilde{x}) := \prod_{\ell=1}^m (1 - \tilde{h}_{\tilde{Q}_\varepsilon}(\ell|\tilde{x}))^{\mathbb{1}\{t_\ell \leq t\}}.$$

As a corner case, if all the kernel weights are zero for test feature vector x , then we output the training set Kaplan-Meier survival function estimate (2.4) as the prediction.

Note that if $\varepsilon = 0$ (i.e., the ε -net consists of all training embeddings), and the pre-training and training sets are set to be identical, then survival kernels becomes an approximate version of the original deep kernel survival analysis model by Chen [2020]. In particular, the approximation comes from the kernel function being truncated (set to be 0 beyond the critical threshold distance τ) at test time. Separately, if the base neural net is the identity function $\phi(x) = x$ (which would require no pre-training data to learn, so we skip steps 1 and 2 of the survival kernel training procedure), then we obtain a non-neural-net extension of the original kernel netting procedure by Kpotufe and Verma [2017] to the survival analysis setting.

Outline for the remainder of this section In the remainder of this section, we discuss three main topics. First, we discuss model interpretability in Section 3.1, where the two key ideas we use are that the training procedure is clustering the training data and that the predicted hazard function at any time step is a weighted combination of clusters (from looking at equation (3.3)).

Next, we provide an overview of the theory we have developed for survival kernels in Section 3.2, starting from assumptions and the generalization error used to stating the main finite-sample guarantee and some interpretations and implications. In a nutshell, our theory says that if the embeddings are in some sense “nice” (satisfying standard theoretical assumptions made in nonparametric estimation and survival analysis), then a survival kernel estimates the conditional survival function arbitrarily accurately (up to some pre-specified time horizon) with high probability as the amount of training data grows large. The error bound we obtain has an order of growth that, ignoring a log factor, is optimal.

Lastly, we present a variant of our training procedure in Section 3.3 that turns out to yield significant accuracy improvements in practice although it is not covered by our theoretical analysis. This variant adds a step at the end of survival kernel training that fine-tunes the summary functions from training step 5. Specifically, note that the summary functions $\mathbf{D}_{\tilde{q}}(t)$ and $\mathbf{R}_{\tilde{q}}^+(t)$ in equation (3.2) are constructed from training data, and it could be that these are noisy or inaccurate. After training the base neural net ϕ and treating it as fixed, we could then set up a fine-tuning step in which we learn $\tilde{\mathbf{D}}_{\tilde{q}}(t)$ and $\tilde{\mathbf{R}}_{\tilde{q}}^+(t)$ in a neural net framework.

3.1 Model Interpretability

Visualizing clusters Recall that each exemplar $\tilde{q} \in \tilde{\mathcal{Q}}_\varepsilon$ corresponds to a cluster of training points, i.e., there is a one-to-one correspondence between exemplars and clusters. For tabular data, we can create a heatmap visualization to help us quickly identify how clusters differ in terms of whether specific feature values are more prominent for specific clusters. In particular, we set the rows of the heatmap to correspond to different features, the columns to correspond to different clusters, and the heatmap intensity values to correspond to the fraction of points in a cluster with a specific feature value. As a concrete example, we show this heatmap visualization in Figure 1(a) for a dataset on predicting time until death of hospitalized patients from the Study to Understand Prognoses, Preferences, Outcomes, and Risks of Treatment (SUPPORT) [Knaus et al., 1995]. For instance, we see that the leftmost cluster (column) in the heatmap corresponds to patients who often have cancer and who tend to be older, have at least one comorbidity, and have a high temperature (indicative of a fever). In contrast, the rightmost cluster corresponds to young patients without cancer.

Moreover, per cluster, we can compute its Kaplan-Meier survival curve using the equation:

$$\hat{S}_{\tilde{q}}^{\text{KM}}(t) := \prod_{\ell=1}^m \left(1 - \frac{\mathbf{D}_{\tilde{q}}(\ell)}{\mathbf{R}_{\tilde{q}}^+(\ell)}\right)^{\mathbf{1}_{\{t_\ell \leq t\}}} \quad \text{for } \tilde{q} \in \tilde{\mathcal{Q}}_\varepsilon, t \geq 0. \quad (3.4)$$

This is simply the Kaplan-Meier estimator equation (2.4) restricted to data points in the cluster corresponding to exemplar \tilde{q} . We can plot these survival curves as shown in Figure 1(b), where we have also included 95% confidence intervals using the standard exponential Greenwood formula [Kalbfleisch and Prentice, 1980]. Note that for this dataset, per patient, the time until death is counted starting from when the patient entered the study, and only patients who have been in the

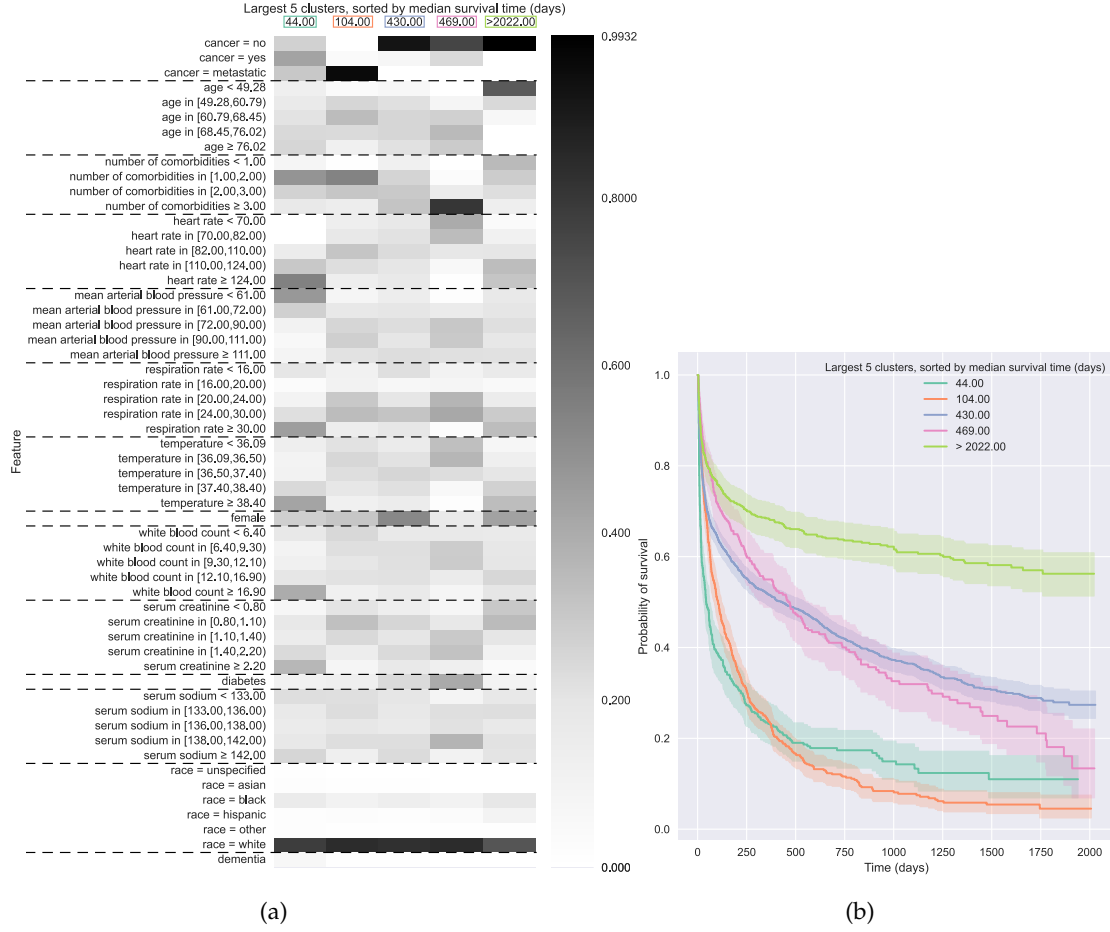


Figure 1: Visualization of the largest 5 clusters found by a survival kernel model trained on the SUPPORT dataset (we limit the number of clusters shown for ease of exposition and to prevent the plots from being too cluttered); more information on how the model is trained is in Section 5. Panel (a) shows a heatmap visualization that readily provides information on how the clusters are different, highlighting feature values that are prominent for specific clusters; the dotted horizontal lines separate features that correspond to the same underlying variable. Panel (b) shows Kaplan-Meier survival curves with 95% confidence intervals for the same clusters as in panel (a); the x-axis measures the number of days since a patient entered the study.

study for at least 3 days are included (since a number of features are collected on the third day). Thus, the x-axis in Figure 1(b) is the time since a patient entered the study.

Note that the time (x-axis value) at which a Kaplan-Meier survival curve crosses probability 1/2 (y-axis value) corresponds to a median survival time estimate (since half the patients survived up to this time and the rest survive beyond this time). Thus, per cluster, we can obtain a median survival time estimate (if the cluster's Kaplan-Meier curve never crosses probability 1/2, then the median survival time is greater than the largest observed time for the cluster). In fact, for the heatmap in Figure 1(a), we have sorted the clusters (i.e., the columns) by median survival time from smallest to largest (the rightmost cluster has median survival time > 2022 days since its Kaplan-Meier curve never crosses probability 1/2, and the last observed time for this cluster is 2022 days).

Comparing Kaplan-Meier curves across different groups of individuals is standard practice in survival analysis and gives a quick way to see which group is better or worse off over time. For instance, in this case, the lime green cluster (with median survival time > 2022 days) generally has higher survival probability across time compared to the four other clusters that have been plotted.

Meanwhile, initially the turquoise cluster (median survival time 44 days) appears worse off than the orange cluster (median survival time 104 days) but then the orange cluster becomes worse off after around 375 days since patients entered the study.

We provide a few technical details regarding how we generated Figure 1(a). Only for visualization purposes, continuous features have been discretized into 5 equal-sized bins (fewer bins are used if there are not enough data points in a cluster, or if the 20/40/60/80 percentile threshold values for a continuous feature are not all unique). The survival kernel models themselves do *not* require continuous features to be discretized first. Moreover, we have sorted the features (i.e., rows of the heatmap) in the following manner: per row, we compute the intensity range (i.e., maximum minus minimum intensity values), and then we sort the rows from largest to smallest intensity range, with the constraint that rows corresponding to the same underlying variable (the same continuous feature that has been discretized, or the same categorical variable) are still grouped together. For example, the reason why the variable “cancer” shows up first in Figure 1(a) is that among the three different cancer rows, one of them has the highest intensity range across all heatmap rows.

Data-point-specific information Next, we observe that for any test feature vector x with embedding $\tilde{x} = \hat{\phi}(x)$, its hazard estimate is given by equation (3.3), reproduced below for ease of exposition:

$$\tilde{h}_{\tilde{\mathcal{Q}}_\epsilon}(\ell|\tilde{x}) = \frac{\sum_{\tilde{q} \in \tilde{\mathcal{Q}}_\epsilon} \tilde{\mathbb{K}}(\tilde{x}, \tilde{q}) \mathbf{D}_{\tilde{q}}(\ell)}{\sum_{\tilde{q} \in \tilde{\mathcal{Q}}_\epsilon} \tilde{\mathbb{K}}(\tilde{x}, \tilde{q}) \mathbf{R}_{\tilde{q}}^+(\ell)}.$$

In the numerator and denominator summations, the only exemplars \tilde{q} that contribute to the calculation are ones for which $\tilde{\mathbb{K}}(\tilde{x}, \tilde{q})$ is positive. Again, since there is a one-to-one correspondence between exemplars and clusters, this means that each test feature vector’s hazard is modeled by only a subset of the clusters.

For any test feature vector x , we can readily determine which exemplars/clusters could possibly contribute to the prediction for x by figuring out which $\tilde{q} \in \tilde{\mathcal{Q}}_\epsilon$ satisfy $\tilde{\mathbb{K}}(\tilde{x}, \tilde{q}) > 0$. Of course, how large these weights are can also give a sense of the relative importance of the clusters for x . We could, for instance, make the same plots as in Figure 1 but only show the clusters that have nonzero weight for a specific test feature vector x .

3.2 Theory of Survival Kernels

We now provide an overview of our theoretical analysis of survival kernels. We begin with assumptions on the embedding space that are standard in nonparametric estimation theory (Section 3.2.1), although these assumptions are typically imposed on the raw feature space rather than the embedding space. We then state our assumption on how the embedding space relates to survival and censoring times (Section 3.2.2). All proofs are in Appendix A.

3.2.1 The Embedding Space

We assume that the raw feature vectors are sampled i.i.d. from a marginal distribution \mathbb{P}_X . As we treat the pre-trained neural net $\hat{\phi}$ as fixed, then the random embedding $\tilde{X} = \hat{\phi}(X)$ is sampled from some distribution $\mathbb{P}_{\tilde{X}}$ instead. We require $\mathbb{P}_{\tilde{X}}$ to satisfy some mild regularity conditions.

As an example, we remark that an embedding space that is uniform over a unit hypersphere (i.e., embeddings are Euclidean vectors with norm 1) satisfies all the assumptions of this subsection. For ways to encourage the learned embedding to be uniform over the unit hypersphere, see the papers by Wang and Isola [2020] and Liu et al. [2021].

Our theory requires a technical assumption that ensures that the event that \tilde{X} lands within distance τ of an embedding $\tilde{x} \in \tilde{\mathcal{X}}$ has a well-defined probability. This event could be phrased as \tilde{X} landing in the closed ball of radius τ centered at \tilde{x} , denoted as $B(\tilde{x}, \tau) := \{\tilde{x}' \in \tilde{\mathcal{X}} : \|\tilde{x} - \tilde{x}'\|_2 \leq \tau\}$.

Assumption A^{technical}. Distribution $\mathbb{P}_{\tilde{\mathcal{X}}}$ is a Borel probability measure with compact support $\tilde{\mathcal{X}} \subseteq \mathbb{R}^d$.

Compactness of $\tilde{\mathcal{X}}$ eases the exposition. Our results trivially extend to the case where embeddings sampled from $\mathbb{P}_{\tilde{\mathcal{X}}}$ land in a compact region (where our theory applies) with probability at least $1 - \delta$ for some $\delta \geq 0$, and otherwise when the embeddings land outside the compact region, we tolerate a worst-case prediction error with probability δ .

We use the standard notion of covers, packings, and nets (all specialized to Euclidean distance).

Definition 1. For any radius $\varepsilon > 0$:

- A subset $\tilde{\mathcal{Q}}$ of $\tilde{\mathcal{X}}$ is called an ε -cover of $\tilde{\mathcal{X}}$ if for any $\tilde{x} \in \tilde{\mathcal{X}}$, there exists $\tilde{q} \in \tilde{\mathcal{Q}}$ such that $\|\tilde{x} - \tilde{q}\|_2 \leq \varepsilon$.
- A subset $\tilde{\mathcal{Q}}$ of $\tilde{\mathcal{X}}$ is called an ε -packing of $\tilde{\mathcal{X}}$ if for any two distinct \tilde{q} and \tilde{q}' in $\tilde{\mathcal{Q}}$, we have $\|\tilde{q} - \tilde{q}'\|_2 > \varepsilon$.
- A subset $\tilde{\mathcal{Q}}$ of $\tilde{\mathcal{X}}$ is called an ε -net of $\tilde{\mathcal{X}}$ if $\tilde{\mathcal{Q}}$ is both an ε -cover and an ε -packing of $\tilde{\mathcal{X}}$.

Next, our theory makes use of the standard complexity notions of covering numbers and intrinsic dimension to describe the embedding space, where lower complexity will correspond to tighter error bounds. As an illustrative example, we explain how these behave when the embedding space is the unit hypersphere $\mathbb{S}^{d-1} = \{\tilde{x} \in \mathbb{R}^d : \|\tilde{x}\|_2 = 1\}$ (with $d \geq 2$).

Definition 2. The ε -covering number of $\tilde{\mathcal{X}}$ (for Euclidean distance) is the smallest size possible for an ε -cover for $\tilde{\mathcal{X}}$. We denote this number by $N(\varepsilon; \tilde{\mathcal{X}})$.

The embedding space $\tilde{\mathcal{X}}$ being compact implies that for every $\varepsilon > 0$, we have $N(\varepsilon; \tilde{\mathcal{X}}) < \infty$, and moreover, that $\tilde{\mathcal{X}}$ has a finite diameter $\Delta_{\tilde{\mathcal{X}}} := \max_{\tilde{x}, \tilde{x}' \in \tilde{\mathcal{X}}} \|\tilde{x} - \tilde{x}'\|_2 < \infty$. For example, the unit hypersphere \mathbb{S}^{d-1} clearly has diameter 2. Moreover, its covering number is bounded as follows.

Claim 1 (Follows from Corollary 4.2.13 by Vershynin [2018]). For any $\varepsilon > 0$, the unit hypersphere has covering number $N(\varepsilon; \mathbb{S}^{d-1}) \leq (\frac{4}{\varepsilon} + 1)^d$.

Covering numbers provide a way to derive error bounds. Another way is to assume a known “intrinsic dimension” of the embedding space. We use the following notion of intrinsic dimension.

Assumption A^{intrinsic}. There exist a positive integer $d' > 0$ (called the intrinsic dimension of $\mathbb{P}_{\tilde{\mathcal{X}}}$) and positive constants $C_{d'}$ and r^* such that for any $\tilde{x} \in \tilde{\mathcal{X}}$ and $r \in (0, r^*]$, we have $\mathbb{P}_{\tilde{\mathcal{X}}}(B(\tilde{x}, r)) \geq C_{d'} r^{d'}$.

When embeddings are on the unit hypersphere, then under a mild regularity condition, the embedding space has intrinsic dimension $d - 1$.

Claim 2. If $\mathbb{P}_{\tilde{\mathcal{X}}}$ has a probability density function that is 0 outside of \mathbb{S}^{d-1} and lower-bounded by a constant $c_{\min} > 0$ over \mathbb{S}^{d-1} , then the embedding space has intrinsic dimension $d - 1$.

We remark that for embeddings on the hypersphere, one desirable property is that they are uniformly distributed [Wang and Isola, 2020, Liu et al., 2021], which is of course a special case of Claim 2.

3.2.2 Relating Embeddings to Survival and Censoring Times

Next, we impose a survival analysis assumption by Chen [2019], which is a slight variant on an earlier assumption by Dabrowska [1989].

Assumption A^{survival}. In addition to Assumption A^{technical}, we further assume that the conditional survival, censoring, and observed time distributions $\mathbb{P}_{T|\tilde{\mathcal{X}}}$, $\mathbb{P}_{C|\tilde{\mathcal{X}}}$, and $\mathbb{P}_{Y|\tilde{\mathcal{X}}}$ correspond to continuous random variables with PDF's $\tilde{f}_{T|\tilde{\mathcal{X}}}$, $\tilde{f}_{C|\tilde{\mathcal{X}}}$, and $\tilde{f}_{Y|\tilde{\mathcal{X}}}$. The conditional survival function that we aim to predict is precisely $\tilde{S}(t|\tilde{x}) := \int_t^\infty \tilde{f}_{T|\tilde{\mathcal{X}}}(s|\tilde{x}) ds$. To be able to estimate this function, censoring cannot almost surely happen. Moreover, we assume the following:

- (a) (Observed time distribution has large enough tails) For a user-specified time $t_{\text{horizon}} > 0$, there exists a constant $\theta > 0$ such that $\int_{t_{\text{horizon}}}^{\infty} f_{Y|\tilde{X}}(s|\tilde{x})ds \geq \theta$ for all $\tilde{x} \in \tilde{\mathcal{X}}$.
- (b) (Smoothness: embeddings that are close by should have similar survival time distributions and also similar censoring time distributions) PDF's $\tilde{f}_{T|\tilde{X}}$ and $\tilde{f}_{C|\tilde{X}}$ are assumed to be Hölder continuous with respect to embeddings, i.e., there exist constants $\lambda_T > 0$, $\lambda_C > 0$, and $\alpha > 0$ such that for all $\tilde{x}, \tilde{x}' \in \tilde{\mathcal{X}}$,

$$|\tilde{f}_{T|\tilde{X}}(t|\tilde{x}) - \tilde{f}_{T|\tilde{X}}(t|\tilde{x}')| \leq \lambda_T \|\tilde{x} - \tilde{x}'\|_2^\alpha,$$

$$|\tilde{f}_{C|\tilde{X}}(t|\tilde{x}) - \tilde{f}_{C|\tilde{X}}(t|\tilde{x}')| \leq \lambda_C \|\tilde{x} - \tilde{x}'\|_2^\alpha.$$

For any estimate \tilde{G} of the true conditional survival function \tilde{S} , our theory uses the generalization error

$$\mathcal{L}_{\text{survival}}(\tilde{G}, \tilde{S}) := \mathbb{E}_{\tilde{X} \sim \mathbb{P}_{\tilde{X}}} \left[\frac{\int_0^{t_{\text{horizon}}} (\tilde{G}(t|\tilde{X}) - \tilde{S}(t|\tilde{X}))^2 dt}{t_{\text{horizon}}} \right].$$

We only aim to accurately estimate $\tilde{S}(t|\tilde{x})$ up to the user-specified time t_{horizon} (that appears in Assumption $\mathbf{A}^{\text{survival}}(\text{a})$). We shall plug in the survival kernel conditional survival function estimate $\tilde{S}_{\tilde{\mathcal{Q}}_\epsilon}$ (from step 6 of the survival kernel procedure) in place of \tilde{G} .

3.2.3 Theoretical Guarantee on Prediction Accuracy

We are now ready to state the main theoretical result of the paper, which states a generalization error bound for survival kernels.

Theorem 1. Suppose that Assumptions $\mathbf{A}^{\text{technical}}$, $\mathbf{A}^{\text{intrinsic}}$, and $\mathbf{A}^{\text{survival}}$ hold, and we train a survival kernel with $\epsilon = \beta\tau$ when constructing $\tilde{\mathcal{Q}}_\epsilon$, where $\beta \in (0, 1)$ and $\tau > 0$ are user-specified parameters, and the truncated kernel used is of the form in equation (3.1). Let $\Psi = \min\{N(\frac{(1-\beta)\tau}{2}; \tilde{\mathcal{X}}), \frac{1}{C_{d'}((1-\beta)\tau)^{d'}}\}$, where d' is the intrinsic dimension. Then when $n \geq \mathcal{O}(\frac{K(0)}{K(\tau)((1-\beta)\tau)^{d'}})$,

$$\mathbb{E}_{\tilde{X}_{1:n}, Y_{1:n}, D_{1:n}} [\mathcal{L}_{\text{survival}}(\tilde{S}_{\tilde{\mathcal{Q}}_\epsilon}, \tilde{S})] \leq \tilde{\mathcal{O}}\left(\frac{1}{n} \cdot \frac{K^4(0)}{K^4(\tau)} \cdot \Psi\right) + (1 + \beta)^{2\alpha} \tau^{2\alpha} \cdot \mathcal{O}\left(\frac{K^2(0)}{K^2(\tau)}\right),$$

where $\tilde{\mathcal{O}}$ ignores log factors.

The error bound consists of two terms, which correspond to variance and bias respectively. When the embedding space has intrinsic dimension d' , this error bound is, up to a log factor, optimal in the case where $K(u) = 1$ for $u \geq 0$, and $\tau = \tilde{\mathcal{O}}(n^{-1/(2\alpha+d')})$. In this scenario, the survival error bound is $\tilde{\mathcal{O}}(n^{-2\alpha/(2\alpha+d')})$, which matches the lower bound for conditional CDF estimation by Chagny and Roche [2014] (this is a special case of the survival analysis setup in which there is no censoring). Of course, in practice, K is typically chosen to decay, so τ should be chosen to not be too large due to the error bound's dependence on the ratio $K(0)/K(\tau)$.

3.3 Summary Fine-Tuning

Our theoretical analysis crucially relies on the summary functions being the ones stated in equation (3.2). However, in practice, it turns out that learning the summary functions improves prediction accuracy in practice. We now discuss how to do this. Specifically, we add a “summary fine-tuning” step that refines the summary functions $\mathbf{D}_{\tilde{q}}(\ell)$ and $\mathbf{R}_{\tilde{q}}^+(\ell)$ that are used in the test-time hazard predictor (given in equation (3.3)).

To do summary fine-tuning, we treat everything in the survival kernel model as fixed except for the summary functions $\mathbf{D}_{\tilde{q}}(\ell)$ and $\mathbf{R}_{\tilde{q}}^+(\ell)$ for each exemplar $\tilde{q} \in \tilde{\mathcal{Q}}_\epsilon$ and each time step $\ell \in \{1, \dots, m\}$, where as a reminder the time steps $t_1 < t_2 < \dots < t_m$ are at the unique times of

death in the training data. We now use the survival kernel predicted hazard function given in equation (3.3), which we plug into the deep kernel survival analysis loss L_{DKSA} given in equation (2.7). Importantly, now when we minimize the loss L_{DKSA} , we are not learning the base neural net ϕ from earlier (as it is treated as fixed); we are only learning the summary functions. Thus, the only additional details needed in explaining how summary fine-tuning works are in how we parameterize the summary functions. This requires a little bit of care to encode the constraints that the number of people at risk monotonically decreases over time and is always at least as large as the number of people who die over time.

Parameterizing summary functions for number of deaths We parameterize the summary function $\mathbf{D}_{\tilde{q}}(\ell)$ for the number of deaths at time step ℓ specific to exemplar \tilde{q} as

$$\mathbf{D}_{\tilde{q}}(\ell) := \exp(\gamma_{\tilde{q},\ell}) + \exp(\gamma_{\ell}^{\text{baseline}}),$$

where $\gamma_{\tilde{q},\ell} \in \mathbb{R}$ and $\gamma_{\ell}^{\text{baseline}} \in \mathbb{R}$ are unconstrained neural net parameters. We initialize $\mathbf{D}_{\tilde{q}}(\ell)$ to be approximately equal to the value given in equation (3.2) by using the initial values

$$\gamma_{\tilde{q},\ell} = \log \left(\sum_{j \in \mathcal{I}_{\tilde{q}}} D_j \mathbb{1}\{Y_j = t_{\ell}\} \right), \quad (3.5)$$

$$\gamma_{\ell}^{\text{baseline}} = \log(10^{-12}) \approx -27.631. \quad (3.6)$$

Note that the 10^{-12} number in equation (3.6) is just an arbitrarily chosen small constant. Meanwhile, in computing equation (3.5), to prevent numerical issues, if the summation inside the log is less than 10^{-12} , then we also set $\gamma_{\tilde{q},\ell} = \log(10^{-12})$.

Parameterizing summary functions for number of individuals at risk To parameterize the summary function for the number of individuals at risk, we first introduce a new variable for the number of individuals censored at time step ℓ specific to exemplar \tilde{q} :

$$\mathbf{C}_{\tilde{q}}(\ell) := \exp(\omega_{\tilde{q},\ell}) + \exp(\omega_{\ell}^{\text{baseline}}),$$

where $\omega_{\tilde{q},\ell} \in \mathbb{R}$ and $\omega_{\ell}^{\text{baseline}} \in \mathbb{R}$ are unconstrained neural net parameters. How these parameters are initialized works the same way as for the number of deaths and requires that we count how many people are censored at each time step ℓ , which is straightforward to compute from the training data (the only minor complication is that the time steps are for unique times of death, and times of censoring could happen at other times—the simple fix is to consider the number of individuals censored at time step ℓ to be summed across all individuals censored at times within the interval $(t_{\ell-1}, t_{\ell}]$).

Finally, it suffices to note that the number of individuals at risk at time step ℓ specific to exemplar \tilde{q} is given by the recurrence relation

$$\mathbf{R}_{\tilde{q}}^+(\ell) = \mathbf{D}_{\tilde{q}}(\ell) + \mathbf{C}_{\tilde{q}}(\ell) + \mathbf{R}_{\tilde{q}}^+(\ell + 1), \quad (3.7)$$

where $\mathbf{R}_{\tilde{q}}^+(m + 1) := 0$. In particular, for a specific exemplar \tilde{q} , once we have computed $\mathbf{D}_{\tilde{q}}(\ell)$ and $\mathbf{C}_{\tilde{q}}(\ell)$ for all ℓ , then we can easily compute $\mathbf{R}_{\tilde{q}}(m)$, $\mathbf{R}_{\tilde{q}}(m - 1)$, $\mathbf{R}_{\tilde{q}}(m - 2)$, \dots , $\mathbf{R}_{\tilde{q}}(1)$ using equation (3.7)—note that we compute these in reverse chronological order.

Final remarks on summary fine-tuning To summarize, summary fine-tuning minimizes the deep kernel survival analysis loss L_{DKSA} (equation (2.7)) using the hazard function given in equation (3.3). We treat the pre-trained base neural net $\hat{\phi}$ and survival kernel clustering assignments as fixed. In fact, the only neural net parameters that we optimize over are the newly introduced variables $\gamma_{\tilde{q},\ell}, \gamma_{\ell}^{\text{baseline}}, \omega_{\tilde{q},\ell}, \omega_{\ell}^{\text{baseline}} \in \mathbb{R}$ for $\tilde{q} \in \tilde{\mathcal{Q}}_{\varepsilon}$ and $\ell \in \{1, 2, \dots, m\}$.

Note that in terms of model interpretation, summary fine-tuning does not change survival kernel cluster assignments and only changes the summary functions of the different clusters. We still compute survival curves using equation (3.4) but instead plug in the refined summary functions. Consequently, the survival curves are no longer the standard Kaplan-Meier ones, and we can no longer use the 95% confidence intervals that are meant for Kaplan-Meier survival curves.

We remark that simultaneously optimizing the summary functions *and* the base neural net ϕ would be difficult in terms of how we set up the survival kernel framework because we only determine the exemplars after the base neural net ϕ has been learned and treated as fixed (the exemplars are chosen based on the embedding space). If we update the base neural net, the exemplars would change as would their summary functions, and in fact even the number of exemplars (and thus, the number of summary functions) could change. An alternating optimization could potentially be done (i.e., alternate between optimizing ϕ , choosing which training points are the exemplars, and then optimizing the summary functions) but would be computationally costly; for simplicity, we do not do such an optimization.

4 Scalable Tree Ensemble Warm-Start

Whereas Section 3 focused on constructing a test-time predictor that can scale to large datasets, we now turn to accelerating the training of the base neural net ϕ , which happens in the very first step of survival kernel training. Specifically, we now present a warm-start strategy for initializing ϕ prior to optimizing the parameters of ϕ by minimizing the DKSA loss L_{DKSA} given in equation (2.7).

Our warm-start strategy begins by learning a kernel function using a scalable tree ensemble approach such as XGBOOST [Chen and Guestrin, 2016]. Because a kernel function learned by a tree ensemble is not represented as a neural net, we then fit a neural net to the tree ensemble’s kernel function via minibatch gradient descent. In short, we warm-start ϕ using a *Tree ensemble Under a Neural Approximation* (TUNA). After the warm-start, we then fine-tune ϕ using the DKSA loss L_{DKSA} (this is not to be confused with summary fine-tuning; here we in fact are fine-tuning the base neural net ϕ and we are *not* optimizing over any sort of summary functions). Importantly, at the end of this section, we explain how TUNA can accelerate neural architecture search. Note that our theory in Section 3.2 trivially supports TUNA: simply train base neural net ϕ with TUNA on the pre-training data.

Approximating a tree ensemble kernel The key idea behind TUNA is that decision trees and their ensembles implicitly learn kernel functions [Breiman, 2000]. Thus, by using any scalable decision tree or decision tree ensemble learning approach, we can learn an initial kernel function guess \mathbb{K}_0 . For example, a decision tree has $\mathbb{K}_0(x, x') = \mathbb{1}\{x \text{ and } x' \text{ are in the same leaf}\}$. For a decision forest $\mathbb{K}_0(x, x')$ is equal to the fraction of trees for which x and x' are in the same leaf. For gradient tree boosting, the kernel function is a bit more involved and the general case is given by Chen and Shah [2018, Section 7.1.3]. For XGBOOST when we add one tree at a time and the final ensemble has equal weight across trees, then it suffices to set $\mathbb{K}_0(x, x')$ to be the fraction of trees for which x and x' are in the same leaf.

The kernel function \mathbb{K}_0 of a tree ensemble does not give us an embedding representation of the data, where the embedding function is a neural net. However, we can train the base neural net ϕ to approximate \mathbb{K}_0 by minimizing the mean-squared error

$$\frac{1}{n_o(n_o - 1)/2} \sum_{i=1}^{n_o} \sum_{j=i+1}^{n_o} \left(\underbrace{\mathbb{K}(X_i^\circ, X_j^\circ)}_{\text{to be learned}} - \underbrace{\mathbb{K}_0(X_i^\circ, X_j^\circ)}_{\text{given by the tree ensemble}} \right)^2. \quad (4.1)$$

As a reminder, “ \circ ” indicates that a quantity is part of pre-training data, and \mathbb{K} depends on the base neural net ϕ : $\mathbb{K}(x, x') = K(\|\phi(x) - \phi(x')\|_2^2)$, where for example $K(u) = \exp(-u^2)$ for a Gaussian kernel. To scale to large datasets, we minimize loss (4.1) in minibatches. The TUNA warm-start strategy is as follows:

1. Train a scalable tree ensemble (e.g., XGBOOST) on the pre-training data; denote its learned kernel function by \mathbb{K}_0 . For a subset $\mathcal{S} \subseteq \{X_1^\circ, \dots, X_{n_o}^\circ\}$ of the pre-training feature vectors, let $\mathbf{K}_{\mathcal{S}}$ denote the $|\mathcal{S}|$ -by- $|\mathcal{S}|$ Gram matrix formed so that the (i, j) -th entry is given by $\mathbb{K}_0(x_i^\circ, x_j^\circ)$ where x_i° and x_j° are the i -th and j -th pre-training feature vectors in \mathcal{S} (with elements of \mathcal{S} ordered arbitrarily).
2. For each minibatch consisting of pre-training feature vectors $x_1^\circ, \dots, x_b^\circ$ where b is the batch size:
 - (a) Compute the batch's tree ensemble Gram matrix $\mathbf{K}_{\{x_1^\circ, \dots, x_b^\circ\}}$ (defined in step 1) using \mathbb{K}_0 .
 - (b) Compute the current neural net's Gram matrix estimate $\hat{\mathbf{K}}_{\{x_1^\circ, \dots, x_b^\circ\}}$, which has (i, j) -th entry given by $\mathbb{K}(x_i^\circ, x_j^\circ) = K(\|\phi(x_i^\circ) - \phi(x_j^\circ)\|_2^2)$.
 - (c) Let this minibatch's loss be the MSE loss (4.1) restricted to feature vectors of the current minibatch, i.e., the MSE loss between $\hat{\mathbf{K}}_{\{x_1^\circ, \dots, x_b^\circ\}}$ and $\mathbf{K}_{\{x_1^\circ, \dots, x_b^\circ\}}$. Update parameters of neural net ϕ based on the gradient of this minibatch's loss.

As a slight refinement of this warm-start procedure, in our experiments later, between steps 1 and 2, we initialize the base neural net ϕ using a different warm-start strategy by Chen [2020] that is based on multidimensional scaling (MDS) [Borg and Groenen, 2005] (i.e, within our warm-start strategy, we further use another warm-start strategy). Chen's warm-start strategy is computationally expensive to compute, so we use this strategy only over a small subset of the training data. For details, see Appendix B.

Neural architecture search Step 2 of TUNA can be run using different base neural nets (and step 1 only needs to be run once). Thus, we can search over different base neural net architectures and choose whichever one achieves the lowest average minibatch loss (the one described in step 2(c) above). Then when fine-tuning by minimizing the DKSA loss L_{DKSA} , we do not repeat a search over neural net architectures. Put another way, when searching over neural net architectures (whether using grid search or a more sophisticated approach to selecting architectures to try), we focus on minimizing a batched version of the loss (4.1). We remark that step 2 of TUNA does a simple least squares fit without accounting for any survival analysis problem structure.

5 Experiments

Our experiments are designed to help us understand the empirical performance of survival kernels in terms of prediction accuracy (Section 5.1) and computation time (Section 5.2). We consider survival kernels with and without the summary fine tuning, and also with and without our TUNA warm-start procedure. We also provide additional examples of cluster visualizations for different datasets that we use (Section 5.3). Our code is publicly available.²

Datasets and basic experimental setup We benchmark survival kernels on three datasets chosen to be sufficiently large. We provide basic characteristics of these datasets in Table 5.1. The first two datasets are on predicting time until death. We already mentioned the first dataset previously in Section 3.1: this is the dataset for hospitalized patients from the Study to Understand Prognoses, Preferences, Outcomes, and Risks of Treatment (SUPPORT) [Knaus et al., 1995]. The second dataset is for patients receiving heart transplants from the United Network for Organ Sharing (UNOS).³ The third dataset KKBOX is the one on customer churn mentioned in Section 1. These datasets have appeared in literature although not necessarily all at once in the same paper (e.g., Chapfuwa et al. 2018, Giunchiglia et al. 2018, Katzman et al. 2018, Lee et al. 2018, Kvamme et al. 2019, Chen 2020, Nagpal et al. 2021). Data preprocessing details are in Appendix C.1. For all datasets, we use a

²<https://github.com/georgehc/survival-kernels>

³We use the UNOS Standard Transplant and Analysis Research data from the Organ Procurement and Transplantation Network as of September 2019, requested at: <https://www.unos.org/data/>

Table 5.1: Dataset characteristics.

Dataset	Number of data points	Number of features	Censoring rate
SUPPORT	8,873	14 (19*)	31.97%
UNOS	62,644	49 (127*)	50.23%
KKBOX	2,814,735	15 (45*)	34.67%

* after preprocessing

random 70%/30% train/test split, and we hold out 20% of the training data to treat as a validation set, which is used to select hyperparameters/neural architectures. For measuring validation/test set accuracy, we use the time-dependent concordance index C^{td} [Antolini et al., 2005].

Baseline survival models As baselines, we use an elastic-net-regularized Cox model (denoted as ELASTIC-NET COX), XGBOOST [Chen and Guestrin, 2016], DEEPSURV [Katzman et al., 2018], DEEPHIT [Lee et al., 2018], and DKSA [Chen, 2020]. All neural net models use a multilayer perceptron as the base neural net. Hyperparameter grids and optimization details are in Appendix C.2. Note that our hyperparameter grid for ELASTIC-NET COX includes no regularization, which corresponds to the standard Cox model [Cox, 1972]. We remark that DEEPHIT has been previously reported to obtain state-of-the-art accuracy on the three datasets we have tested (cf., Lee et al. 2018, Kvamme et al. 2019; as these authors use different experimental setups, their accuracy numbers are not directly comparable to each other or to ours; however, our accuracy results yield trends similar to what was found by these authors in terms of how the baseline methods compare to each other).

Variants of survival kernels For survival kernels, as part of hyperparameter tuning, we try a number of variants. We always use the Gaussian kernel $K(u) = \exp(-u^2)$. We fix the truncation distance to be $\tau = \sqrt{\log 10} \approx 1.517$ (i.e., training points contributing to prediction must have kernel weight at least 0.1), and we further only consider at most 128 approximate nearest neighbors, which are found using the HNSW algorithm [Malkov and Yashunin, 2018]. For constructing ε -nets, we set $\varepsilon = \beta\tau$ and try $\beta \in \{1/2, 1/4\}$. For the embedding space, motivated by Claims 1 and 2, we constrain the embeddings to be on a hypersphere (in preliminary experiments, we found that leaving the embedding space unconstrained would occasionally lead to numerical issues during training and did not yield better validation accuracy scores than having a hypersphere constraint). We try standard neural net initialization [He et al., 2015] with an exhaustive hyperparameter grid/neural architecture sweep vs our strategy TUNA (denoted in tables as KERNET vs TUNA-KERNET).

When dividing data so that pre-training and training data are not the same, we split the full training data into 60%/20%/20% pre-training/training/validation sets (neural net training uses the pre-training and validation sets, with the latter used for early stopping). When we use this sample splitting, we add the suffix “(SPLIT)” to the method name in tables (e.g., “TUNA-KERNET (SPLIT)” refers to a survival kernel model trained with TUNA warm-start and with pre-training and training sets disjoint). Otherwise, if the pre-training and training sets are set to be the same, then we split the full training data into 80%/20% training/validation sets similar to all the baselines, using the validation set for hyperparameter tuning (including early stopping during neural net training); in this case, we add the suffix “(NO SPLIT)” to the method name in tables.

Finally, if summary fine-tuning (abbreviated SFT) is used, then we also add the suffix “SFT”. For instance, “(NO SPLIT, SFT)” means that pre-training and training data are set to be the same, and summary fine-tuning is used.

5.1 Results on Prediction Accuracy

We report test set C^{td} indices in Table 5.2, where for each final model trained, we construct a 95% bootstrap confidence interval (resample the test set 200 times with replacement, and for each bootstrap sample, compute the C^{td} index; the 2.5 and 97.5 percentiles of C^{td} indices are reported). The

Table 5.2: Test set C^{td} indices with 95% bootstrap confidence intervals.

Model	Dataset		
	SUPPORT	UNOS	KKBOX
ELASTIC-NET COX	0.6061 (0.5929, 0.6194)	0.5925 (0.5862, 0.5993)	0.8438 (0.8433, 0.8443)
XGBOOST	0.6318 (0.6189, 0.6439)	0.6025 (0.5963, 0.6096)	0.8714 (0.8709, 0.8719)
DEEPSURV	0.6145 (0.6014, 0.6294)	0.5910 (0.5847, 0.5975)	0.8688 (0.8683, 0.8693)
DEEPHIT	0.6276 (0.6142, 0.6398)	0.6141 (0.6082, 0.6208)	0.9147 (0.9143, 0.9151)
DKSA	0.6391 (0.6259, 0.6511)	out of memory	out of memory
KERNET (SPLIT)	0.5994 (0.5841, 0.6123)	0.5940 (0.5879, 0.6012)	0.8940 (0.8935, 0.8945)
KERNET (SPLIT, SFT)	0.5994 (0.5841, 0.6123)*	0.5991 (0.5931, 0.6062)	0.9020 (0.9016, 0.9025)
KERNET (NO SPLIT)	0.6245 (0.6102, 0.6373)	0.6045 (0.5988, 0.6114)	0.8946 (0.8942, 0.8951)
KERNET (NO SPLIT, SFT)	0.6249 (0.6106, 0.6383)	0.6110 (0.6048, 0.6179)	0.9025 (0.9021, 0.9030)
TUNA-KERNET (SPLIT)	0.6148 (0.6023, 0.6257)	0.5962 (0.5908, 0.6022)	0.8955 (0.8951, 0.8960)
TUNA-KERNET (SPLIT, SFT)	0.6148 (0.6023, 0.6257)*	0.6004 (0.5949, 0.6067)	0.9045 (0.9040, 0.9049)
TUNA-KERNET (NO SPLIT)	0.6500 (0.6365, 0.6635)	0.6067 (0.6009, 0.6139)	0.8964 (0.8960, 0.8968)
TUNA-KERNET (NO SPLIT, SFT)	0.6504 (0.6368, 0.6627)	0.6167 (0.6106, 0.6229)	0.9050 (0.9046, 0.9055)

* summary fine-tuning did not result in higher validation accuracy, so the final model is the same as without summary fine-tuning

main findings are as follows:

- (a) The TUNA-KERNET (NO SPLIT, SFT) model (i.e., a survival kernel trained with TUNA, pre-training data set to be the same as training data, and summary fine-tuning) achieves the highest test set C^{td} indices on SUPPORT and UNOS and the second highest on KKBOX (second to DEEPHIT).

Accounting for the 95% bootstrap confidence intervals though, we would not claim that TUNA-KERNET (NO SPLIT, SFT) is significantly better than DEEPHIT on the SUPPORT and UNOS datasets (as the two different model's confidence intervals overlap for these datasets). Rather, we find that TUNA-KERNET (NO SPLIT, SFT) is competitive with DEEPHIT on SUPPORT and UNOS.

- (b) By making the pre-training and training sets disjoint as required by our theory, the accuracy decreases (this trend generally holds for any variant of survival kernels where the only difference is whether pre-training and training sets are disjoint vs set to be the same).
- (c) Using summary fine-tuning improves accuracy compared to setting the summary functions based on equation (3.2) (this trend generally holds for any variant of survival kernels where the only difference is whether summary fine-tuning is used).
- (d) Using the TUNA warm-start strategy improves accuracy compared to standard neural net initialization (this trend generally holds for any variant of survival kernels where the only difference is whether TUNA is used).

As a minor remark, our KKBOX C^{td} index is significantly higher for DEEPHIT than previously reported in literature (e.g., Kvamme et al. 2019) because we also try setting the time discretization grid to be all unique observed times in the dataset, which turns out to significantly improve DEEPHIT's accuracy for the KKBOX dataset (when we discretize to 64 or 128 time steps, the C^{td} indices we get are on par with what Kvamme et al get).

5.2 Results on Computation Time

We next report wall clock computation times for training survival kernel variants and the baselines in Table 5.3. These training times are inclusive of hyperparameter tuning (and searching over neural net architectures). Per model, the hyperparameter that achieves the highest validation set C^{td}

Table 5.3: Total training time (minutes), which includes training using different hyperparameters. Note that TUNA-KERNEL (SPLIT) and TUNA-KERNEL (SPLIT, SFT) include the time needed to train an XGBOOST warm-start model only using *pre-training data*, whereas TUNA-KERNEL (NO SPLIT) and TUNA-KERNEL (NO SPLIT, SFT) include time to train XGBOOST on the *full training data*.

Model	Total training time (minutes)		
	SUPPORT	UNOS	KKBOX
ELASTIC-NET COX	0.852	3.617	63.510
XGBOOST	16.802	72.356	280.404
DEEPSURV	0.332	3.441	54.986
DEEPHIT	13.499	705.289	1653.543
DKSA	164.876	out of memory	out of memory
KERNEL (SPLIT)	58.130	1588.978	11153.036
KERNEL (SPLIT, SFT)	59.739	1629.146	11351.090
KERNEL (NO SPLIT)	197.856	2027.346	14288.763
KERNEL (NO SPLIT, SFT)	198.067	2114.303	14634.500
TUNA-KERNEL (SPLIT)	22.247	229.508	1671.926
TUNA-KERNEL (SPLIT, SFT)	22.721	293.200	2072.020
TUNA-KERNEL (NO SPLIT)	38.805	455.257	2164.797
TUNA-KERNEL (NO SPLIT, SFT)	41.482	530.305	2728.134

index is the one that is used in obtaining the test set C^{td} indices previously reported in Table 5.2. Our computation time results aim to show how much our TUNA warm-start strategy accelerates training and also to give a sense of the time needed to train the different models under consideration. All code was run under similar conditions on identical Ubuntu 20.04.2 LTS instances, each with an Intel Core i9-10900K CPU (3.70 GHz, 10 cores, 20 threads), 64GB RAM, and an Nvidia Quadro RTX 4000 (8GB GPU RAM). These compute instances accessed code and data that were centrally stored on a single network-attached storage (NAS) system.

Note that the timing results in Table 5.3 are fair in comparing between the different variants of survival kernels but *not* fair in comparing between a survival kernel variant and a baseline or between two different baselines. The reason for this is that, as aforementioned, we report training times that are inclusive of hyperparameter tuning. Different models can have drastically different hyperparameters and hyperparameter grid sizes. We can easily increase or decrease the number of hyperparameters we try for a model, which can significantly increase or decrease the overall training time of the model as a result. Because we use the exact same hyperparameter grid across survival kernel variants, comparing computation times across them is fair. However, comparing the training times of a survival kernel variant and that of a baseline or of two different baselines does not lead to a fair comparison due to the hyperparameter grids being different.⁴ That said, we present the overall training times across models anyways in Table 5.3. Due to how expensive model training is, the reported times are point estimates; we did not repeat training to obtain error bars.

The main takeaways from Table 5.3 are as follows:

- (a) For each TUNA-KERNEL variant, when we compare it to its corresponding variant that does not use TUNA, then we consistently find that using TUNA dramatically reduces computation time, with savings of 61.7% to 85.6% depending on the specific variant of survival kernels used and on the dataset.

⁴Note that reporting “per epoch” training times does not give a fair comparison either since, for instance, training the TUNA-KERNEL (NO SPLIT, SFT) model involves three different kinds of neural net minibatch gradient descent optimizations (the first is for approximating the XGBOOST tree ensemble kernel, the second is for fine-tuning the base neural net using the DKSA loss, and the third is for summary fine-tuning) whereas, for instance, the baselines DEEPSURV and DEEPHIT each only involve one kind of neural net minibatch gradient descent optimization. Reporting “per hyperparameter setting” training times is not straightforward since, for instance, the TUNA warm-start strategy could be viewed as further expanding the hyperparameter grid to include the hyperparameters of the base tree ensemble model being trained while at the same time never doing an exhaustive grid search.

Table 5.4: Time breakdown in training the TUNA-KERNEL (NO SPLIT, SFT) model on the KKBOX dataset for our experimental setup. The time breakdown for training TUNA-KERNEL (NO SPLIT) is the same without the final summary fine-tuning time. Note that our TUNA warm-start strategy corresponds to the combination of the first two tasks listed below. Also, note that every task listed below involves tuning different hyperparameters. For details on hyperparameters, see Appendix C.2.

Task	Hyperparameter settings	Time (minutes)
Train XGBOOST model	192*	280.404
Approximate XGBOOST kernel with base neural net	18 [†]	111.146
Fine-tune base neural net with DKSA loss ($\beta = 1/2$)	36 [‡]	841.466
Fine-tune base neural net with DKSA loss ($\beta = 1/4$)	36 [‡]	931.782
Summary fine-tuning	2 [§]	563.336
Total		2728.134

* corresponds to the full XGBOOST hyperparameter grid that we use

[†] base neural net hyperparameters (number of hidden layers, nodes per hidden layer), learning rate

[‡] survival loss hyperparameters (η and σ_{rank} from equation (2.7)), number of time steps to discretize to, learning rate

[§] learning rate

- (b) Using summary fine-tuning clearly increases training time compared to not using it, with an increase of 0.1% to 27.8% additional time depending on the specific variant of survival kernels used and on the dataset.
- (c) Even though survival kernels with TUNA are significantly faster to train than survival kernels without TUNA, survival kernels with TUNA are still relatively expensive to train when compared to baselines tested (aside from DKSA) at least for the hyperparameter grids that we have used.

We reiterate that are trivial ways to reduce or increase the computation time of either survival kernels or any of the baseline models by simply removing or adding hyperparameter settings to try. For example, we suspect that for the survival kernel variants and for DEEPHIT, we could remove some of the hyperparameter settings that we had tried while retaining a similar test set accuracy. Note that the hyperparameter grid we used for every survival kernel variant is a superset of the one we used for DEEPHIT, so we expected the computation times to be higher for survival kernel variants than DEEPHIT. It turns out though that all the survival kernel variants with TUNA have lower overall training times than DEEPHIT on the UNOS dataset for the hyperparameter grids we used.

As an illustrative example to provide more insight on how much time is spent on different parts of survival kernel training, we provide a timing breakdown for the TUNA-KERNEL (NO SPLIT, SFT) model trained on the KKBOX dataset in Table 5.4. Note that in this table, we have separated the computation times for using different ε values in ε -net construction (as a reminder, we set $\varepsilon = \beta\tau$ where the threshold distance is set to be $\tau = \sqrt{\log(10)} \approx 1.517$, and we sweep over $\beta \in \{1/2, 1/4\}$). For example, we see that if we only tried using $\beta = 1/4$ and did not try $\beta = 1/2$, then we would reduce the computation time by about 31% in this case.⁵ In Table 5.4, we also provide some detail on the hyperparameters that we sweep over for the different steps during training. As a reminder, for the TUNA warm-start strategy, the neural net architecture is treated as fixed after we approximate the XGBOOST kernel with the base neural net (in particular, trying different neural net architectures happens during the step labeled “Approximate XGBOOST kernel with base neural net” in Table 5.4).

⁵Note that which β value is “best” depends on the dataset. In our experiments specifically with the TUNA-KERNEL (NO SPLIT, SFT) model, the best hyperparameter setting chosen for the three datasets did not always use the same β (after hyperparameter tuning, the β values chosen for SUPPORT, UNOS, and KKBOX were 1/2, 1/4, and 1/4 respectively).

5.3 Cluster Visualizations

SUPPORT dataset For the final TUNA-KERNET (NO SPLIT) model trained on the SUPPORT dataset that we used to evaluate test set accuracy, we visualize the largest 5 clusters in Figure 1 using our visualization strategies from Section 3.1. In Section 3.1, we had already pointed out how one could interpret the different clusters, for instance finding the rightmost cluster in Figure 1(a) to be of mostly young, cancer-free patients. Meanwhile, the Kaplan-Meier curves in Figure 1(b) quickly give us a sense of which clusters appear to be better or worse off than others over time. For this dataset, the largest 5 clusters contain 68.6% of the training data. There are a total of 34 clusters, many of which are small. Of course, more clusters can be visualized at once; the plots get more cluttered but can still be interpreted.

If instead summary fine-tuning is used and we want to visualize the largest 5 clusters of the final TUNA-KERNET (NO SPLIT, SFT) model, then we would make the following changes. First, note that the final TUNA-KERNET (NO SPLIT, SFT) model is actually identical to the final TUNA-KERNET (NO SPLIT) model except that summary fine-tuning is used at the very end, which does not change the survival kernel cluster assignments. Thus, in terms of cluster visualization, the only main change would be that instead of computing the survival curve for each cluster using a Kaplan-Meier plot as in Figure 1(b), we would instead compute the survival curve using equation (3.4) with the learned summary functions. Next, based on these newly estimated survival curves, we can look at when they cross probability $1/2$ to obtain median survival time estimates. The survival curves from summary fine-tuning in this case are shown in Figure 2; note that these curves are in the exact same ordering and correspond to the same clusters as in Figure 1 (the same color means the same cluster although the median survival times change), but as we can readily see, they look different from the Kaplan-Meier curves from Figure 1(b). Since the survival curves in Figure 2 are no longer the standard Kaplan-Meier ones, we do not have confidence intervals for them. Note that Figure 1(a) remains the same except that the median survival times at the top should be updated to the new values computed (and that appear in the legend of Figure 2).

We have found that for some clusters, the survival curve from summary fine-tuning is relatively close to that of the Kaplan-Meier estimate without summary fine-tuning whereas for other clusters, there could be a more dramatic difference (such as the lime green cluster shifting dramatically downward in Figure 2 compared to Figure 1(b)). Some possible explanations could be that the lime green cluster is in a region of the embedding space that is close to other clusters and its survival function that gets learned could be thought of as being estimated from a larger region of the embedding space (rather than just getting averaged over points in points assigned to the lime green cluster), or that even among the points in the cluster, calculating the survival curve by weighting every point equally (as in the standard Kaplan-Meier survival curve estimate) does not make as much sense as using some sort of unequal/nonuniform weighting.

Although there are a total of 34 clusters, we have shown only 5 of them thus far. While we could visualize all 34 at once using the same visualization ideas as above, the heatmap and survival curve plots would get cluttered. One way to still visualize information from all 34 clusters is to use agglomerative clustering [Hastie et al., 2009, Section 14.3.12] to merge many clusters into larger “superclusters”. For the new superclusters, we can make visualizations similar to Figure 1. For instance, using standard complete-linkage agglomerative clustering, we partition the 34 clusters into 10 superclusters in Figure 3. The resulting feature heatmap in Figure 3(a) gives a more comprehensive view of how features vary across the entire training dataset. In this case, the leftmost and rightmost superclusters in the heatmap (corresponding to the superclusters with the shortest and longest median survival times) actually only contain a single data point each and could be considered outliers among the training data. The rest of the superclusters, however, exhibit some of the same trends we pointed out earlier when only looking at the largest 5 clusters, such as the superclusters having higher median survival times tending to be for younger, cancer-free patients who often have no comorbidities. Meanwhile, the survival curves in Figure 3(b) are more spread out compared to those in Figure 2; the lowest curve and the highest curve correspond to the two superclusters that we mentioned are outliers.

Note that when we merge clusters into a supercluster, there is a question of how to compute an

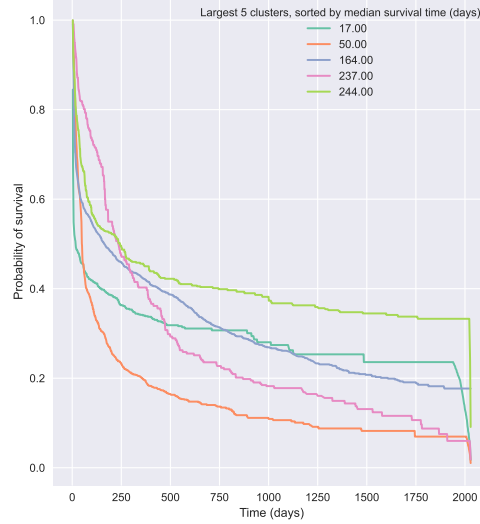


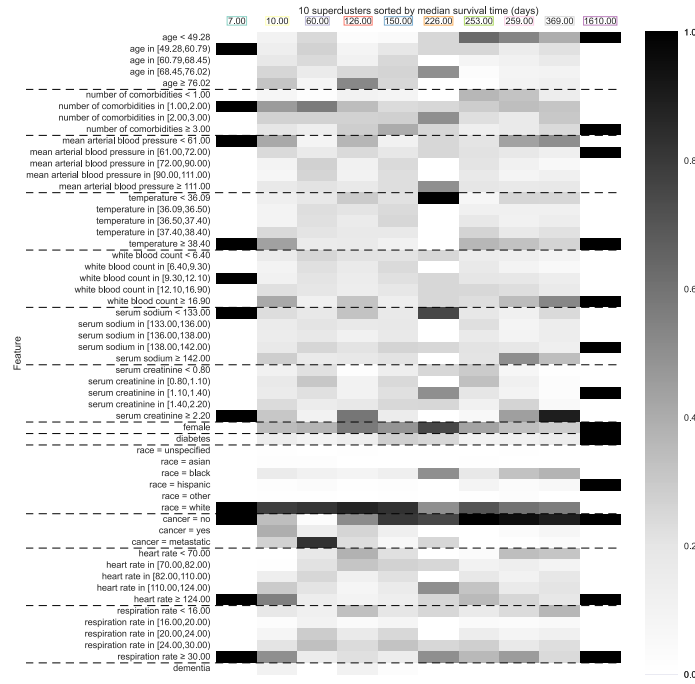
Figure 2: Survival curves for the largest 5 clusters found by the final TUNA-KERNET (NO SPLIT, SFT) model trained on the SUPPORT dataset; the x-axis measures the number of days since a patient entered the study.

aggregated survival curve for the supercluster. If we are not using summary fine-tuning, then the aggregation is straightforward: we continue to use the standard Kaplan-Meier survival curve estimator but instead now use data from all patients in a supercluster to compute that supercluster’s survival curve. However, when using summary fine-tuning, there is no standard way to aggregate information from different clusters’ learned summary functions. For simplicity, to come up with the survival curves in Figure 3(b), for the clusters that are being merged into a supercluster, we take these clusters’ survival curves and then just take a weighted average to obtain the survival curve for the supercluster (the weights are proportional to how many points are in each cluster belonging to the supercluster). The median survival times are then estimated by finding the times in which these survival curves cross probability $1/2$.

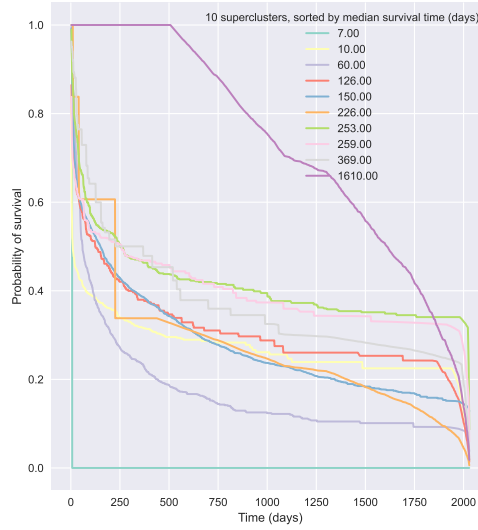
UNOS dataset Next, we plot the feature heatmap and survival curves for the final TUNA-KERNET (NO SPLIT, SFT) model trained on the UNOS dataset in Figure 4. Note that for the heatmap, to prevent it from getting cluttered, we are only showing 59 rows in the heatmap even though there are a total of 160 rows after feature discretization (as mentioned in Section 3.1, we sort features largest to smallest based on the maximum minus minimum intensity value per row although we keep the same variable together, e.g., the different discretized values for “age” remain in sequence together).

From the heatmap in Figure 4(a), we can readily tease apart some trends. For instance, of the 5 largest clusters, the two with the lowest median survival times tend to be for elderly patients with high creatinine values at transplant time (possibly indicative of kidney problems). However, between these two clusters, there are also noticeable differences such as the leftmost cluster tending to have lower donor ages and higher ischemic times compared to the second-to-leftmost cluster (note that there’s a known interaction between donor age and ischemic times in predicting survival times of heart transplant patients [Russo et al., 2007]).

From the survival curves in Figure 4(b), we see that these curves are much closer to each other compared to the survival curves we previously saw for the SUPPORT dataset in Figure 2. This is just by chance and if we look at more clusters concurrently, we can see a larger spread across survival curves. We can still tease out some trends among the five clusters shown, such as the magenta cluster (median survival time 10.19 years) tending to be the worst off initially, and the lime green cluster (median survival time 13.09 years) tending to have the highest probability of



(a)



(b)

Figure 3: Visualization of 10 superclusters for the final TUNA-KERNET (NO SPLIT, SFT) model trained on the SUPPORT dataset. These 10 superclusters summarize all 34 clusters found by the TUNA-KERNET (NO SPLIT, SFT) model by merging clusters using complete-linkage agglomerative clustering. Panel (a) shows a feature heatmap visualization. Panel (b) shows survival curves for the same superclusters as in panel (a); the x-axis measures the number of days since a patient entered the study. Note that the superclusters with the shortest and, separately, longest median survival times actually each only consist of a single data point and could be considered outliers.

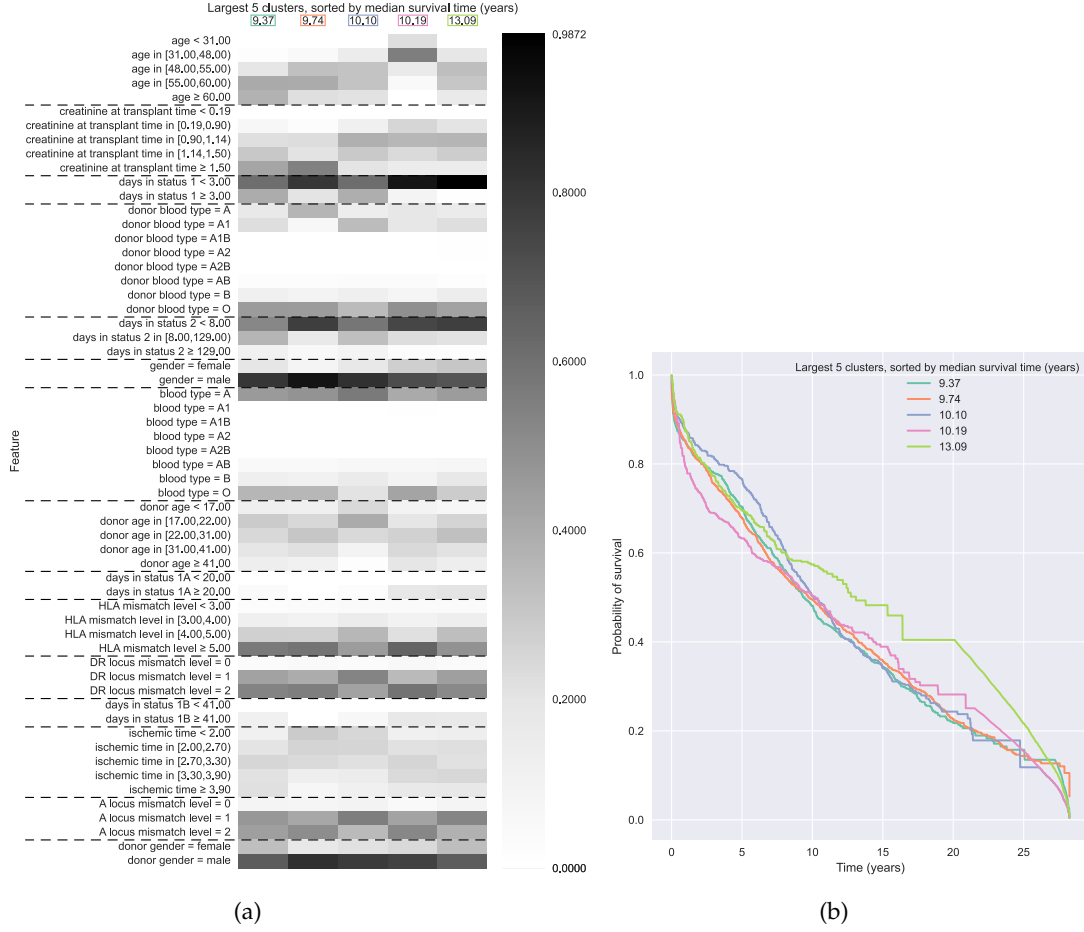
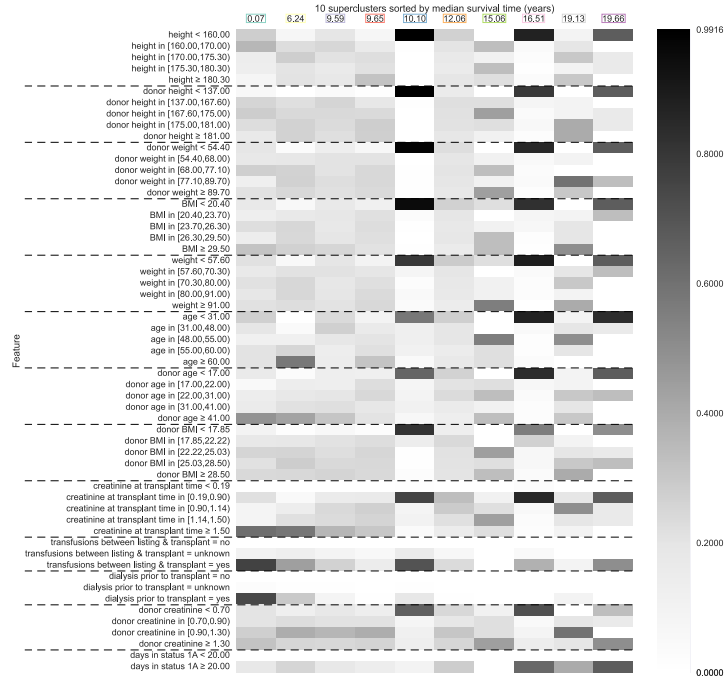


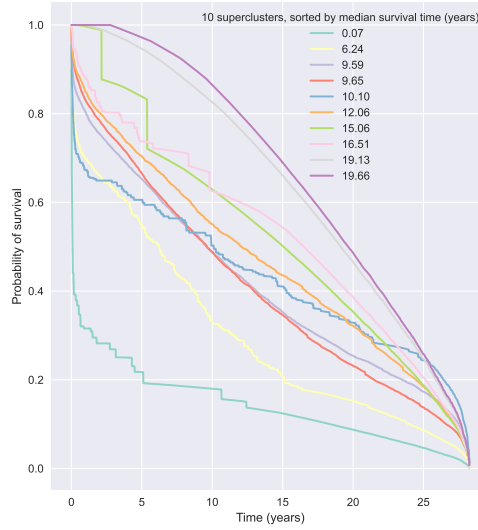
Figure 4: Visualization of the largest 5 clusters found by the final TUNA-KERNEL (NO SPLIT, SFT) model trained on the UNOS dataset. Panel (a) shows a heatmap visualization that readily provides information on how the clusters are different, highlighting feature values that are prominent for specific clusters; the dotted horizontal lines separate features that correspond to the same underlying variable. Panel (b) shows survival curves (estimated from learned summary functions) for the same clusters as in panel (a); the x-axis measures the number of years since a patient received a heart transplant.

survival between around 8 to 27 years after a patient receives a heart transplant.

For the UNOS dataset, automatic hyperparameter tuning led to a final TUNA-KERNEL (NO SPLIT, SFT) model with a total of 2,794 clusters that altogether contain 35,080 training points. The largest 5 clusters only account for 11.6% of the training data. Visualizing all clusters simultaneously in this case is not feasible. We again use complete-linkage agglomerative clustering, this time partitioning the 2,794 clusters into 10 superclusters, which we then visualize in Figure 5. The resulting feature heatmap in Figure 5(a) provides a more complete picture of how features vary across the training dataset compared to the earlier heatmap in Figure 4(a). For instance, the columns corresponding to superclusters with median survival times 10.10, 16.51, and 19.66 years are all for young patients who receive heart transplants from young donors but the superclusters have very different outcomes in terms of median survival time, which could be explained in part by differences in whether the patients received transfusions or had dialysis, how many days they were in status 1A, and also the donor’s creatinine level. Meanwhile, the survival curves in Figure 5(b) show much larger differences compared to the earlier plot in Figure 4(b) that was only of the 5 largest clusters.



(a)



(b)

Figure 5: Visualization of 10 superclusters for the final TUNA-KERNET (NO SPLIT, SFT) model trained on the UNOS dataset. These 10 superclusters summarize all 2,794 clusters found by the TUNA-KERNET (NO SPLIT, SFT) model by merging clusters using complete-linkage agglomerative clustering. Panel (a) shows a feature heatmap visualization (only 57 rows of features are shown out of 160). Panel (b) shows survival curves for the same superclusters as in panel (a); the x-axis measures the number of years since a patient received a heart transplant.

KKBOX dataset We can repeat the same visualization ideas for the KKBOX dataset. As the ideas are the same, we provide only a summary of findings. Using the same supercluster idea presented previously, we visualize 10 superclusters in Figure 6 for the final TUNA-KERNET (NO SPLIT, SFT) model trained on the KKBOX dataset. These superclusters summarize all 122,748 clusters found by the final TUNA-KERNET (NO SPLIT, SFT) model and contain 1,576,251 training data. We also provide a visualization of just the largest 10 clusters (containing 29.0% of training data) in Appendix C.3. Among superclusters corresponding to users who subscribed to the music streaming service for less than a month, there’s a higher fraction of users who are less than 19 years old and who have the lowest amount of payment. Among superclusters corresponding to the longest subscription times, there tends to be fewer previous churns for these users. Many of the survival curves show a steep drop in survival probability at around the 30-day mark, corresponding to a one-month promotion period.

Final remarks on visualization We end this section with a reminder that as pointed out at the end of Section 3.1, a survival kernel model represents the hazard of any feature vector as a weighted combination of clusters. We can determine which clusters have nonzero weight for any given feature vector and only visualize these particular clusters. This visualization could be helpful to provide as “forecast evidence” or to assist model debugging. As an example, we can find test data with predictions that are inconsistent with the ground truth (e.g., if the test data point is not censored and its observed survival time is far from the predicted median survival time, or if the test data point is censored and the predicted median survival time is much lower than the observed time). For these test data that the model has difficulty with, we could examine which clusters have high weight, what features are prominent for these clusters, and what the clusters’ survival curves are. After all, the predictions are made with these clusters’ summary functions.

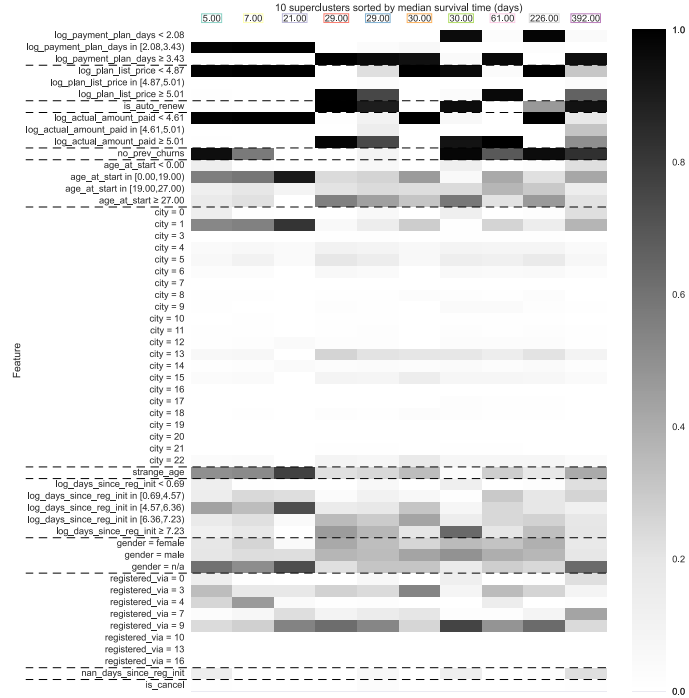
6 Discussion

In high-stakes applications such as healthcare, for survival models to be deployed in practice and producing time-to-event predictions using large (potentially live) streams of data in years to come, we believe that these models should be accurate, scalable, robust, interpretable, and theoretically sound. Our proposed survival kernel model achieves many of these properties although some only partially. Specifically, survival kernels are accurate, scalable, interpretable, and for a special case of the model has a theoretical guarantee. We discuss a number of limitations of our work next.

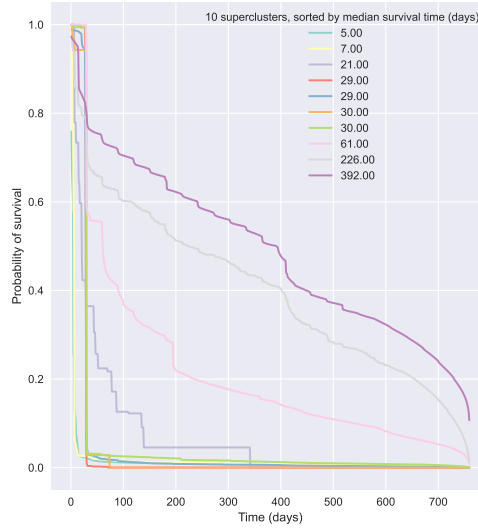
Theoretical analysis of the best-performing survival kernel variant As our experimental results show, the best-performing variant of survival kernels sets pre-training and training data to be the same and also uses summary fine-tuning. However, neither of these are covered by our theoretical analysis.

From a technical standpoint, sample splitting (i.e., having pre-training and training data be disjoint and moreover appear i.i.d.) is crucial in our theoretical analysis. Specifically, our proof of Theorem 1 routinely uses the fact that the training embeddings $\tilde{X}_1 = \hat{\phi}(X_1), \dots, \tilde{X}_n = \hat{\phi}(X_n)$ appear i.i.d. If the pre-training and training data are actually the same, then the learned base neural net $\hat{\phi}$ is a function of X_1, \dots, X_n (along with their observed times and event indicators), so the embeddings are no longer guaranteed to be independent. We do not currently know of a good way to resolve this technical issue. We expect that a proof technique that can address this issue would be quite broadly applicable beyond analyzing survival kernels.

As for summary fine-tuning, we suspect that if one treats the learned kernel function as fixed, then theoretical analysis should be possible although the theory would not say anything about the learned kernel function. Of course, the theory that we have presented does not say anything about the learned kernel function either since we treat the base neural net as a black box. Future work could consider the case when the base neural net is chosen from a specific family (e.g., a multilayer perceptron with ReLU activations), which could lead to a more nuanced theoretical guarantee (for instance, this is done by Zhong et al. [2021, 2022] for other deep survival analysis models).



(a)



(b)

Figure 6: Visualization of 10 superclusters for the final TUNA-KERNET (NO SPLIT, SFT) model trained on the KKBOX dataset. These 10 superclusters summarize all 122,748 clusters found by the TUNA-KERNET (NO SPLIT, SFT) model by merging clusters using complete-linkage agglomerative clustering. Panel (a) shows a feature heatmap visualization. Panel (b) shows survival curves for the same superclusters as in panel (a); the x-axis measures the number of days since an individual subscribed to the music streaming service.

Impact of clustering on accuracy and interpretability For survival kernels, one could easily replace the ε -net-based clustering with another clustering approach. We chose the ε -net-based clustering for theoretical convenience: ε -nets can easily be constructed in the greedy manner we had mentioned, and importantly, the resulting clusters come with theoretical properties. Consequently, ε -nets have been used to prove that “compressed” versions of nearest neighbor or kernel regression are consistent [Kpotufe and Verma, 2017, Kontorovich et al., 2017, Hanneke et al., 2021]. In contrast, had we used, for instance, k-means for clustering, then even though k-means at this point also has a lot of known theory (e.g., Rakhlin and Caponnetto 2006, Ben-David et al. 2007, Kumar and Kannan 2010, von Luxburg 2010, Fränti and Sieranoja 2019), it can be quite unstable in practice and the resulting clusters do not in general come with theoretical assurances. As such, we suspect that using k-means clustering with survival kernels would lead to a test-time predictor that is harder to theoretically analyze.

Putting aside theoretical convenience, by empirically evaluating how a wider range of clustering algorithms work with our survival kernel framework, we could potentially find that some of these lead to better prediction accuracy or better model interpretability compared to using ε -net clustering. We remark that especially as our experiments use embeddings that are on a hypersphere, then hyperspherical clustering methods could be used such as fitting a mixture of von Mises-Fisher distributions [Banerjee et al., 2005]. We leave an empirical study of using different clustering methods with survival kernels for future work.

Handling outliers Separately, we point out that even with our ε -net clustering approach, in practice many clusters could have very few data points assigned to them. Currently we are not removing such small clusters, although it might make sense to do so or to somehow flag these clusters as outliers and treat them a bit differently. Even pointing these clusters out to the user and visualizing them using the cluster visualization approach we had presented could be useful for model debugging purposes. In fact, this problem of addressing outliers would also arise if we replace the clustering method with, for instance, DBSCAN [Ester et al., 1996], which automatically flags various data points as outliers as part of the clustering procedure.

Calibration When a survival model’s predicted number of critical events within a time interval closely resembles the observed number, then the model is considered well-calibrated [Haider et al., 2020]. This could be thought of as a different notion of accuracy than the one we used in our experiments (namely time-dependent concordance index by Antolini et al. [2005]). We have not considered calibration in our paper, which in practice can be important. A straightforward way to incorporate calibration is to introduce an additional loss term such as the X-CAL loss by Goldstein et al. [2020]. We leave a thorough investigation of the calibration properties of survival kernels, with and without the addition of the X-CAL loss, to future work.

Robustness We have not discussed robustness of survival kernels thus far although in some sense they already have a limited amount of robustness built-in. Specifically, survival kernels do not assume a parametric form for the underlying survival distribution; the base neural net is used only to parameterize the kernel function, which is then plugged into the nonparametric conditional Kaplan-Meier estimator. By being nonparametric, survival kernels should be more robust to the data coming from different survival distributions. In fact, our theoretical guarantee works under a fairly broad range of settings. However, survival kernels are currently not designed to handle changes in the data distribution such as covariate shift, where test feature vectors come from a different distribution than that of training but how feature vectors relate to survival and censoring times remains unchanged at test time. Modifying survival kernels to better accommodate test data appearing different from training data is an important future research direction to explore.

Acknowledgments

This work was supported in part by NSF CAREER award #2047981, and by Health Resources and Services Administration contract 234-2005-370011C. The content is the responsibility of the author alone and does not necessarily reflect the views or policies of the National Science Foundation or the Department of Health and Human Services, nor does mention of trade names, commercial products, or organizations imply endorsement by the U.S. Government. Many thanks to Shu Hu for pointing out some typos in an earlier draft.

A Proofs

We present the proofs for Claim 1 (unit hypersphere's covering number) and Claim 2 (intrinsic dimension of the unit hypersphere) in Appendices A.1 and A.2, respectively. The proof of our main theoretical result Theorem 1 (survival kernel error bound) is in Appendix A.3.

A.1 Proof of Claim 1

Let $\{\zeta_1, \zeta_2, \dots, \zeta_N\}$ be an $\varepsilon/2$ -covering of the d -dimensional unit Euclidean ball (denoted by \mathcal{B}_d) such that N is the smallest value possible, i.e., $N = N(\varepsilon/2; \mathcal{B}_d)$; note that the unit Euclidean ball includes the interior of the ball whereas the unit hypersphere \mathbb{S}^{d-1} is only the outer shell. We recall a standard result of covering numbers (Corollary 4.2.13 of Vershynin [2018]) that

$$N = N(\varepsilon/2; \mathcal{B}_d) \leq \left(\frac{4}{\varepsilon} + 1\right)^d. \quad (\text{A.1})$$

Then since $\mathbb{S}^{d-1} \subseteq \mathcal{B}_d$, for every $v \in \mathbb{S}^{d-1}$, there exists some ζ_j such that $\|v - \zeta_j\| \leq \varepsilon/2$. This implies that there exists a subset Ξ of $\{\zeta_1, \zeta_2, \dots, \zeta_N\}$ such that every point in \mathbb{S}^{d-1} is at most a distance $\varepsilon/2$ from some point in Ξ . Let Ξ^* be such a subset that has the smallest size, and denote its unique elements as $\xi_1, \xi_2, \dots, \xi_{|\Xi^*|}$.

We next show how to construct an ε -cover for \mathbb{S}^{d-1} using $\xi_1, \xi_2, \dots, \xi_{|\Xi^*|}$. For each point ξ_i , note that there exists some $s_i \in \mathbb{S}^{d-1}$ such that $s_i \in B(\xi_i, \varepsilon/2)$ (if such an s_i does not exist, then ξ_i would not have been included in Ξ^* , i.e., Ξ^* does not actually have the smallest size possible while still covering \mathbb{S}^{d-1}). Next, we observe that for any $v \in B(\xi_i, \varepsilon/2)$, the triangle inequality implies that

$$\|s_i - v\|_2 = \|s_i - \xi_i + \xi_i - v\|_2 \leq \underbrace{\|s_i - \xi_i\|_2}_{\leq \varepsilon/2} + \underbrace{\|\xi_i - v\|_2}_{\leq \varepsilon/2},$$

which means that v is also in $B(s_i, \varepsilon)$. Hence,

$$B(s_i, \varepsilon) \supseteq B(\xi_i, \varepsilon/2).$$

This means that $\bigcup_{i=1}^{|\Xi^*|} B(s_i, \varepsilon) \supseteq \bigcup_{i=1}^{|\Xi^*|} B(\xi_i, \varepsilon/2)$, and since the latter covers \mathbb{S}^{d-1} , so does the former. We thus conclude that $\{s_1, s_2, \dots, s_{|\Xi^*|}\}$ forms a valid ε -cover of \mathbb{S}^{d-1} . The ε -cover of \mathbb{S}^{d-1} that has the smallest size possible is thus upper-bounded by $|\Xi^*| \leq N \leq \left(\frac{4}{\varepsilon} + 1\right)^d$ using inequality (A.1). ■

A.2 Proof of Claim 2

Let $f_{\tilde{\chi}}$ denote the pdf of $\mathbb{P}_{\tilde{\chi}}$, where we assume that $f_{\tilde{\chi}}(\tilde{z}) \geq c_{\min} > 0$ for all $\tilde{z} \in \mathbb{S}^{d-1}$, and $f_{\tilde{\chi}}(\tilde{z}) = 0$ for all $\tilde{z} \notin \mathbb{S}^{d-1}$. Thus, $\mathbb{S}^{d-1} = \hat{\phi}(\text{supp}(\mu))$. Let $\tilde{x} \in \hat{\phi}(\text{supp}(\mu))$ and $r \in (0, 1]$. Then

$$\mathbb{P}_{\tilde{\chi}}(B(\tilde{x}, r)) = \int_{B(\tilde{x}, r)} f_{\tilde{\chi}}(\tilde{z}) d\tilde{z} \geq \int_{B(\tilde{x}, r)} c_{\min} \cdot d\tilde{z} = c_{\min} \cdot \underbrace{\text{area}(\mathbb{S}^{d-1} \cap B(\tilde{x}, r))}_{\mathcal{C}(\tilde{x}, r):=}$$

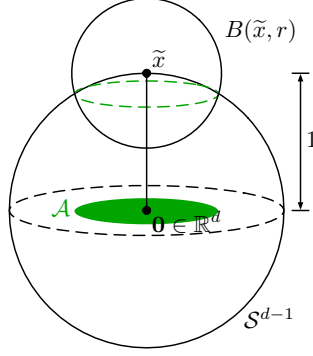


Figure 7: This diagram shows the geometric observation in the proof for the case of $d = 3$ dimensional Euclidean space. The intersection of the closed ball $B(\tilde{x}, r)$ with the unit hypersphere S^{d-1} is a hyperspherical cap, with the “top” of the cap at \tilde{x} , and the bottom is shown in the dotted green line. The surface area of this cap is lower-bounded by the area of the projection (the solid green circle \mathcal{A} ; in higher dimensions, this is a ball in \mathbb{R}^{d-1}).

Note that $\mathcal{C}(\tilde{x}, r)$ is a hyperspherical cap. We make a geometric observation:

$$\text{area}(\mathcal{C}(\tilde{x}, r)) \geq \underbrace{\text{volume}(\mathcal{C}(\tilde{x}, r) \text{ projected down to } \mathbb{R}^{d-1} \text{ in the direction of } \tilde{x})}_{\mathcal{A}:=}$$

where \mathcal{A} is depicted as a solid shaded green circle in Figure 7. The core of the remaining analysis is in determining the volume of \mathcal{A} . With a bit of trigonometry, we can derive that \mathcal{A} is precisely equal to a ball centered at the origin with radius $\frac{1}{2}r\sqrt{4-r^2}$; see Figure 8. Since $r \in (0, 1]$, the radius of \mathcal{A} satisfies the bound $\frac{1}{2}r\sqrt{4-r^2} \geq \frac{1}{2}r\sqrt{3}$. Thus, the volume of \mathcal{A} is lower-bounded by the volume of a ball in \mathbb{R}^{d-1} with radius $\frac{\sqrt{3}}{2}r$, which is $\frac{\pi^{(d-1)/2}}{\Gamma(\frac{d-1}{2}+1)} \left(\frac{\sqrt{3}}{2}r\right)^{d-1}$, where $\Gamma(z) := \int_0^\infty u^{z-1}e^{-u}du$. Putting everything together,

$$\begin{aligned} \mathbb{P}_{\tilde{x}}(B(\tilde{x}, r)) &\geq c_{\min} \cdot \text{area}(\mathcal{C}(\tilde{x}, r)) \\ &\geq c_{\min} \cdot \text{volume}(\mathcal{A}) \\ &\geq c_{\min} \cdot \frac{\pi^{(d-1)/2}}{\Gamma(\frac{d-1}{2}+1)} \left(\frac{\sqrt{3}}{2}r\right)^{d-1} \\ &= \left[c_{\min} \cdot \frac{\pi^{(d-1)/2}}{\Gamma(\frac{d-1}{2}+1)} \left(\frac{\sqrt{3}}{2}\right)^{d-1} \right] r^{d-1}, \end{aligned}$$

which establishes that the embedding space has intrinsic dimension $d - 1$.

A.3 Proof of Survival Kernet Error Bound (Theorem 1)

To keep the notation from getting cluttered, we use different notation than what is in the main paper. We drop tildes and instead write the embedding space as $\mathcal{U} \subset \mathbb{R}^d$. The training (and not pre-training) embeddings (treated as random variables) are written as $U_1, U_2, \dots, U_n \in \mathcal{U}$. Just as in the main paper, we use the notation $U_{1:n} = (U_1, \dots, U_n) \in \mathcal{U}^n$. The random test feature vector’s embedding is denoted by the random variable U . The marginal distribution of embeddings is denoted by \mathbb{P}_U . We denote the ε -net as Q (treated as a set), which is a subsample of the indices in $U_{1:n}$ (treated as a sequence). Just as in the main paper, we denote $\mathcal{I}_q \subseteq \{1, 2, \dots, n\}$ to be the indices of the training points assigned to $q \in Q$. We denote the true conditional survival, censoring, and observed time distributions as $\mathbb{P}_{T|U}$, $\mathbb{P}_{C|U}$, and $\mathbb{P}_{Y|U}$. We write their PDFs as $f_{T|U}(t|u)$, $f_{C|U}(t|u)$, and $f_{Y|U}(t|u)$; their CDFs as $F_{T|U}(t|u)$, $F_{C|U}(t|u)$, and $F_{Y|U}(t|u)$; and their tail functions

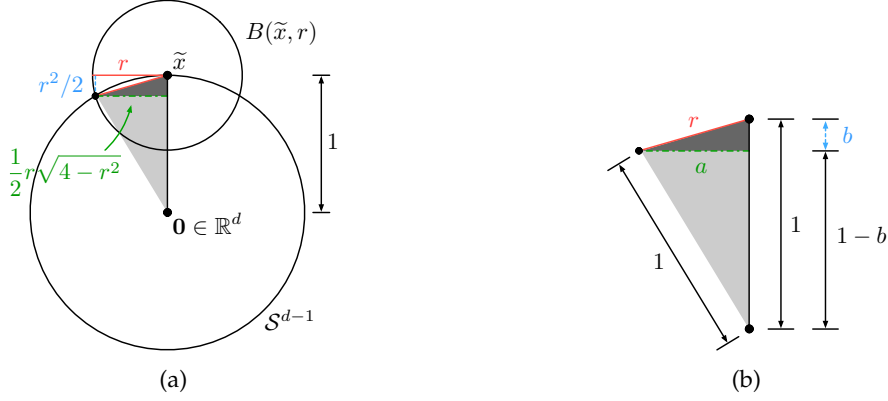


Figure 8: The radius of both the dotted and solid green circles in Figure 7 can be computed to be equal to $\frac{1}{2}r\sqrt{4-r^2}$. Specifically, in panel (a), we show a 2D view of Figure 7. To verify that the lengths specified in red, blue, and green in panel (a) are correct, we show the two shaded right triangles from panel (a) with more detail in panel (b), where we denote the green and blue lengths as a and b respectively: the Pythagorean theorem says that for the darker triangle, we have $a^2 + b^2 = r^2$, and for the lighter triangle, we have $a^2 + (1-b)^2 = 1^2$; by solving this system of two equations, we get $a = \frac{1}{2}r\sqrt{4-r^2}$ and $b = \frac{r^2}{2}$.

as $S_{T|U}(t|u) = 1 - F_{T|U}(t|u)$, $S_{C|U}(t|u) = 1 - F_{C|U}(t|u)$, and $S_{Y|U}(t|u) = 1 - F_{Y|U}(t|u)$. For a test embedding u , the conditional survival function we aim to predict is precisely $S_{T|U}(t|u)$ for $t \geq 0$.

For survival kernels, the only training points that can possibly contribute to the prediction for test embedding u (i.e., they have nonzero truncated kernel weight) are the ones with indices in

$$\mathcal{N}_Q(u) := \bigsqcup_{q \in Q \text{ s.t. } \|u-q\|_2 \leq \tau} \mathcal{I}_q,$$

where “ \bigsqcup ” denotes disjoint union. This union is disjoint since the survival kernel training procedure assigns each training point to exactly one exemplar in Q . The set $\mathcal{N}_Q(u)$ could be thought of as the “neighbors” of u .

For $Y_{\max}(u) := \max_{j \in \mathcal{N}_Q(u)} Y_j$, the survival kernel hazard function estimate (equation (3.3)) can be written as follows, using the new notation:

$$\hat{g}_Q(t|u) := \begin{cases} \frac{\sum_{j \in \mathcal{N}_Q(u)} K(\|u - q_j\|_2) D_j \mathbb{1}\{Y_j = t\}}{\sum_{j \in \mathcal{N}_Q(u)} K(\|u - q_j\|_2) \mathbb{1}\{Y_j \geq t\}} & \text{if } \mathcal{N}_Q(u) \neq \emptyset \text{ and } 0 \leq t \leq Y_{\max}(u), \\ 0 & \text{otherwise.} \end{cases} \quad (\text{A.2})$$

Let \mathcal{T} be the set of (unique) times until death within the training data, i.e., $\mathcal{T} := \{t' \in [0, \infty) : \exists j \in \{1, \dots, n\} \text{ s.t. } Y_j = t' \text{ and } D_j = 1\}$. Then the survival kernel conditional survival function estimator can be written as

$$\hat{S}_{T|U}(t|u) := \prod_{t' \in \mathcal{T}} (1 - \hat{g}_Q(t'|u))^{\mathbb{1}\{t' \leq t\}}.$$

In the main paper, this estimator is written as $\tilde{S}_{\tilde{Q}_\varepsilon}(t|\tilde{x})$. Using the new notation, we state the survival kernel error guarantee (Theorem 1) in the following proposition (note that this proposition is more detailed than Theorem 1 and includes constants that we have not tried to optimize).

Proposition 1. Suppose that assumptions $\mathbf{A}^{\text{technical}}$, $\mathbf{A}^{\text{intrinsic}}$, and $\mathbf{A}^{\text{survival}}$ hold, and that for training a survival kernel, we choose $\varepsilon = \beta\tau$ when constructing the ε -net Q using $U_{1:n}$, where $\beta \in (0, 1)$ and $\tau > 0$ are user-specified parameters. Let

$$\Psi = \min \left\{ N\left(\frac{(1-\beta)\tau}{2}; \tilde{\mathcal{X}}\right), \frac{1}{C_{d'}((1-\beta)\tau)^{d'}} \right\}.$$

Then for

$$n \geq \frac{2}{C_{d'}((1-\beta)\tau)^{d'}} \max \left\{ \frac{K(0)}{K(\tau)\theta}, \left(\frac{9K^2(0)}{144K^2(\tau)} (2+\sqrt{2}) \right)^{1/3} \right\},$$

we have

$$\begin{aligned} & \mathbb{E}_{Y_{1:n}, D_{1:n}, U_{1:n}, U} \left[\frac{\int_0^{t_{\text{horizon}}} (\widehat{S}_{T|U}(t|U) - S_{T|U}(t|U))^2 dt}{t_{\text{horizon}}} \right] \\ & \leq \frac{1}{n} \cdot \frac{346K^4(0) \log(n^3 \frac{144K^2(\tau)}{9K^2(0)})}{\theta^4 K^4(\tau)} \Psi \\ & \quad + (1+\beta)^{2\alpha} \tau^{2\alpha} \left[\frac{t_{\text{horizon}}^2}{\theta^2} \left(\lambda_T^2 + \frac{3\lambda_T f_T^* \lambda_C t_{\text{horizon}}}{4} + \frac{3(f_T^*)^2 \lambda_C^2 t_{\text{horizon}}^2}{20} \right) \right. \\ & \quad \left. + \frac{12K^2(0)}{K^2(\tau)\theta^4} (\lambda_T + \lambda_C)^2 t_{\text{horizon}}^2 \right], \end{aligned}$$

where

$$f_T^* := \max_{s \in [0, t_{\text{horizon}}], u \in \mathcal{U}} f_{T|U}(s|u).$$

In our theoretical analysis, we assume that the ε -net Q is a random variable that depends on $U_{1:n}$, where if we condition on $U_{1:n}$, then Q becomes deterministic. Note that as stated previously, we treat $U_{1:n}$ as a sequence (so ordering matters) whereas Q is treated as a set. Thus, an algorithm that constructs Q from $U_{1:n}$ need not produce the exact same Q if the ordering of $U_{1:n}$ is shuffled. If a randomized algorithm is used to construct Q , we assume that it has a random seed that can be fixed, making the algorithm behave deterministically given $U_{1:n}$.

A key lemma used in proving Proposition 1 is a lower bound on the number of neighbors of a test embedding u .

Lemma 1. (Number of training points contributing to prediction – lower bound) *Let $\beta \in (0, 1)$. Suppose that we train a survival kernel with threshold distance $\tau > 0$ and compression parameter $\varepsilon = \beta\tau$, i.e., training embeddings $U_{1:n}$ are used to construct a $\beta\tau$ -net Q . For a fixed choice of embedding $u \in \mathcal{U}$, let $U_{1:n}(u; \beta, \tau)$ denote the multiset of training data that land within the closed ball $B(u, (1-\beta)\tau)$. We have the inclusion relationship*

$$U_{1:n}(u; \beta, \tau) \subseteq \bigcup_{j \in \mathcal{N}_Q(u)} \underbrace{[U_j]}_{\text{multiset with single element}}. \quad (\text{A.3})$$

In particular, taking the cardinality of both sides, we have the inequality

$$|\Xi_u| := |U_{1:n}(u; \beta, \tau)| \leq |\mathcal{N}_Q(u)|. \quad (\text{A.4})$$

Proof. Let $u' \in U_{1:n}(u; \beta, \tau)$. Since $U_{1:n}(u; \beta, \tau) = U_{1:n} \cap B(u, (1-\beta)\tau)$, we have $\|u' - u\|_2 \leq (1-\beta)\tau$. Next, let $q \in Q$ be the exemplar point that u' is assigned to by step 4 of the survival kernel training procedure. By how step 4 works, we have $\|u' - q\|_2 \leq \beta\tau$. We can then bound the distance between q and u using the triangle inequality:

$$\|q - u\|_2 \leq \underbrace{\|q - u'\|_2}_{\leq \beta\tau} + \underbrace{\|u' - u\|_2}_{\leq (1-\beta)\tau} \leq \tau.$$

This means that u' is a training embedding that is assigned to an exemplar point q that satisfies $\|u - q\|_2 \leq \tau$, i.e., u' corresponds to a training point in $\mathcal{N}_Q(u)$. This establishes the subset relationship (A.3). \square

Throughout our theoretical analysis, we assume that Q is constructed to be an ε -net of $U_{1:n}$ with $\varepsilon = \beta\tau$ just as in Lemma 1, i.e., $\beta \in (0, 1)$ and $\tau > 0$ is the threshold distance for the truncated kernel.

We also regularly use the variable Ξ_u defined in equation (A.4). Importantly, since $U_{1:n}$ are sampled i.i.d. from \mathbb{P}_U , then Ξ_u is binomially distributed with parameters n and $\mathbb{P}_U(B(u, (1 - \beta)\tau))$. We can ensure that test embedding u has enough neighbors with high probability by asking that Ξ_u be sufficiently large (for which Lemma 1 guarantees that $|\mathcal{N}_Q(u)| \geq \Xi_u$). Specifically, define the good event

$$\mathcal{E}_\beta(u) := \left\{ \Xi_u > \frac{1}{2} n \mathbb{P}_U(B(u, (1 - \beta)\tau)) \right\}. \quad (\text{A.5})$$

We denote the complement of this event as $\mathcal{E}_\beta^c(u)$.

Lemma 2. (Sufficiently many number of neighbors) *Suppose that Assumption $\mathbf{A}^{\text{technical}}$ holds and $U_{1:n}$ are sampled i.i.d. from \mathbb{P}_U . Let $\beta \in (0, 1)$, $\tau > 0$, and $u \in \mathcal{U}$. Then the probability that good event $\mathcal{E}_\beta(u)$ does not happen is bounded above as*

$$\mathbb{P}(\mathcal{E}_\beta^c(u)) \leq \exp\left(-\frac{n \mathbb{P}_U(B(u, (1 - \beta)\tau))}{8}\right) \leq \frac{8}{n \mathbb{P}_U(B(u, (1 - \beta)\tau))}.$$

Proof. The claim readily follows from a multiplicative Chernoff bound of the binomial distribution and noting that $\exp(-z) \leq 1/z$ for all $z > 0$. \square

Another argument used in the proof is that if the j -th training point is a neighbor of embedding u —i.e., $j \in \mathcal{N}_Q(u)$ —then their embeddings cannot be too far apart, i.e., $\|U_j - u\|_2$ is not too large.

Lemma 3. (Neighbor embeddings are close) *Suppose that we train a survival kernet as in Lemma 1. Let $u \in \mathcal{U}$. If $j \in \mathcal{N}_Q(u)$, then*

$$\|U_j - u\|_2 \leq (1 + \beta)\tau.$$

Proof. Let $j \in \mathcal{N}_Q(u)$. This means that the exemplar that the j -th training point is assigned to, namely $q_j \in Q$, must be within distance τ of u . Thus,

$$\|U_j - u\|_2 \leq \underbrace{\|U_j - q_j\|_2}_{\leq \beta\tau} + \underbrace{\|q_j - u\|_2}_{\leq \tau} \leq (1 + \beta)\tau,$$

where we have used the fact that Q is a $\beta\tau$ -net, and $\mathcal{N}_Q(u)$ is defined to consider all exemplars within distance τ of u . \square

We remark that proving the special case when $\varepsilon = 0$ is easier precisely because Lemmas 1, 2, and 3 simplify — we no longer need ε -net arguments. Instead of Lemma 1, we directly consider training points within distance τ of fixed embedding u . Instead of Lemma 2, we directly consider points landing in the ball $B(u, \tau)$. In Lemma 3, there is no multiplicative approximation error $(1 + \beta)$ to worry about. In short, we get the same conclusions as these lemmas except plugging in $\beta = 0$.

We present proof of Proposition 1 next.

A.3.1 Proof of Proposition 1

We focus on proving “pointwise” bounds first, which in this case means that we fix both the test embedding $u \in \mathcal{U}$ and time $t \in [0, t_{\text{horizon}}]$. (At the end of the proof, we take an expectation over the test embedding and integrate over time.)

First off, we have the trivial bound $|\hat{S}_{\text{TU}}(t|u) - S_{\text{TU}}(t|u)| \leq 1$. Under some good events holding, we can obtain a nontrivial error bound. The first good event is the same as for regression

$\mathcal{E}_\beta(u) = \{\Xi_u > \frac{1}{2}n\mathbb{P}_U(B(u, (1-\beta)\tau))\}$. We introduce two additional good events. We define the second good event as

$$\mathcal{E}_{\text{horizon}}(u) := \left\{ \underbrace{\sum_{j \in \mathcal{N}_Q(u)} \mathbb{1}\{Y_j > t_{\text{horizon}}\}}_{d^+(u, t_{\text{horizon}}) := \frac{|\mathcal{N}_Q(u)|\theta}{2}} > \frac{|\mathcal{N}_Q(u)|\theta}{2} \right\}. \quad (\text{A.6})$$

Note that for any $s \geq 0$, $d^+(u, s)$ is the number of neighbors of u that have observed times Y_j 's exceeding s . When event $\mathcal{E}_{\text{horizon}}(u)$ holds, we have $t_{\text{horizon}} \leq Y_{\max}(u)$. We define the third and final good event later when we relate estimating the tail function $S_{T|U}(t|u)$ (that is for survival times T_j 's that we do not always get to observe in the training data), to estimating the tail function $S_{Y|U}(t|u)$ (that is of observed times Y_j 's that we see all of in the training data).

Importantly, when both $\mathcal{E}_\beta(u)$ and $\mathcal{E}_{\text{horizon}}(u)$ hold, then for every time $t \in [0, t_{\text{horizon}}]$, the hazard estimator $\hat{g}_Q(t|u)$ takes on a nontrivial value given by the first case of equation (A.2), rather than just being 0. As we show later (Lemma 8), good events $\mathcal{E}_\beta(u)$ and $\mathcal{E}_{\text{horizon}}(u)$ simultaneously hold with high probability as n grows large. These good events holding enable us to write the survival kernel conditional survival function estimate $\hat{S}_{T|U}(t|u)$ in a form that will be easier to work with.

Lemma 4. (Convenient form of the kernel survival estimator) *Suppose that Assumptions $\mathbf{A}^{\text{technical}}$ and $\mathbf{A}^{\text{survival}}$ hold, and that the kernel function K is of the form described in equation (3.1). Consider training a survival kernel with parameter $\varepsilon = \beta\tau$, where $\tau > 0$ is the truncated kernel threshold distance, and $\beta \in (0, 1)$ is a user-specified parameter. Fix $u \in \mathcal{U}$, and condition on events $\mathcal{E}_\beta(u)$ and $\mathcal{E}_{\text{horizon}}(u)$ occurring. Recall that $q_j \in Q$ is the exemplar that the j -th training point is assigned to during survival kernel training. With probability 1, for all $t \in [0, t_{\text{horizon}}]$,*

$$\hat{S}_{T|U}(t|u) = \prod_{i \in \mathcal{N}_Q(u)} \left(\frac{d_K^+(u, Y_i)}{K_i + d_K^+(u, Y_i)} \right)^{D_i \mathbb{1}\{Y_i \leq t\}}, \quad (\text{A.7})$$

where $K_i := K(\|u - q_i\|_2) \mathbb{1}\{\|u - q_i\|_2 \leq \tau\}$, and for any $s \geq 0$,

$$d_K^+(u, s) := \sum_{j \in \mathcal{N}_Q(u)} K_j \mathbb{1}\{Y_j > s\}.$$

Moreover, since $\mathcal{E}_{\text{horizon}}(u) = \{d^+(u, t_{\text{horizon}}) > \frac{|\mathcal{N}_Q(u)|\theta}{2}\}$ holds, we are guaranteed that $\hat{S}_{T|U}(t|u) > 0$ for $t \in [0, t_{\text{horizon}}]$.

Note that $d_K^+(u, s)$ is not the same as $d^+(u, s)$ defined earlier (in equation (A.6), which does not use kernel weights). These quantities are related via the bound $d_K^+(u, s) \geq K(\tau)d^+(u, s)$.

Proof. Fix $u \in \mathcal{U}$ and $t \in [0, t_{\text{horizon}}]$. First off, due to events $\mathcal{E}_\beta(u)$ and $\mathcal{E}_{\text{horizon}}(u)$ holding, $\hat{g}_Q(t|u)$ is nonzero. Next, Assumption $\mathbf{A}^{\text{survival}}$ implies that ties in Y_j 's happen with probability 0. Thus, with probability 1, there are no ties in Y_j 's, so

$$\hat{S}_{T|U}(t|u) = \prod_{t' \in \mathcal{T}} (1 - \hat{g}_Q(t'|u))^{\mathbb{1}\{t' \leq t\}} = \prod_{i=1}^n (1 - \hat{g}_Q(Y_i|u))^{D_i \mathbb{1}\{Y_i \leq t\}}. \quad (\text{A.8})$$

Next, since there are no ties in Y_j 's, the expression for $\hat{g}_Q(Y_i|u)$ simplifies as

$$\hat{g}_Q(Y_i|u) = \frac{K_i D_i}{\sum_{j \in \mathcal{N}_Q(u)} K_j \mathbb{1}\{Y_j \geq Y_i\}} = \frac{K_i D_i}{K_i + \sum_{j \in \mathcal{N}_Q(u)} K_j \mathbb{1}\{Y_j > Y_i\}} = \frac{K_i D_i}{K_i + d_K^+(u, Y_i)}.$$

Hence,

$$\begin{aligned}
(1 - \hat{g}_Q(Y_i|u))^{D_i \mathbb{1}\{Y_i \leq t\}} &= \left(1 - \frac{K_i D_i}{K_i + d_K^+(u, Y_i)}\right)^{D_i \mathbb{1}\{Y_i \leq t\}} \\
&= \left(1 - \frac{K_i}{K_i + d_K^+(u, Y_i)}\right)^{D_i \mathbb{1}\{Y_i \leq t\}} \\
&= \left(\frac{d_K^+(u, Y_i)}{K_i + d_K^+(u, Y_i)}\right)^{D_i \mathbb{1}\{Y_i \leq t\}}.
\end{aligned}$$

Combining this with equation (A.8), we get

$$\hat{S}_{T|U}(t|u) = \prod_{i=1}^n \left(\frac{d_K^+(u, Y_i)}{K_i + d_K^+(u, Y_i)}\right)^{D_i \mathbb{1}\{Y_i \leq t\}}.$$

In the RHS, if $K_i = 0$, then the i -th factor is 1 and thus does not affect the overall product. Note that $K_i > 0$ precisely for $i \in \mathcal{N}_Q(u)$. Thus, it suffices to only take the product over $i \in \mathcal{N}_Q(u)$, which establishes equality (A.7). \square

When we can write $\hat{S}_{T|U}(t|u)$ using the expression (A.7), then using the Taylor expansion $\log(1+z) = \sum_{\ell=1}^{\infty} \frac{1}{\ell} \left(\frac{z}{z+1}\right)^\ell$ that is valid for any $z > 0$, we get

$$\begin{aligned}
\log \hat{S}_{T|U}(t|u) &= \sum_{i \in \mathcal{N}_Q(u)} D_i \mathbb{1}\{Y_i \leq t\} \log \left(\frac{d_K^+(u, Y_i)}{K_i + d_K^+(u, Y_i)}\right) \\
&= - \sum_{i \in \mathcal{N}_Q(u)} D_i \mathbb{1}\{Y_i \leq t\} \log \left(1 + \frac{K_i}{d_K^+(u, Y_i)}\right) \\
&= - \sum_{i \in \mathcal{N}_Q(u)} \frac{D_i \mathbb{1}\{Y_i \leq t\} K_i}{K_i + d_K^+(u, Y_i)} - \sum_{i \in \mathcal{N}_Q(u)} D_i \mathbb{1}\{Y_i \leq t\} \sum_{\ell=2}^{\infty} \frac{1}{\ell [1 + (d_K^+(u, Y_i)/K_i)]^\ell} \\
&= W_1(t|u) + W_2(t|u) + W_3(t|u),
\end{aligned}$$

where

$$\begin{aligned}
W_1(t|u) &:= \sum_{i \in \mathcal{N}_Q(u)} \left(\frac{K_i}{\sum_{j \in \mathcal{N}_Q(u)} K_j}\right) \left(-\frac{D_i \mathbb{1}\{Y_i \leq t\}}{S_{Y|U}(Y_i|u)}\right), \\
W_2(t|u) &:= - \sum_{i \in \mathcal{N}_Q(u)} \frac{K_i D_i \mathbb{1}\{Y_i \leq t\} \left[\frac{\sum_{\ell \in \mathcal{N}_Q(u)} K_\ell}{K_i + d_K^+(u, Y_i)} - \frac{1}{S_{Y|U}(Y_i|u)}\right]}{\sum_{j \in \mathcal{N}_Q(u)} K_j}, \\
W_3(t|u) &:= - \sum_{i \in \mathcal{N}_Q(u)} D_i \mathbb{1}\{Y_i \leq t\} \sum_{\ell=2}^{\infty} \frac{1}{\ell [1 + (d_K^+(u, Y_i)/K_i)]^\ell}.
\end{aligned}$$

The high-level idea is to show that $W_1(t|u) \rightarrow \log S_{T|U}(t|u)$, $W_2(t|u) \rightarrow 0$, and $W_3(t|u) \rightarrow 0$.

As previously pointed out by Chen [2019], the term $W_1(t|u)$ could be thought of as a kernel regression estimate that averages over hypothetical labels of the form $-\frac{D_i \mathbb{1}\{Y_i \leq t\}}{S_{Y|U}(Y_i|u)}$ across i , which knows the true tail function $S_{Y|U}$ (of observed times and not survival times). Of course this true tail function is not actually known.

The term $W_2(t|u)$ focuses on how accurately we can estimate the tail function $S_{Y|U}$. Note that estimating the CDF of the observed times Y_j 's is simpler than estimating the CDF of the survival times T_j 's since observed times are known for all training data whereas survival times are only known for uncensored training data (although the censored data provide information on survival times as well since censored times are lower bounds on survival times).

Lastly, the term $W_3(t|u)$ vanishes when the number of neighbors of u with observed times Y_j 's exceeding t_{horizon} is sufficiently large.

For now, we assume that good events $\mathcal{E}_\beta(u)$ and $\mathcal{E}_{\text{horizon}}(u)$ hold, along with Assumptions $\mathbf{A}^{\text{technical}}$ and $\mathbf{A}^{\text{survival}}$ before introducing the third and final good event that comes into play in showing that $W_2(t|u) \rightarrow 0$. Lemma 4 guarantees that under these conditions, $\widehat{S}_{\mathbf{T}|\mathbf{U}}(t|u) \neq 0$ (recall that $t \in [0, t_{\text{horizon}}]$). Moreover, using Assumption $\mathbf{A}^{\text{survival}}(\text{a})$ and since $S_{\mathbf{T}|\mathbf{U}}(\cdot|u)$ monotonically decreases, we have $S_{\mathbf{T}|\mathbf{U}}(t|u) \geq S_{\mathbf{T}|\mathbf{U}}(t_{\text{horizon}}|u) \geq \theta > 0$. Using the fact that for any $a, b \in (0, 1]$, we have $|a - b| \leq |\log a - \log b|$, we get

$$\begin{aligned} & \mathbb{E}_{Y_{1:n}, D_{1:n} | U_{1:n}} [(\widehat{S}_{\mathbf{T}|\mathbf{U}}(t|u) - S_{\mathbf{T}|\mathbf{U}}(t|u))^2] \\ & \leq \mathbb{E}_{Y_{1:n}, D_{1:n} | U_{1:n}} [(\log \widehat{S}_{\mathbf{T}|\mathbf{U}}(t|u) - \log S_{\mathbf{T}|\mathbf{U}}(t|u))^2] \\ & = \mathbb{E}_{Y_{1:n}, D_{1:n} | U_{1:n}} [W_1(t|u) - \log S_{\mathbf{T}|\mathbf{U}}(t|u) + W_2(t|u) + W_3(t|u)]^2. \end{aligned}$$

Next, recall that for any $a_1, a_2, \dots, a_\ell \in \mathbb{R}$, a consequence of Jensen's inequality is that $(\sum_{i=1}^\ell a_i)^2 \leq \ell \sum_{i=1}^\ell a_i^2$. By applying this inequality to the RHS above, we get

$$\begin{aligned} & \mathbb{E}_{Y_{1:n}, D_{1:n} | U_{1:n}} [(\widehat{S}_{\mathbf{T}|\mathbf{U}}(t|u) - S_{\mathbf{T}|\mathbf{U}}(t|u))^2] \\ & \leq \mathbb{E}_{Y_{1:n}, D_{1:n} | U_{1:n}} [W_1(t|u) - \log S_{\mathbf{T}|\mathbf{U}}(t|u) + W_2(t|u) + W_3(t|u)]^2 \\ & \leq 3 \underbrace{\mathbb{E}_{Y_{1:n}, D_{1:n} | U_{1:n}} [(W_1(t|u) - \log S_{\mathbf{T}|\mathbf{U}}(t|u))^2]}_{\text{term I}} + 3 \underbrace{\mathbb{E}_{Y_{1:n}, D_{1:n} | U_{1:n}} [(W_2(t|u))^2]}_{\text{term II}} \\ & \quad + 3 \underbrace{\mathbb{E}_{Y_{1:n}, D_{1:n} | U_{1:n}} [(W_3(t|u))^2]}_{\text{term III}}. \end{aligned} \tag{A.9}$$

We proceed to bound each of the RHS expectations.

Bounding term I As stated previously, $W_1(t|u)$ is like a kernel regression estimate. By a standard bias-variance decomposition,

$$\begin{aligned} & \mathbb{E}_{Y_{1:n}, D_{1:n} | U_{1:n}} [(W_1(t|u) - \log S_{\mathbf{T}|\mathbf{U}}(t|u))^2] \\ & = \underbrace{\mathbb{E}_{Y_{1:n}, D_{1:n} | U_{1:n}} [(W_1(t|u) - \mathbb{E}_{Y_{1:n}, D_{1:n} | U_{1:n}} [W_1(t|u)])^2]}_{\text{variance}} \\ & \quad + \underbrace{(\mathbb{E}_{Y_{1:n}, D_{1:n} | U_{1:n}} [W_1(t|u)] - \log S_{\mathbf{T}|\mathbf{U}}(t|u))^2}_{\text{bias}}. \end{aligned}$$

We bound the right-hand side.

Lemma 5. (Bound on term I) *Under the same setting as Lemma 4, except where we only condition on good event $\mathcal{E}_\beta(u)$ (i.e., good event $\mathcal{E}_{\text{horizon}}(u)$ can optionally hold),*

$$\mathbb{E}_{Y_{1:n}, D_{1:n} | U_{1:n}} [(W_1(t|u) - \log S_{\mathbf{T}|\mathbf{U}}(t|u))^2] \leq \underbrace{\frac{K(0)}{4\theta^2 K(\tau) \Xi_u}}_{\text{variance term bound}} + \underbrace{\frac{(1+\beta)^{2\alpha} \tau^{2\alpha}}{\theta^2} \left(\lambda_{\mathbf{T}} t + \frac{f_{\mathbf{T}}^* \lambda_{\mathbf{C}} t^2}{2} \right)^2}_{\text{bias term bound}}.$$

Proof. (Variance term bound) The variance term equals

$$\begin{aligned} & \mathbb{E}_{Y_{1:n}, D_{1:n} | U_{1:n}} [(W_1(t|u) - \mathbb{E}_{Y_{1:n}, D_{1:n} | U_{1:n}} [W_1(t|u)])^2] \\ & = \sum_{i \in \mathcal{N}_Q(u)} \left(\frac{K_i}{\sum_{j \in \mathcal{N}_Q(u)} K_j} \right)^2 \underbrace{\mathbb{E}_{Y_i, D_i | U_i} \left[\left(-\frac{D_i \mathbb{1}\{Y_i \leq t\}}{S_{\mathbf{Y}|\mathbf{U}}(Y_i|u)} - \mathbb{E}_{Y_{1:n}, D_{1:n} | U_{1:n}} \left[-\frac{D_i \mathbb{1}\{Y_i \leq t\}}{S_{\mathbf{Y}|\mathbf{U}}(Y_i|u)} \right] \right)^2 \right]}_{\text{variance of } -\frac{D_i \mathbb{1}\{Y_i \leq t\}}{S_{\mathbf{Y}|\mathbf{U}}(Y_i|u)} \text{ conditioned on } U_i}. \end{aligned}$$

Note that this sum is not vacuous since under event $\mathcal{E}_\beta(u)$ and using Lemma 1, $|\mathcal{N}_Q(u)| > 0$. Next, note that $-\frac{D_i \mathbb{1}\{Y_i \leq t\}}{S_{Y|U}(Y_i|u)}$ is a bounded random variable. It is nonzero only when $Y_i \leq t$, for which the denominator could be as large as 1 and as small as $S_{Y|U}(Y_i|u) \geq S_{Y|U}(t|u) \geq S_{Y|U}(t_{\text{horizon}}|u) \geq \theta$ using the fact that $S_{Y|U}(\cdot|u)$ monotonically decreases and using Assumption **A**^{survival}(a). Consequently, $-\frac{D_i \mathbb{1}\{Y_i \leq t\}}{S_{Y|U}(Y_i|u)} \in [-\frac{1}{\theta}, 0]$, which by a standard result on bounded random variables implies that the variance of this random variable is at most $\frac{1}{4\theta^2}$. Hence,

$$\mathbb{E}_{Y_{1:n}, D_{1:n} | U_{1:n}} [(W_1(t|u) - \mathbb{E}_{Y_{1:n}, D_{1:n} | U_{1:n}} [W_1(t|u)])^2] \leq \sum_{i \in \mathcal{N}_Q(u)} \left(\frac{K_i}{\sum_{j \in \mathcal{N}_Q(u)} K_j} \right)^2 \frac{1}{4\theta^2}.$$

Then by Hölder's inequality and Lemma 1,

$$\begin{aligned} \sum_{i \in \mathcal{N}_Q(u)} \left(\frac{K_i}{\sum_{j \in \mathcal{N}_Q(u)} K_j} \right)^2 \frac{1}{4\theta^2} &\leq \frac{1}{4\theta^2} \left[\max_{i \in \mathcal{N}_Q(u)} \frac{K_i}{\sum_{j \in \mathcal{N}_Q(u)} K_j} \right] \underbrace{\sum_{i \in \mathcal{N}_Q(u)} \frac{K_i}{\sum_{j \in \mathcal{N}_Q(u)} K_j}}_{=1} \\ &\leq \frac{1}{4\theta^2} \max_{i \in \mathcal{N}_Q(u)} \frac{K(0)}{K(\tau) |\mathcal{N}_Q(u)|} \\ &= \frac{K(0)}{4\theta^2 K(\tau) |\mathcal{N}_Q(u)|} \leq \frac{K(0)}{4\theta^2 K(\tau) \Xi_u}, \end{aligned}$$

which establishes the variance term bound.

(Bias term bound) First, recall from equation (2.1) that the hazard function is $-\frac{\partial}{\partial t} \log S_{T|U}(t|u) = \frac{f_{T|U}(s|u)}{S_{T|U}(s|u)}$. Then by the fundamental theorem of calculus,

$$\begin{aligned} \log S_{T|U}(t|u) &= - \int_0^t \frac{f_{T|U}(s|u)}{S_{T|U}(s|u)} ds \\ &= - \int_0^t \frac{1}{S_{T|U}(s|u) S_{C|U}(s|u)} S_{C|U}(s|u) f_{T|U}(s|u) ds \\ &= - \int_0^t \frac{1}{S_{Y|U}(s|u)} S_{C|U}(s|u) f_{T|U}(s|u) ds, \end{aligned} \tag{A.10}$$

where the last step uses the result that for two independent random variables A_1 and A_2 , the random variable $\min\{A_1, A_2\}$ has a tail function (1 minus CDF) that is the product of the tail functions of A_1 and A_2 ; in our setting, $Y_j = \min\{T_j, C_j\}$ where T_j and C_j are conditionally independent given U_j , so $S_{Y|U}(s|u) = S_{T|U}(s|u) S_{C|U}(s|u)$.

Next, we have

$$\mathbb{E}_{Y_{1:n}, D_{1:n} | U_{1:n}} [W_1(t|u)] = \sum_{i \in \mathcal{N}_Q(u)} \left(\frac{K_i}{\sum_{j \in \mathcal{N}_Q(u)} K_j} \right) \mathbb{E}_{Y_i, D_i | U_i} \left[- \frac{D_i \mathbb{1}\{Y_i \leq t\}}{S_{Y|U}(Y_i|u)} \right], \tag{A.11}$$

where

$$\begin{aligned} \mathbb{E}_{Y_i, D_i | U_i} \left[- \frac{D_i \mathbb{1}\{Y_i \leq t\}}{S_{Y|U}(Y_i|u)} \right] &= - \int_0^t \left[\int_s^\infty \frac{1}{S_{Y|U}(s|u)} d\mathbb{P}_{C|U}(c|U_i) \right] d\mathbb{P}_{T|U}(s|U_i) \\ &= - \int_0^t \frac{1}{S_{Y|U}(s|u)} S_{C|U}(s|U_i) f_{T|U}(s|U_i) ds. \end{aligned}$$

We take the difference of equations (A.11) and (A.10) to get

$$\begin{aligned} &\mathbb{E}_{Y_{1:n}, D_{1:n} | U_{1:n}} [W_1(t|u)] - \log S_{T|U}(t|u) \\ &= \sum_{i \in \mathcal{N}_Q(u)} \left(\frac{K_i}{\sum_{j \in \mathcal{N}_Q(u)} K_j} \right) \int_0^t \frac{S_{C|U}(s|u) f_{T|U}(s|u) - S_{C|U}(s|U_i) f_{T|U}(s|U_i)}{S_{Y|U}(s|u)} ds. \end{aligned}$$

Note that Assumption $\mathbf{A}^{\text{survival}}(\mathbf{b})$ implies that $S_{C|U}(s|\cdot)f_{T|U}(s|\cdot)$ is Hölder continuous with parameters $(\lambda_T + f_T^* \lambda_C s)$ and α , where $f_T^* = \max_{s \in [0, t_{\text{horizon}}], u \in \mathcal{U}} f_{T|U}(s|u)$; this maximum exists by compactness of $[0, t_{\text{horizon}}]$ and \mathcal{U} . Then by Hölder's inequality, Assumption $\mathbf{A}^{\text{survival}}$, and Lemma 3,

$$\begin{aligned}
& |\mathbb{E}_{Y_{1:n}, D_{1:n} | U_{1:n}} [W_1(t|u)] - \log S_{T|U}(t|u)| \\
& \leq \max_{i \in \mathcal{N}_Q(u)} \left| \int_0^t \frac{1}{\underbrace{S_{Y|U}(s|u)}_{\geq S_{Y|U}(t_{\text{horizon}}|u) \geq \theta}} [S_{C|U}(s|u)f_{T|U}(s|u) - S_{C|U}(s|U_i)f_{T|U}(s|U_i)] ds \right| \\
& \leq \frac{1}{\theta} \max_{i \in \mathcal{N}_Q(u)} \int_0^t |S_{C|U}(s|u)f_{T|U}(s|u) - S_{C|U}(s|U_i)f_{T|U}(s|U_i)| ds \\
& \leq \frac{1}{\theta} \max_{i \in \mathcal{N}_Q(u)} \int_0^t (\lambda_T + f_T^* \lambda_C s) \|u - U_i\|_2^\alpha ds \\
& \leq \frac{1}{\theta} \max_{i \in \mathcal{N}_Q(u)} \int_0^t (\lambda_T + f_T^* \lambda_C s) ((1 + \beta)\tau)^\alpha ds \\
& = \frac{(1 + \beta)^\alpha \tau^\alpha}{\theta} \int_0^t (\lambda_T + f_T^* \lambda_C s) ds \\
& = \frac{(1 + \beta)^\alpha \tau^\alpha}{\theta} \left(\lambda_T t + \frac{f_T^* \lambda_C t^2}{2} \right).
\end{aligned}$$

Squaring both sides yields the bias term bound. \square

Bounding term II The term $W_2(t|u)$ is related to a CDF estimation problem. Specifically, define the following estimate of $S_{Y|U}(s|u)$:

$$\hat{S}_{Y|U}(s|u) := \frac{d_K^+(u, s)}{\sum_{\ell \in \mathcal{N}_Q(u)} K_\ell} = \sum_{j \in \mathcal{N}_Q(u)} \frac{K_j}{\sum_{\ell \in \mathcal{N}_Q(u)} K_\ell} \mathbb{1}\{Y_j > s\}.$$

Then $1 - \hat{S}_{Y|U}(s|u)$ is a weighted empirical distribution that estimates $1 - S_{Y|U}(s|u)$. We introduce the third and final good event

$$\mathcal{E}_{\text{CDF}}(u) := \underbrace{\left\{ \sup_{s \geq 0} |\hat{S}_{Y|U}(s|u) - \mathbb{E}_{Y_{1:n} | U_{1:n}} [\hat{S}_{Y|U}(s|u)]| \leq \varepsilon_{\text{CDF}} \right\}}_{\spadesuit :=}, \quad (\text{A.12})$$

where

$$\varepsilon_{\text{CDF}} = \sqrt{\frac{9K^2(0)}{4K^2(\tau)|\mathcal{N}_Q(u)|} \log \left(|\mathcal{N}_Q(u)|^3 \frac{144K^2(\tau)}{9K^2(0)} \right)}.$$

We show later (Lemma 8) that this event holds with high probability for large n . Note that event $\mathcal{E}_{\text{CDF}}(u)$ is like a variance term, saying that $\hat{S}_{Y|U}(s|u)$ is close to its expectation. We also define a bias term

$$\heartsuit := \sup_{s \in [0, t]} |\hat{S}_{Y|U}(s|u) - \mathbb{E}_{Y_{1:n} | U_{1:n}} [\hat{S}_{Y|U}(s|u)]|. \quad (\text{A.13})$$

Then the following lemma relates $W_2(t|u)$ to the variance and bias terms.

Lemma 6. (Bound on term II) *Under the same setting as Lemma 4, except where we now condition on all three good events $\mathcal{E}_\beta(u)$, $\mathcal{E}_{\text{horizon}}(u)$, and $\mathcal{E}_{\text{CDF}}(u)$ holding,*

$$(W_2(t|u))^2 \leq \frac{12K^2(0)}{K^2(\tau)\theta^4\Xi_u^2} + \frac{12K^2(0)}{K^2(\tau)\theta^4} (\spadesuit^2 + \heartsuit^2).$$

where

$$\spadesuit^2 \leq \varepsilon_{CDF}^2, \quad \heartsuit^2 \leq (\lambda_T + \lambda_C)^2 t^2 (1 + \beta)^{2\alpha} \tau^{2\alpha}.$$

Thus,

$$\mathbb{E}_{Y_{1:n}, D_{1:n} | U_{1:n}} [(W_2(t|u))^2] \leq \frac{12K^2(0)}{K^2(\tau)\theta^4\Xi_u^2} + \frac{12K^2(0)}{K^2(\tau)\theta^4} [\varepsilon_{CDF}^2 + (\lambda_T + \lambda_C)^2 t^2 (1 + \beta)^{2\alpha} \tau^{2\alpha}].$$

Proof. We use Hölder's inequality and a bit of algebra to get

$$\begin{aligned} |W_2(t|u)| &= \left| \sum_{i \in \mathcal{N}_Q(u)} \frac{K_i D_i \mathbb{1}\{Y_i \leq t\} \left[\frac{1}{S_{Y|U}(Y_i|u)} - \frac{\sum_{\ell \in \mathcal{N}_Q(u)} K_\ell}{K_i + d_K^+(u, Y_i)} \right]}{\sum_{j \in \mathcal{N}_Q(u)} K_j} \right| \\ &\leq \max_{i \in \mathcal{N}_Q(u)} \left| D_i \mathbb{1}\{Y_i \leq t\} \left[\frac{1}{S_{Y|U}(Y_i|u)} - \frac{\sum_{\ell \in \mathcal{N}_Q(u)} K_\ell}{K_i + d_K^+(u, Y_i)} \right] \right| \\ &= \max_{i \in \mathcal{N}_Q(u)} \left| \frac{D_i \mathbb{1}\{Y_i \leq t\} \sum_{\ell \in \mathcal{N}_Q(u)} K_\ell}{(K_i + d_K^+(u, Y_i)) S_{Y|U}(Y_i|u)} \left[\frac{K_i + d_K^+(u, Y_i)}{\sum_{\ell \in \mathcal{N}_Q(u)} K_\ell} - S_{Y|U}(Y_i|u) \right] \right| \\ &= \max_{i \in \mathcal{N}_Q(u)} \left| \underbrace{\frac{D_i \mathbb{1}\{Y_i \leq t\} \sum_{\ell \in \mathcal{N}_Q(u)} K_\ell}{(K_i + d_K^+(u, Y_i)) S_{Y|U}(Y_i|u)}}_{\clubsuit_i :=} \left[\frac{K_i}{\sum_{\ell \in \mathcal{N}_Q(u)} K_\ell} + \underbrace{\widehat{S}_{Y|U}(Y_i|u) - S_{Y|U}(Y_i|u)}_{\text{CDF/tail estimation}} \right] \right| \\ &\leq \sup_{\substack{i \in \mathcal{N}_Q(u), \\ s \in [0, t]}} \left| \clubsuit_i \left[\frac{K_i}{\sum_{\ell \in \mathcal{N}_Q(u)} K_\ell} + \widehat{S}_{Y|U}(s|u) - S_{Y|U}(s|u) \right] \right|, \end{aligned} \quad (\text{A.14})$$

where the last step uses the fact that for \clubsuit_i to be nonzero, we must have $Y_i \leq t$, for which we then replace Y_i with a worst case $s \in [0, t]$ in the CDF/tail estimation problem.

By squaring both sides of inequality (A.14) (and noting that the square can go into the sup on the RHS) followed by using the fact that $(\sum_{i=1}^\ell a_i)^2 \leq \ell \sum_{i=1}^\ell a_i^2$,

$$\begin{aligned} (W_2(t|u))^2 &\leq \sup_{\substack{i \in \mathcal{N}_Q(u), \\ s \in [0, t]}} \clubsuit_i^2 \left[\frac{K_i}{\sum_{\ell \in \mathcal{N}_Q(u)} K_\ell} + \widehat{S}_{Y|U}(s|u) - S_{Y|U}(s|u) \right]^2 \\ &= \sup_{\substack{i \in \mathcal{N}_Q(u), \\ s \in [0, t]}} \clubsuit_i^2 \left[\frac{K_i}{\sum_{\ell \in \mathcal{N}_Q(u)} K_\ell} + \widehat{S}_{Y|U}(s|u) - \mathbb{E}_{Y_{1:n}, D_{1:n} | U_{1:n}} [\widehat{S}_{Y|U}(s|u)] \right. \\ &\quad \left. + \mathbb{E}_{Y_{1:n}, D_{1:n} | U_{1:n}} [\widehat{S}_{Y|U}(s|u)] - S_{Y|U}(s|u) \right]^2 \\ &\leq \sup_{\substack{i \in \mathcal{N}_Q(u), \\ s \in [0, t]}} \left[3\clubsuit_i^2 \left(\frac{K_i}{\sum_{\ell \in \mathcal{N}_Q(u)} K_\ell} \right)^2 + 3\clubsuit_i^2 (\widehat{S}_{Y|U}(s|u) - \mathbb{E}_{Y_{1:n}, D_{1:n} | U_{1:n}} [\widehat{S}_{Y|U}(s|u)])^2 \right. \\ &\quad \left. + 3\clubsuit_i^2 (\mathbb{E}_{Y_{1:n}, D_{1:n} | U_{1:n}} [\widehat{S}_{Y|U}(s|u)] - S_{Y|U}(s|u))^2 \right] \\ &\leq 3 \max_{i \in \mathcal{N}_Q(u)} \clubsuit_i^2 \left(\frac{K_i}{\sum_{\ell \in \mathcal{N}_Q(u)} K_\ell} \right)^2 + \left(3 \max_{i \in \mathcal{N}_Q(u)} \clubsuit_i^2 \right) \spadesuit^2 + \left(3 \max_{i \in \mathcal{N}_Q(u)} \clubsuit_i^2 \right) \heartsuit^2, \end{aligned} \quad (\text{A.15})$$

where the variance term \spadesuit and bias term \heartsuit are defined in equations (A.12) and (A.13). We now bound $\clubsuit_i^2 \left(\frac{K_i}{\sum_{\ell \in \mathcal{N}_Q(u)} K_\ell} \right)^2$, \clubsuit_i^2 , and \heartsuit^2 .

Since $d_K^+(u, \cdot)$ and $S_{Y|U}(\cdot|u)$ are monotonically decreasing and with the constraint in the numerator that $Y_i \leq t$, we have

$$\begin{aligned}
\clubsuit_i^2 \left(\frac{K_i}{\sum_{\ell \in \mathcal{N}_Q(u)} K_\ell} \right)^2 &= \left(\frac{D_i \mathbb{1}\{Y_i \leq t\} K_i}{(K_i + d_K^+(u, Y_i)) S_{Y|U}(Y_i|u)} \right)^2 \\
&\leq \left(\frac{D_i \mathbb{1}\{Y_i \leq t\} K_i}{d_K^+(u, t) S_{Y|U}(t|u)} \right)^2 \\
&\leq \left(\frac{D_i \mathbb{1}\{Y_i \leq t\} K_i}{K(\tau) \cdot \frac{|\mathcal{N}_Q(u)|\theta}{2} \cdot \theta} \right)^2 && \text{by } \mathcal{E}_{\text{horizon}}(u), \mathbf{A}^{\text{survival}}(\mathbf{a}) \\
&\leq \left(\frac{K(0)}{K(\tau) \cdot \frac{|\mathcal{N}_Q(u)|\theta}{2} \cdot \theta} \right)^2 \\
&= \frac{4K^2(0)}{K^2(\tau)\theta^4 |\mathcal{N}_Q(u)|^2} \\
&\leq \frac{4K^2(0)}{K^2(\tau)\theta^4 \Xi_u^2} && \text{by Lemma 1.} \tag{A.16}
\end{aligned}$$

By similar ideas,

$$\clubsuit_i^2 = \left(\frac{D_i \mathbb{1}\{Y_i \leq t\} \sum_{\ell \in \mathcal{N}_Q(u)} K_\ell}{(K_i + d_K^+(u, Y_i)) S_{Y|U}(Y_i|u)} \right)^2 \leq \left(\frac{|\mathcal{N}_Q(u)| K(0)}{(K(\tau) |\mathcal{N}_Q(u)| \theta / 2) \theta} \right)^2 = \frac{4K^2(0)}{K^2(\tau) \theta^4}. \tag{A.17}$$

Lastly, we bound $\heartsuit = \sup_{s \in [0, t]} \diamond(s)$, where $\diamond(s) := |\mathbb{E}_{Y_{1:n}|U_{1:n}}[\widehat{S}_{Y|U}(s|u)] - S_{Y|U}(s|u)|$. For $s \in [0, t]$, we have

$$\begin{aligned}
\mathbb{E}_{Y_{1:n}|U_{1:n}}[\widehat{S}_{Y|U}(s|u)] &= \mathbb{E}_{Y_{1:n}|U_{1:n}} \left[\sum_{j \in \mathcal{N}_Q(u)} \frac{K_j}{\sum_{\ell \in \mathcal{N}_Q(u)} K_\ell} \mathbb{1}\{Y_j > s\} \right] \\
&= \sum_{j \in \mathcal{N}_Q(u)} \frac{K_j}{\sum_{\ell \in \mathcal{N}_Q(u)} K_\ell} \mathbb{E}_{Y_j|U_j}[\mathbb{1}\{Y_j > s\}]. \\
&= \sum_{j \in \mathcal{N}_Q(u)} \frac{K_j}{\sum_{\ell \in \mathcal{N}_Q(u)} K_\ell} S_{Y|U}(s|U_j). \tag{A.18}
\end{aligned}$$

Note that Assumption $\mathbf{A}^{\text{survival}}(\mathbf{b})$ implies that $S_{Y|U}(s|\cdot)$ is Hölder continuous with parameters $(\lambda_T + \lambda_C)s$ and α . Then using equation (A.18), Hölder's inequality, Hölder continuity, and Lemma 3,

$$\begin{aligned}
\diamond(s) &= \left| \sum_{j \in \mathcal{N}_Q(u)} \frac{K_j}{\sum_{\ell \in \mathcal{N}_Q(u)} K_\ell} (S_{Y|U}(s|U_j) - S_{Y|U}(s|u)) \right| \\
&\leq \max_{j \in \mathcal{N}_Q(u)} |S_{Y|U}(s|U_j) - S_{Y|U}(s|u)| \\
&\leq \max_{j \in \mathcal{N}_Q(u)} (\lambda_T + \lambda_C) s \|U_j - u\|_2^\alpha \\
&\leq \max_{j \in \mathcal{N}_Q(u)} (\lambda_T + \lambda_C) s (1 + \beta)^\alpha \tau^\alpha \\
&= (\lambda_T + \lambda_C) t (1 + \beta)^\alpha \tau^\alpha.
\end{aligned}$$

Therefore,

$$\heartsuit = \sup_{s \in [0, t]} \diamond(s) \leq (\lambda_T + \lambda_C) t (1 + \beta)^\alpha \tau^\alpha. \tag{A.19}$$

Combining inequalities (A.15), (A.16), (A.17), and (A.19) yields the claim. \square

Bounding term III Lastly, we have the following bound.

Lemma 7. (Bound on term III) *Under the same setting as Lemma 4 (conditioning on $\mathcal{E}_\beta(u)$ and $\mathcal{E}_{\text{horizon}}(u)$) and with the addition of Assumption $\mathbf{A}^{\text{intrinsic}}$ and the requirement that $n \geq \frac{2K(0)}{K(\tau)\theta C_{d'}((1-\beta)\tau)^{d'}}$, we have*

$$\mathbb{E}_{Y_{1:n}, D_{1:n} | U_{1:n}} [(W_3(t|u))^2] \leq \frac{16K^4(0)}{K^4(\tau)\theta^4 \Xi_u^2}.$$

Proof. We write $|W_3(t|u)| = \sum_{i \in \mathcal{N}_Q(u)} Y_i$, where

$$Y_i := D_i \mathbb{1}\{Y_i \leq t\} \sum_{\ell=2}^{\infty} \frac{1}{\ell [1 + (d_K^+(u, Y_i)/K_i)]^\ell}.$$

Using the constraint that $Y_i \leq t$, that $d_K^+(u, \cdot)$ monotonically decreases, and that $t \leq t_{\text{horizon}}$, we have

$$\begin{aligned} Y_i &\leq D_i \mathbb{1}\{Y_i \leq t\} \sum_{\ell=2}^{\infty} \frac{1}{\ell [1 + (d_K^+(u, t)/K_i)]^\ell} \\ &\leq \sum_{\ell=2}^{\infty} \frac{1}{\ell [1 + (d_K^+(u, t)/K_i)]^\ell} \\ &\leq \sum_{\ell=2}^{\infty} \frac{1}{\ell [1 + (d_K^+(u, t_{\text{horizon}})/K_i)]^\ell}. \end{aligned}$$

Next, recall that good event $\mathcal{E}_{\text{horizon}}(u)$ ensures that $d^+(u, t_{\text{horizon}}) > \frac{|\mathcal{N}_Q(u)|\theta}{2}$. Furthermore, $d_K^+(u, t_{\text{horizon}}) \geq K(\tau)d^+(u, t_{\text{horizon}})$, and $K_i \leq K(0)$, so

$$\frac{1}{\ell [1 + (d_K^+(u, t_{\text{horizon}})/K_i)]^\ell} \leq \frac{1}{\ell [1 + \frac{K(\tau)|\mathcal{N}_Q(u)|\theta}{2K(0)}]^\ell}.$$

Hence,

$$Y_i \leq \sum_{\ell=2}^{\infty} \frac{1}{\ell [1 + \frac{K(\tau)|\mathcal{N}_Q(u)|\theta}{2K(0)}]^\ell}.$$

Noting that $\sum_{\ell=2}^{\infty} \frac{1}{\ell(1+z)^\ell} = \log(1 + \frac{1}{z}) - \frac{1}{1+z} \leq \frac{1}{(1+z)^2}$ for all $z \geq 0.46241$, then provided that

$$\frac{K(\tau)|\mathcal{N}_Q(u)|\theta}{2K(0)} \geq 0.46241, \tag{A.20}$$

we have

$$Y_i \leq \frac{1}{(1 + \frac{K(\tau)|\mathcal{N}_Q(u)|\theta}{2K(0)})^2} \leq \frac{1}{(\frac{K(\tau)|\mathcal{N}_Q(u)|\theta}{2K(0)})^2} = \frac{4K^2(0)}{K^2(\tau)|\mathcal{N}_Q(u)|^2\theta^2}.$$

Thus,

$$\begin{aligned} |W_3(t|u)| &= \sum_{i \in \mathcal{N}_Q(u)} Y_i \leq \sum_{i \in \mathcal{N}_Q(u)} \frac{4K^2(0)}{K^2(\tau)|\mathcal{N}_Q(u)|^2\theta^2} \\ &= \frac{4K^2(0)}{K^2(\tau)|\mathcal{N}_Q(u)|\theta^2} \leq \frac{4K^2(0)}{K^2(\tau)\theta^2} \cdot \frac{1}{\Xi_u}. \end{aligned}$$

Squaring and taking expectation $\mathbb{E}_{Y_{1:n}, D_{1:n} | U_{1:n}}$ of both sides, we have

$$\mathbb{E}_{Y_{1:n}, D_{1:n} | U_{1:n}} [(W_3(t|u))^2] \leq \frac{16K^4(0)}{K^4(\tau)\theta^4} \cdot \frac{1}{\Xi_u^2}.$$

The only missing piece is to ensure that condition (A.20) holds. Under event $\mathcal{E}_\beta(u)$ and Assumption $\mathbf{A}^{\text{intrinsic}}$, with the help of Lemma 1,

$$|\mathcal{N}_Q(u)| \geq \Xi_u > \frac{1}{2} n \mathbb{P}_U(B(u, (1-\beta)\tau)) \geq \frac{1}{2} n C_{d'}((1-\beta)\tau)^{d'}.$$

Thus, since we assume that $n \geq \frac{2K(0)}{K(\tau)\theta C_{d'}((1-\beta)\tau)^{d'}}$, we have

$$\begin{aligned} \frac{K(\tau)|\mathcal{N}_Q(u)|\theta}{2} &\geq \frac{K(\tau)\frac{1}{2}nC_{d'}((1-\beta)\tau)^{d'}\theta}{2} \\ &\geq \frac{K(\tau)\frac{1}{2}\left[\frac{2K(0)}{K(\tau)\theta C_{d'}((1-\beta)\tau)^{d'}}\right]C_{d'}((1-\beta)\tau)^{d'}\theta}{2} \\ &= \frac{1}{2} \geq 0.46241, \end{aligned}$$

which verifies that condition (A.20) holds. \square

Deriving a final pointwise bound Putting together bound (A.9) and Lemmas 5, 6, and 7, we have that when all three good events $\mathcal{E}_\beta(u)$, $\mathcal{E}_{\text{horizon}}(u)$, and $\mathcal{E}_{\text{CDF}}(u)$ hold, and $n \geq \frac{2K(0)}{K(\tau)\theta C_{d'}((1-\beta)\tau)^{d'}}$,

$$\begin{aligned} &\mathbb{E}_{Y_{1:n}, D_{1:n} | U_{1:n}} [(\hat{S}_{T|U}(t|u) - S_{T|U}(t|u))^2] \\ &\leq 3\mathbb{E}_{Y_{1:n}, D_{1:n} | U_{1:n}} [(W_1(t|u) - \log S_{T|U}(t|u))^2] + 3\mathbb{E}_{Y_{1:n}, D_{1:n} | U_{1:n}} [(W_2(t|u))^2] \\ &\quad + 3\mathbb{E}_{Y_{1:n}, D_{1:n} | U_{1:n}} [(W_3(t|u))^2] \\ &\leq 3 \left[\frac{K(0)}{4\theta^2 K(\tau) \Xi_u} + \frac{(1+\beta)^{2\alpha} \tau^{2\alpha}}{\theta^2} \left(\lambda_T t + \frac{f_T^* \lambda_C t^2}{2} \right)^2 \right] \\ &\quad + 3 \left[\frac{12K^2(0)}{K^2(\tau) \Xi_u^2 \theta^4} + \frac{12K^2(0)}{K^2(\tau) \theta^4} \varepsilon_{\text{CDF}}^2 + \frac{12K^2(0)}{K^2(\tau) \theta^4} (\lambda_T + \lambda_C)^2 t^2 (1+\beta)^{2\alpha} \tau^{2\alpha} \right] \\ &\quad + 3 \left[\frac{16K^4(0)}{K^4(\tau) \theta^4 \Xi_u^2} \right] \\ &\leq \frac{1}{n} \cdot \frac{332K^4(0)}{\theta^4 K^4(\tau) \mathbb{P}_U(B(u, (1-\beta)\tau))} \log \left(n^3 \frac{144K^2(\tau)}{9K^2(0)} \right) \\ &\quad + (1+\beta)^{2\alpha} \tau^{2\alpha} \left[\frac{3}{\theta^2} \left(\lambda_T t + \frac{f_T^* \lambda_C t^2}{2} \right)^2 + \frac{36K^2(0)}{K^2(\tau) \theta^4} (\lambda_T + \lambda_C)^2 t^2 \right]. \end{aligned}$$

When not all good events occur, we resort to the trivial bound

$$\mathbb{E}_{Y_{1:n}, D_{1:n} | U_{1:n}} [(\hat{S}_{T|U}(t|u) - S_{T|U}(t|u))^2] \leq 1.$$

Abbreviating the three good events as $\mathcal{E}_{\text{good}}(u) := \mathcal{E}_\beta(u) \cup \mathcal{E}_{\text{horizon}}(u) \cup \mathcal{E}_{\text{CDF}}(u)$,

$$\begin{aligned} &\mathbb{E}_{Y_{1:n}, D_{1:n}, U_{1:n}} [(\hat{S}_{T|U}(t|u) - S_{T|U}(t|u))^2] \\ &= \mathbb{E}_{U_{1:n}} [\mathbb{E}_{Y_{1:n}, D_{1:n} | U_{1:n}} [(\hat{S}_{T|U}(t|u) - S_{T|U}(t|u))^2 \mathbb{1}\{\mathcal{E}_{\text{good}}(u)\} \\ &\quad + (\hat{S}_{T|U}(t|u) - S_{T|U}(t|u))^2 \mathbb{1}\{\mathcal{E}_{\text{good}}^c(u)\}]] \\ &\leq \mathbb{E}_{U_{1:n}} [\mathbb{E}_{Y_{1:n}, D_{1:n} | U_{1:n}} [(\hat{S}_{T|U}(t|u) - S_{T|U}(t|u))^2 \mathbb{1}\{\mathcal{E}_{\text{good}}(u)\} + \mathbb{1}\{\mathcal{E}_{\text{good}}^c(u)\}]] \\ &\leq \frac{1}{n} \cdot \frac{332K^4(0)}{\theta^4 K^4(\tau) \mathbb{P}_U(B(u, (1-\beta)\tau))} \log \left(n^3 \frac{144K^2(\tau)}{9K^2(0)} \right) \\ &\quad + (1+\beta)^{2\alpha} \tau^{2\alpha} \left[\frac{3}{\theta^2} \left(\lambda_T t + \frac{f_T^* \lambda_C t^2}{2} \right)^2 + \frac{36K^2(0)}{K^2(\tau) \theta^4} (\lambda_T + \lambda_C)^2 t^2 \right] \\ &\quad + \mathbb{E}_{U_{1:n}, Y_{1:n}, D_{1:n}} [\mathbb{1}\{\mathcal{E}_{\text{good}}^c(u)\}]. \end{aligned} \tag{A.21}$$

We next bound $\mathbb{E}_{U_{1:n}, Y_{1:n}, D_{1:n}}[\mathbb{1}\{\mathcal{E}_{\text{good}}^c(u)\}]$.

Lemma 8. (The survival analysis good events hold with high probability) *Consider the same setting as Lemma 4 except without conditioning on any good events. Moreover, we add Assumption $\mathbf{A}^{\text{intrinsic}}$ and require that $n \geq \frac{2}{C_{d'}((1-\beta)\tau)^{d'}} \left(\frac{9K^2(0)}{144K^2(\tau)}(2+\sqrt{2})\right)^{1/3}$. Then*

$$\mathbb{E}_{U_{1:n}, Y_{1:n}, D_{1:n}}[\mathbb{1}\{\mathcal{E}_{\text{good}}^c(u)\}] \leq \frac{14}{\theta^2 n \mathbb{P}_U(B(u, (1-\beta)\tau))}.$$

We defer the proof of this lemma to Appendix A.3.2 as it is somewhat technical.

Putting together bound (A.21) and Lemma 8, and in particular absorbing Lemma 8's bound into the leading error term in (A.21), we get the final pointwise bound: for $n \geq \frac{2}{C_{d'}((1-\beta)\tau)^{d'}} \max\left\{\frac{K(0)}{K(\tau)\theta}, \left(\frac{9K^2(0)}{144K^2(\tau)}(2+\sqrt{2})\right)^{1/3}\right\}$,

$$\begin{aligned} & \mathbb{E}_{Y_{1:n}, D_{1:n}, U_{1:n}}[(\widehat{S}_{T|U}(t|u) - S_{T|U}(t|u))^2] \\ & \leq \frac{346K^4(0)}{n\theta^4 K^4(\tau) \mathbb{P}_U(B(u, (1-\beta)\tau))} \log\left(n^3 \frac{144K^2(\tau)}{9K^2(0)}\right) \\ & \quad + (1+\beta)^{2\alpha} \tau^{2\alpha} \left[\frac{3}{\theta^2} \left(\lambda_T t + \frac{f_T^* \lambda_C t^2}{2}\right)^2 + \frac{36K^2(0)}{K^2(\tau)\theta^4} (\lambda_T + \lambda_C)^2 t^2 \right]. \end{aligned} \quad (\text{A.22})$$

Completing the proof Finally, we account for randomness in the test embedding $U \sim \mathbb{P}_U$ and integrate over time. Suppose that $n \geq \frac{2}{C_{d'}((1-\beta)\tau)^{d'}} \max\left\{\frac{K(0)}{K(\tau)\theta}, \left(\frac{9K^2(0)}{144K^2(\tau)}(2+\sqrt{2})\right)^{1/3}\right\}$. By Fubini's theorem, iterated expectation, and the final pointwise bound (A.22),

$$\begin{aligned} & \mathbb{E}_{Y_{1:n}, D_{1:n}, U_{1:n}, U} \left[\frac{\int_0^{t_{\text{horizon}}} (\widehat{S}_{T|U}(t|U) - S_{T|U}(t|U))^2 dt}{t_{\text{horizon}}} \right] \\ & = \int_{[0, t_{\text{horizon}}]} \frac{\mathbb{E}_U[\mathbb{E}_{Y_{1:n}, D_{1:n}, U_{1:n}|U}[(\widehat{S}_{T|U}(t|U) - S_{T|U}(t|U))^2]]}{t_{\text{horizon}}} dt \\ & \leq \int_{[0, t_{\text{horizon}}]} \frac{1}{t_{\text{horizon}}} \mathbb{E}_U \left[\frac{1}{n} \cdot \frac{346K^4(0) \log(n^3 \frac{144K^2(\tau)}{9K^2(0)})}{\theta^4 K^4(\tau) \mathbb{P}_U(B(U, (1-\beta)\tau))} \right. \\ & \quad \left. + (1+\beta)^{2\alpha} \tau^{2\alpha} \left[\frac{3}{\theta^2} \left(\lambda_T t + \frac{f_T^* \lambda_C t^2}{2}\right)^2 + \frac{36K^2(0)}{K^2(\tau)\theta^4} (\lambda_T + \lambda_C)^2 t^2 \right] \right] dt \\ & = \frac{346K^4(0) \log(n^3 \frac{144K^2(\tau)}{9K^2(0)})}{n\theta^4 K^4(\tau)} \mathbb{E}_U \left[\frac{1}{\mathbb{P}_U(B(U, (1-\beta)\tau))} \right] \\ & \quad + (1+\beta)^{2\alpha} \tau^{2\alpha} \left[\frac{t_{\text{horizon}}^2}{\theta^2} \left(\lambda_T^2 + \frac{3\lambda_T f_T^* \lambda_C t_{\text{horizon}}}{4} + \frac{3(f_T^*)^2 \lambda_C^2 t_{\text{horizon}}^2}{20} \right) \right. \\ & \quad \left. + \frac{12K^2(0)}{K^2(\tau)\theta^4} (\lambda_T + \lambda_C)^2 t_{\text{horizon}}^2 \right]. \end{aligned}$$

At this point, we can bound $\mathbb{E}_U[\frac{1}{\mathbb{P}_U(B(U, (1-\beta)\tau))}]$ using the same approach as in the regression proof, either using covering numbers or Assumption $\mathbf{A}^{\text{intrinsic}}$. Namely, $\mathbb{E}_U[\frac{1}{\mathbb{P}_U(B(U, (1-\beta)\tau))}] \leq N(\frac{(1-\beta)\tau}{2}; U)$, or $\mathbb{E}_U[\frac{1}{\mathbb{P}_U(B(U, (1-\beta)\tau))}] \leq \frac{1}{C_{d'}((1-\beta)\tau)^{d'}}.$ ■

A.3.2 Proof of Lemma 8

Observe that

$$\begin{aligned}\mathcal{E}_{\text{good}}(u) &= (\mathcal{E}_\beta(u) \cap \mathcal{E}_{\text{horizon}}(u) \cap \mathcal{E}_{\text{CDF}}(u))^c \\ &= \mathcal{E}_\beta^c(u) \cup \mathcal{E}_{\text{horizon}}^c(u) \cup \mathcal{E}_{\text{CDF}}^c(u) \\ &= \mathcal{E}_\beta^c(u) \cup [\mathcal{E}_{\text{horizon}}^c(u) \cap \mathcal{E}_\beta(u)] \cup [\mathcal{E}_{\text{CDF}}^c(u) \cap \mathcal{E}_\beta(u)].\end{aligned}$$

Hence, by a union bound

$$\begin{aligned}\mathbb{E}_{U_{1:n}, Y_{1:n}, D_{1:n}}[\mathbb{1}\{\mathcal{E}_{\text{good}}(u)\}] &\leq \underbrace{\mathbb{E}_{U_{1:n}, Y_{1:n}, D_{1:n}}[\mathbb{1}\{\mathcal{E}_\beta^c(u)\}]}_{(a)} + \underbrace{\mathbb{E}_{U_{1:n}, Y_{1:n}, D_{1:n}}[\mathbb{1}\{\mathcal{E}_{\text{horizon}}^c(u) \cap \mathcal{E}_\beta(u)\}]}_{(b)} \\ &\quad + \underbrace{\mathbb{E}_{U_{1:n}, Y_{1:n}, D_{1:n}}[\mathbb{1}\{\mathcal{E}_{\text{CDF}}^c(u) \cap \mathcal{E}_\beta(u)\}]}_{(c)}.\end{aligned}\tag{A.23}$$

We upper-bound each of these three terms next.

Term (a) This term is bounded precisely by Lemma 2. In particular,

$$\text{term (a)} \leq \frac{8}{n\mathbb{P}_{\mathbf{U}}(B(u, (1-\beta)\tau))}.\tag{A.24}$$

Term (b) For term (b), note that within the expectation there is no dependence on $D_{1:n}$. In particular,

$$\begin{aligned}\mathbb{E}_{U_{1:n}, Y_{1:n}, D_{1:n}}[\mathbb{1}\{\mathcal{E}_{\text{horizon}}^c(u) \cap \mathcal{E}_\beta(u)\}] &= \mathbb{E}_{U_{1:n}, Y_{1:n}, D_{1:n}}\left[\mathbb{1}\left\{d^+(u, t_{\text{horizon}}) \leq \frac{|\mathcal{N}_Q(u)|\theta}{2}\right\} \mathbb{1}\left\{\Xi_u > \frac{1}{2}n\mathbb{P}_{\mathbf{U}}(B(u, (1-\beta)\tau))\right\}\right] \\ &= \mathbb{E}_{U_{1:n}, Y_{1:n}}\left[\mathbb{1}\left\{d^+(u, t_{\text{horizon}}) \leq \frac{|\mathcal{N}_Q(u)|\theta}{2}\right\} \mathbb{1}\left\{\Xi_u > \frac{1}{2}n\mathbb{P}_{\mathbf{U}}(B(u, (1-\beta)\tau))\right\}\right] \\ &= \mathbb{E}_{U_{1:n}}\left[\mathbb{1}\left\{\Xi_u > \frac{1}{2}n\mathbb{P}_{\mathbf{U}}(B(u, (1-\beta)\tau))\right\} \mathbb{E}_{Y_{1:n}|U_{1:n}}\left[\mathbb{1}\left\{d^+(u, t_{\text{horizon}}) \leq \frac{|\mathcal{N}_Q(u)|\theta}{2}\right\}\right]\right].\end{aligned}\tag{A.25}$$

By Assumption **A**^{survival}(a),

$$|\mathcal{N}_Q(u)|\theta = \sum_{j \in \mathcal{N}_Q(u)} \theta \leq \sum_{j \in \mathcal{N}_Q(u)} S_{Y|U}(t_{\text{horizon}}|U_j) =: \mu^+.\tag{A.26}$$

Hence, $d^+(u, t_{\text{horizon}}) \leq \frac{|\mathcal{N}_Q(u)|\theta}{2}$ implies that $d^+(u, t_{\text{horizon}}) \leq \frac{\mu^+}{2}$, i.e.,

$$\mathbb{1}\left\{d^+(u, t_{\text{horizon}}) \leq \frac{|\mathcal{N}_Q(u)|\theta}{2}\right\} \leq \mathbb{1}\left\{d^+(u, t_{\text{horizon}}) \leq \frac{\mu^+}{2}\right\}.$$

Thus,

$$\begin{aligned}\mathbb{E}_{U_{1:n}}\left[\mathbb{1}\left\{\Xi_u > \frac{1}{2}n\mathbb{P}_{\mathbf{U}}(B(u, (1-\beta)\tau))\right\} \mathbb{E}_{Y_{1:n}|U_{1:n}}\left[\mathbb{1}\left\{d^+(u, t_{\text{horizon}}) \leq \frac{|\mathcal{N}_Q(u)|\theta}{2}\right\}\right]\right] \\ \leq \mathbb{E}_{U_{1:n}}\left[\mathbb{1}\left\{\Xi_u > \frac{1}{2}n\mathbb{P}_{\mathbf{U}}(B(u, (1-\beta)\tau))\right\} \mathbb{E}_{Y_{1:n}|U_{1:n}}\left[\mathbb{1}\left\{d^+(u, t_{\text{horizon}}) \leq \frac{\mu^+}{2}\right\}\right]\right].\end{aligned}\tag{A.27}$$

We now upper-bound $\mathbb{E}_{Y_{1:n}|U_{1:n}}[\mathbb{1}\{d^+(u, t_{\text{horizon}}) \leq \frac{\mu^+}{2}\}]$, under the constraint that $\Xi_u > \frac{1}{2}n\mathbb{P}_{\mathbf{U}}(B(u, (1-\beta)\tau))$. Importantly, since the $Y_{1:n}$ variables are conditionally independent given $U_{1:n}$ and since $\mathcal{N}_Q(u)$ is deterministic given $U_{1:n}$, then after conditioning on $U_{1:n}$, the sum

$$d^+(u, t_{\text{horizon}}) = \sum_{j \in \mathcal{N}_Q(u)} \mathbb{1}\{Y_j > t_{\text{horizon}}\}$$

is over independent random variables and, furthermore, using Lemma 1, the above summation is not vacuous since $|\mathcal{N}_Q(u)| \geq \Xi_u > 0$. Thus, with $\mathcal{N}_Q(u)$ nonempty, the expectation of the above sum is

$$\mathbb{E}_{Y_{1:n}|U_{1:n}}[d^+(u, t_{\text{horizon}})] = \sum_{j \in \mathcal{N}_Q(u)} \mathbb{E}_{Y_j|U_j}[\mathbb{1}\{Y_j > t_{\text{horizon}}\}] = \sum_{j \in \mathcal{N}_Q(u)} S_{Y|U}(t_{\text{horizon}}|U_j) = \mu^+.$$

Applying Hoeffding's inequality

$$\begin{aligned} \mathbb{E}_{Y_{1:n}|U_{1:n}}\left[\mathbb{1}\left\{d^+(u, t_{\text{horizon}}) \leq \frac{\mu^+}{2}\right\}\right] &\leq \exp\left(-\frac{2(\frac{1}{2}\mu^+)^2}{|\mathcal{N}_Q(u)|}\right) \\ &\leq \exp\left(-\frac{2(\frac{|\mathcal{N}_Q(u)|\theta}{2})^2}{|\mathcal{N}_Q(u)|}\right) \quad \text{by inequality (A.26)} \\ &= \exp\left(-\frac{\theta^2}{2}|\mathcal{N}_Q(u)|\right) \\ &\leq \exp\left(-\frac{\theta^2}{2}\Xi_u\right) \quad \text{by Lemma 1} \\ &\leq \frac{2}{\theta^2\Xi_u} \\ &< \frac{4}{\theta^2n\mathbb{P}_{\mathbf{U}}(B(u, (1-\beta)\tau))} \quad \text{by good event } \mathcal{E}_\beta(u), \quad (\text{A.28}) \end{aligned}$$

where the last step uses the constraint $\Xi_u > \frac{1}{2}n\mathbb{P}_{\mathbf{U}}(B(u, (1-\beta)\tau))$.

Stringing together inequalities (A.25), (A.27), and (A.28), we see that

$$\text{term (b)} \leq \frac{4}{\theta^2n\mathbb{P}_{\mathbf{U}}(B(u, (1-\beta)\tau))}. \quad (\text{A.29})$$

Term (c) Recall that we use the shorthand notation $\spadesuit = \sup_{s \geq 0} |\hat{S}_{Y|U}(s|u) - \mathbb{E}_{Y_{1:n}|U_{1:n}}[\hat{S}_{Y|U}(s|u)]|$. Then term (c) can be written as

$$\begin{aligned} &\mathbb{E}_{U_{1:n}, Y_{1:n}, D_{1:n}}\left[\mathbb{1}\{\spadesuit > \varepsilon_{\text{CDF}}\} \mathbb{1}\left\{\Xi_u > \frac{1}{2}n\mathbb{P}_{\mathbf{U}}(B(u, (1-\beta)\tau))\right\}\right] \\ &= \mathbb{E}_{U_{1:n}, Y_{1:n}}\left[\mathbb{1}\{\spadesuit > \varepsilon_{\text{CDF}}\} \mathbb{1}\left\{\Xi_u > \frac{1}{2}n\mathbb{P}_{\mathbf{U}}(B(u, (1-\beta)\tau))\right\}\right] \\ &= \mathbb{E}_{U_{1:n}}\left[\mathbb{1}\left\{\Xi_u > \frac{1}{2}n\mathbb{P}_{\mathbf{U}}(B(u, (1-\beta)\tau))\right\} \mathbb{E}_{Y_{1:n}|U_{1:n}}\left[\mathbb{1}\{\spadesuit > \varepsilon_{\text{CDF}}\}\right]\right]. \quad (\text{A.30}) \end{aligned}$$

Under the constraint that $\Xi_u > \frac{1}{2}n\mathbb{P}_{\mathbf{U}}(B(u, (1-\beta)\tau))$ and conditioned on $U_{1:n}$,

$$1 - \hat{S}_{Y|U}(s|u) = \sum_{j \in \mathcal{N}_Q(u)} \frac{K_j}{\sum_{\ell \in \mathcal{N}_Q(u)} K_\ell} \mathbb{1}\{Y_j \leq s\}$$

is a weighted empirical distribution constructed from more than $\frac{1}{2}n\mathbb{P}_{\mathbf{U}}(B(u, (1-\beta)\tau))$ samples. Applying Proposition 3.1 of Chen [2019],

$$\begin{aligned}\mathbb{E}_{Y_{1:n}|U_{1:n}}[\mathbb{1}\{\spadesuit > \varepsilon_{\text{CDF}}\}] &\leq \frac{6}{\varepsilon_{\text{CDF}}} \exp\left(-\frac{2\varepsilon_{\text{CDF}}^2(\sum_{j \in \mathcal{N}_Q(u)} K_j)^2}{9 \sum_{\ell \in \mathcal{N}_Q(u)} K_\ell^2}\right) \\ &\leq \frac{6}{\varepsilon_{\text{CDF}}} \exp\left(-\frac{2\varepsilon_{\text{CDF}}^2(|\mathcal{N}_Q(u)|K(\tau))^2}{9|\mathcal{N}_Q(u)|K^2(0)}\right) \\ &= \frac{6}{\varepsilon_{\text{CDF}}} \exp\left(-\frac{2\varepsilon_{\text{CDF}}^2 K^2(\tau)}{9K^2(0)}|\mathcal{N}_Q(u)|\right).\end{aligned}\quad (\text{A.31})$$

We show that our choice of ε_{CDF} ensures that the RHS is at most $\frac{1}{|\mathcal{N}_Q(u)|}$, i.e., we want to show that

$$\frac{6}{\varepsilon_{\text{CDF}}} \exp\left(-\frac{2\varepsilon_{\text{CDF}}^2 K^2(\tau)}{9K^2(0)}|\mathcal{N}_Q(u)|\right) \leq \frac{1}{|\mathcal{N}_Q(u)|}. \quad (\text{A.32})$$

Lemma D.1(b) of Chen [2019] says that inequality (A.32) holds under the sufficient conditions

$$\varepsilon_{\text{CDF}} < 6|\mathcal{N}_Q(u)| \quad \text{and} \quad |\mathcal{N}_Q(u)| \geq \left(\frac{9K^2(0)e}{144K^2(\tau)}\right)^{1/3}. \quad (\text{A.33})$$

The latter holds since we assume that $n \geq \frac{2}{C_{d'}((1-\beta)\tau)^{d'}} \left(\frac{9K^2(0)}{144K^2(\tau)}(2+\sqrt{2})\right)^{1/3}$, so using good event $\mathcal{E}_\beta(u)$, Lemma 1 and Assumption **A**^{intrinsic}, we have

$$\begin{aligned}|\mathcal{N}_Q(u)| &\geq \Xi_u \\ &> \frac{1}{2}n\mathbb{P}_{\mathbf{U}}(B(u, (1-\beta)\tau)) \\ &\geq \frac{1}{2}nC_{d'}((1-\beta)\tau)^{d'} \\ &\geq \frac{1}{2}\left[\frac{2}{C_{d'}((1-\beta)\tau)^{d'}} \left(\frac{9K^2(0)}{144K^2(\tau)}(2+\sqrt{2})\right)^{1/3}\right]C_{d'}((1-\beta)\tau)^{d'} \\ &= \left(\frac{9K^2(0)}{144K^2(\tau)}(2+\sqrt{2})\right)^{1/3},\end{aligned}\quad (\text{A.34})$$

which is strictly greater than $\left(\frac{9K^2(0)e}{144K^2(\tau)}\right)^{1/3}$.

At this point, it suffices for us to show that the condition $\varepsilon_{\text{CDF}} < 6|\mathcal{N}_Q(u)|$ holds. This inequality can be written as

$$|\mathcal{N}_Q(u)|^3 > \frac{9K^2(0)}{144K^2(\tau)} \log\left(|\mathcal{N}_Q(u)|^3 \frac{144K^2(\tau)}{9K^2(0)}\right). \quad (\text{A.35})$$

Define

$$a := \frac{9K^2(0)}{144K^2(\tau)}, \quad b := \frac{9K^2(0)}{144K^2(\tau)} \log\left(\frac{144K^2(\tau)}{9K^2(0)}\right) + \frac{18K^2(0)}{144K^2(\tau)}.$$

Then Lemma D.2(c) of Chen [2019] says that if $\frac{b}{a} + \log a > 1$ and

$$|\mathcal{N}_Q(u)|^3 \geq a\left(1 + \sqrt{2\log(ae^{b/a-1})} + \log(ae^{b/a-1})\right) = \left(\frac{9K^2(0)}{144K^2(\tau)}(2+\sqrt{2})\right)^{1/3}, \quad (\text{A.36})$$

then

$$|\mathcal{N}_Q(u)|^3 \geq a \log(|\mathcal{N}_Q(u)|^3) + b = \frac{9K^2(0)}{144K^2(\tau)} \log\left(|\mathcal{N}_Q(u)|^3 \frac{144K^2(\tau)}{9K^2(0)}\right) + \frac{18K^2(0)}{144K^2(\tau)},$$

which implies that condition (A.35) holds. In fact, we have already shown that condition (A.36) holds (see inequality (A.34)). Thus, it suffices to show that $\frac{b}{a} + \log a > 1$. Indeed,

$$\frac{b}{a} + \log a = \frac{\frac{9K^2(0)}{144K^2(\tau)} \log\left(\frac{144K^2(\tau)}{9K^2(0)}\right) + \frac{18K^2(0)}{144K^2(\tau)}}{\frac{9K^2(0)}{144K^2(\tau)}} + \log\left(\frac{9K^2(0)}{144K^2(\tau)}\right) = 2 > 1.$$

At this point, we can conclude that condition (A.35) holds, which completes our justification that the sufficient conditions (A.33) hold. Thus, we can combine equation (A.30), inequality (A.31), and inequality (A.32) to get that

$$\text{term}(c) \leq \frac{1}{|\mathcal{N}_Q(u)|} \leq \frac{1}{\Xi_u} < \frac{2}{n\mathbb{P}_U(B(u, (1-\beta)\tau))}, \quad (\text{A.37})$$

making use of event $\mathcal{E}_\beta(u)$ and Lemma 1.

Completing the proof Plugging the bounds on terms (a), (b), and (c) (given in inequalities (A.24), (A.29), and (A.37)) back into the union bound (A.23), we get

$$\begin{aligned} & \mathbb{E}_{U_{1:n}, Y_{1:n}, D_{1:n}} [\mathbb{1}\{(\mathcal{E}_\beta(u) \cap \mathcal{E}_{\text{horizon}}(u) \cap \mathcal{E}_{\text{CDF}}(u))^c\}] \\ & \leq \frac{8}{n\mathbb{P}_U(B(u, (1-\beta)\tau))} + \frac{4}{\theta^2 n\mathbb{P}_U(B(u, (1-\beta)\tau))} + \frac{2}{n\mathbb{P}_U(B(u, (1-\beta)\tau))} \\ & \leq \frac{14}{\theta^2 n\mathbb{P}_U(B(u, (1-\beta)\tau))}. \end{aligned} \quad \blacksquare$$

B Details on TUNA

Previously, Chen [2020] showed how to warm-start deep kernel survival analysis using any pre-trained kernel function, such as one obtained from decision trees or their ensembled variants (random forests, gradient tree boosting). However, Chen’s strategy does not scale to large datasets (as we explain shortly). We first state Chen’s strategy (in terms of pre-training data, although Chen originally stated this in terms of training data) and then we say how we incorporate it as a warm-start strategy to our own TUNA warm-start strategy described in Section 4.

Warm-start strategy by Chen [2020] Let \mathbb{K}_0 be a pre-trained kernel function (learned from, for instance, a random survival forest or XGBOOST). Then compute the n_o -by- n_o matrix \mathbf{K} , where $\mathbf{K}_{i,j} = \mathbb{K}_0(X_i^\circ, X_j^\circ)$ for every pair of pre-training feature vectors X_i° and X_j° . Note that computing the matrix \mathbf{K} is prohibitively expensive for large datasets, where even storing this whole matrix can be impractical. For the moment, suppose that we can compute and store this matrix. Next, if we are using a Gaussian kernel $\mathbb{K}(X_i^\circ, X_j^\circ) = \exp(-\|\phi(X_i^\circ) - \phi(X_j^\circ)\|_2^2)$, then by setting this expression equal to $\mathbf{K}_{i,j}$ and with a bit of algebra, we obtain

$$\|\phi(X_i^\circ) - \phi(X_j^\circ)\|_2 = \sqrt{\log \frac{1}{\mathbf{K}_{i,j}}} \quad \text{for all } i, j.$$

To prevent division by 0 in the log, we could for instance add a small constant to all values of \mathbf{K} or clip values of \mathbf{K} under a user-specified threshold to be equal to the threshold.

Next, we can use metric multidimensional scaling (MDS) [Borg and Groenen, 2005] to learn an embedding \tilde{X}_i^{MDS} for each pre-training feature X_i° such that $\|\tilde{X}_i^{\text{MDS}} - \tilde{X}_j^{\text{MDS}}\|_2 \approx \sqrt{\log \frac{1}{\mathbf{K}_{i,j}}}$ for all pairs i and j . Then for a base neural net ϕ with a user-specified architecture, we warm-start ϕ by minimizing the mean squared error loss

$$\frac{1}{n} \sum_{i=1}^n (\phi(X_i^\circ) - \tilde{X}_i^{\text{MDS}})^2.$$

Effectively we are having the neural net ϕ approximate the MDS embedding, which approximates the Euclidean distances induced by the pre-trained kernel function under the assumption of a Gaussian kernel. This MDS-based strategy generalizes to other choices of kernel functions that can be written in terms of the distance function $\rho(x, x') = \|\phi(x) - \phi(x')\|_2$, so long as we can solve the equation $\mathbb{K}(X_i^\circ, X_j^\circ) = \mathbf{K}_{i,j}$ for $\rho(X_i^\circ, X_j^\circ)$; in fact, ρ could even be chosen to be non-Euclidean if generalized MDS is used, which handles non-Euclidean distances [Bronstein et al., 2006].

Incorporating Chen’s warm-start strategy into TUNA To avoid having to compute the full n_o -by- n_o kernel matrix \mathbf{K} (and also having to solve MDS for such a large input matrix), we instead begin by only computing it over a subsample, much like Landmark Isomap [De Silva and Tenenbaum, 2002]. In more detail, our full TUNA warm-start procedure is as follows:

1. Train a scalable tree ensemble (e.g., XGBOOST) on the pre-training data; denote its learned kernel function by \mathbb{K}_0 . For a subset $\mathcal{S} \subseteq \{X_1^\circ, \dots, X_{n_o}^\circ\}$ of the pre-training feature vectors, let $\mathbf{K}_{\mathcal{S}}$ denote the $|\mathcal{S}|$ -by- $|\mathcal{S}|$ Gram matrix formed so that the (i, j) -th entry is given by $\mathbb{K}_0(x_i^\circ, x_j^\circ)$ where x_i° and x_j° are the i -th and j -th pre-training feature vectors in \mathcal{S} (with elements of \mathcal{S} ordered arbitrarily).
- 1'. (MDS initialization by Chen [2020]) Take a subsample of size $n_{\text{subsample}}$ from the pre-training feature vectors (e.g., uniformly at random or using an ε -net). Denote the subsample by $\mathcal{S}_{\text{init}}$. Compute the gram matrix $\mathbf{K}_{\mathcal{S}_{\text{init}}}$. Use Chen’s warm-start strategy restricted to pre-training data in $\mathcal{S}_{\text{init}}$ and using pre-trained kernel matrix $\mathbf{K}_{\mathcal{S}_{\text{init}}}$ to obtain an initial estimate of the base neural net ϕ .
2. For each minibatch consisting of pre-training feature vectors $x_1^\circ, \dots, x_b^\circ$ where b is the batch size:
 - (a) Compute the batch’s tree ensemble Gram matrix $\mathbf{K}_{\{x_1^\circ, \dots, x_b^\circ\}}$ (defined in step 1) using \mathbb{K}_0 .
 - (b) Compute the current neural net’s Gram matrix estimate $\widehat{\mathbf{K}}_{\{x_1^\circ, \dots, x_b^\circ\}}$, which has (i, j) -th entry given by $\mathbb{K}(x_i^\circ, x_j^\circ) = K(\|\phi(x_i^\circ) - \phi(x_j^\circ)\|_2^2)$.
 - (c) Let this minibatch’s loss be the MSE loss (4.1) restricted to feature vectors of the current minibatch, i.e., the MSE loss between $\widehat{\mathbf{K}}_{\{x_1^\circ, \dots, x_b^\circ\}}$ and $\mathbf{K}_{\{x_1^\circ, \dots, x_b^\circ\}}$. Update parameters of neural net ϕ based on the gradient of this minibatch’s loss.

In our experiments later, for simplicity, we construct $\mathcal{S}_{\text{init}}$ in step 1' by taking a uniform subsample of the training data and set $n_{\text{subsample}} = 2048$.

By running minibatch gradient descent (step 2) for a number of epochs (we use 100 for SUPPORT and UNOS, and 10 for KKBOX), we obtain the initial neural net $\hat{\phi}$ that we begin survival kernel training with.

C Details on Experiments

We now provide additional details on data preprocessing (Appendix C.1), and on hyperparameter grids and optimization (Appendix C.2). An additional cluster visualization is in Appendix C.3.

C.1 Preprocessing Notes

Continuous features are standardized (subtract mean and divide by standard deviation). Categorical features are one-hot encoded unless they correspond to features with a clear ordering in which case they are converted to be on a scale from 0 to 1 (evenly spaced for where the levels are). The UNOS data preprocessing is a bit more involved and follows the steps of Yoon et al. [2018] and Lee et al. [2018]. The KKBOX dataset is preprocessed via the pycox package [Kvamme et al., 2019].

C.2 Hyperparameter Grids (Including Neural Net Architecture Settings) and Optimization Details

We provide hyperparameter grids and optimization details in this section. Before doing so, we make a few remarks. First, we implement the elastic-net-regularized Cox model as well as all neural net models in PyTorch [Paszke et al., 2019] so that we can train these models via minibatch gradient descent, which is helpful due to the size of some of our datasets. Note that XGBOOST supports survival analysis with a few losses. We specifically use the Cox loss. We train all models that are implemented in PyTorch (including ELASTIC-NET COX) using Adam [Kingma and Ba, 2014] with a budget of epochs 100 (except for the KKBOX dataset, where we use 10). Early stopping is used based on the validation set (no improvement in the best validation loss within 10 epochs). For simplicity, we always use a batch size of 1024 (from some preliminary experiments, we find that smaller batch sizes such as 128, 256, and 512 yield similar results for baselines but for survival kernels, a larger batch size appears to be helpful).

For the KKBOX dataset, because of how large it is, even computing the validation loss is computationally expensive (C^{td} index is a ranking metric that considers every pair of data points). To make training more practical, we use a subsampling strategy for computing the validation loss where we randomly partition the validation data into groups of size 2^{14} , compute the C^{td} index per group, and then average the indices computed across the groups. We empirically found this approximation to be close to the exact calculation and takes much less time to compute. For the test set as well as bootstrap confidence intervals, we do an exact calculation rather than using this subsampling strategy.

We now list hyperparameter grids of the different methods. Even more details are available in our code.

ELASTIC-NET COX:

- Learning rate: 1.0, 0.1, 0.01, 0.001, 0.0001
- Regularization weight: 0 (corresponds to the standard Cox model [Cox, 1972]), 0.01, 1
- Elastic-net knob for how much to use ℓ_1 regularization vs squared ℓ_2 regularization: 0 (ridge regression), 0.5 (evenly balance ℓ_1 and squared ℓ_2), 1 (lasso)

XGBOOST:

- Number of random features selected per node:
 $\frac{1}{2} \times \text{sqrt of number of features}$, $\text{sqrt of number of features}$, $2 \times \text{sqrt of number of features}$, use all features
- Learning rate “eta”: 0.1, 0.3, 1
- Number of parallel trees: 1, 10
- Training data subsampling when growing trees: 0.6, 0.8
- Max depth: 3, 6, 9, 12
- Max number of rounds: 100 (for KKBOX, only 20)

DEEPSURV:

- Learning rate: 0.01, 0.001
- Number of hidden layers: 2, 4, 6
- Number of nodes per hidden layer: 32, 64, 128
- Nonlinear activation of hidden layers: ReLU
- Use batch norm after each hidden layer: yes

The final layer (a linear layer) is not a hidden layer and corresponds to a Cox model; it has 1 output node and no bias.

DEEPHIT has the same search grid as DEEPSURV and also additionally has the following:

- “alpha”: 0, 0.001, 0.01
- “sigma”: 0.1, 1
- number of time steps to discretize to: 0 (i.e., use all unique observed times), 64, 128

DKSA (we used the reference code by the original author specifically with random survival forest initialization; the only changes made were to get it to work with our experimental harness that loads in data, tunes hyperparameters, and gets test set metrics):

- Number of random features selected per node (for random survival forest warm-start): $\frac{1}{2} \times \text{sqrt of number of features}$, $\text{sqrt of number of features}$, $2 \times \text{sqrt of number of features}$
- Minimum data points per leaf (for random survival forest warm-start): 8, 32, 128
- Learning rate: 0.01, 0.001
- Number of hidden layers: 2, 4, 6
- Number of nodes per hidden layer: 32, 64, 128
- Nonlinear activation of hidden layers: ReLU
- Use batch norm after each hidden layer: yes
- number of durations: 0 (i.e., use all unique observed times), 64, 128

The MLP base neural net’s final number of output nodes is precisely the number of dimensions of the embedding space. We set this number to be the minimum of: (1) the number of nodes per hidden layer, and (2) the number of features in feature space (after preprocessing).

Note that we always project the base neural net’s output onto a hypersphere of radius $\sqrt{0.1}$ (this is mathematically equivalent to projecting to the unit hypersphere but changing the kernel function to instead be $K(u) = \exp(-u^2/0.1)$). In fact, this idea is commonly used in contrastive learning and the radius is a hyperparameter that can be tuned and is equal to the square root of two multiplied by what is commonly called the “temperature” hyperparameter (see for instance the papers by Wang and Isola [2020] and Liu et al. [2021]).

KERNET has the same search grid as DEEPSURV and also additionally has the following:

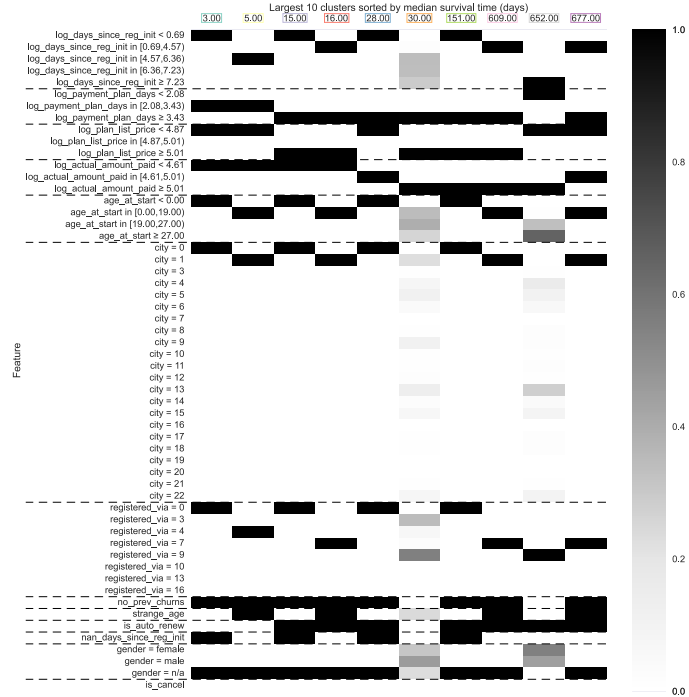
- η : 0, 0.001, 0.01 (defined in L_{rank} as part of equation (2.7); this hyperparameter is analogous to DEEPHIT’s “alpha” hyperparameter)
- σ_{rank} : 0.1, 1 (also defined in L_{rank} as part of equation (2.7); this hyperparameter is analogous to DEEPHIT’s “sigma” hyperparameter)
- number of time steps to discretize to: 0 (i.e., use all unique observed times), 64, 128
- τ : $\sqrt{\log(10)} \approx 1.517$ (we additionally set the maximum number of approximate nearest neighbors to be 128)
- β : 1/4, 1/2 (we construct ε -nets with $\varepsilon = \beta\tau$)

We set the MLP base neural net’s final number of output nodes the same way as the DKSA baseline and again project the base neural net’s output to a hypersphere with radius $\sqrt{0.1}$. From preliminary experiments, using a unit hypersphere (i.e., setting the radius to be equal to 1) typically resulted in worse validation accuracy scores.

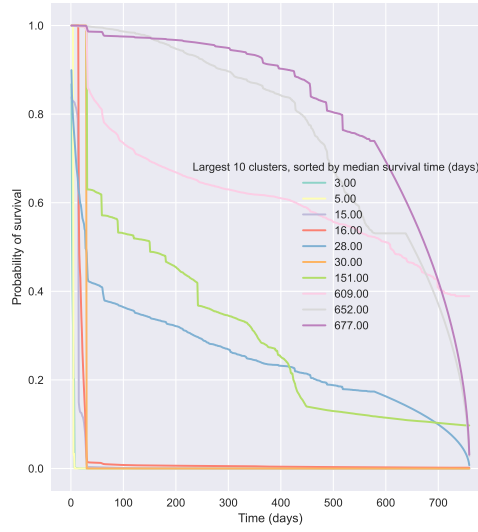
TUNA-KERNET is the same as KERNET except that our TUNA warm-start strategy is used.

C.3 Additional Cluster Visualization

For the KKBOX dataset, we visualize the largest 10 clusters found by the final TUNA-KERNET (NO SPLIT, SFT) model in Figure 9. These largest 10 clusters only contain 29.0% of all training data.



(a)



(b)

Figure 9: Visualization of the largest 10 clusters for the final TUNA-KERNET (NO SPLIT, SFT) model trained on the KKBOX dataset. Panel (a) shows a feature heatmap visualization. Panel (b) shows survival curves for the same clusters as in panel (a); the x-axis measures the number of days since an individual subscribed to the music streaming service.

References

- Alexandr Andoni and Ilya Razenshteyn. Optimal data-dependent hashing for approximate near neighbors. In *Symposium on Theory of Computing*, pages 793–801. ACM, 2015.
- Alexandr Andoni, Piotr Indyk, Thijs Laarhoven, Ilya Razenshteyn, and Ludwig Schmidt. Practical and optimal LSH for angular distance. In *Advances in Neural Information Processing Systems*, pages 1225–1233, 2015.
- Laura Antolini, Patrizia Boracchi, and Elia Biganzoli. A time-dependent discrimination index for survival data. *Statistics in Medicine*, 24(24):3927–3944, 2005.
- Arindam Banerjee, Inderjit S Dhillon, Joydeep Ghosh, Suvrit Sra, and Greg Ridgeway. Clustering on the unit hypersphere using von mises-fisher distributions. *Journal of Machine Learning Research*, 6(9), 2005.
- Shai Ben-David, Dávid Pál, and Hans Ulrich Simon. Stability of k-means clustering. In *International Conference on Computational Learning Theory*, pages 20–34. Springer, 2007.
- Rudolf Beran. Nonparametric regression with randomly censored survival data. *Technical report*, University of California, Berkeley, 1981.
- Ingwer Borg and Patrick J. F. Groenen. *Modern Multidimensional Scaling: Theory and Applications*. Springer Science & Business Media, 2005.
- Leo Breiman. Some infinity theory for predictor ensembles. *Technical report 577*, Statistics Department, University of California, Berkeley, 2000.
- Alexander M. Bronstein, Michael M. Bronstein, and Ron Kimmel. Generalized multidimensional scaling: a framework for isometry-invariant partial surface matching. *Proceedings of the National Academy of Sciences*, 103(5):1168–1172, 2006.
- Charles C. Brown. On the use of indicator variables for studying the time-dependence of parameters in a response-time model. *Biometrics*, 31(4):863–872, 1975.
- Gaëlle Chagny and Angelina Roche. Adaptive and minimax estimation of the cumulative distribution function given a functional covariate. *Electronic Journal of Statistics*, 8(2):2352–2404, 2014.
- Paidamoyo Chapfuwa, Chenyang Tao, Chunyuan Li, Courtney Page, Benjamin Goldstein, Lawrence Carin Duke, and Ricardo Henao. Adversarial time-to-event modeling. In *International Conference on Machine Learning*, pages 735–744. PMLR, 2018.
- George H. Chen. Nearest neighbor and kernel survival analysis: Nonasymptotic error bounds and strong consistency rates. In *International Conference on Machine Learning*, pages 1001–1010, 2019.
- George H. Chen. Deep kernel survival analysis and subject-specific survival time prediction intervals. In *Machine Learning for Healthcare*, 2020.
- George H. Chen and Devavrat Shah. Explaining the success of nearest neighbor methods in prediction. *Foundations and Trends® in Machine Learning*, 10(5-6):337–588, 2018.
- Tianqi Chen and Carlos Guestrin. XGBoost: A scalable tree boosting system. In *ACM SigKDD International Conference on Knowledge Discovery and Data Mining*, pages 785–794, 2016.
- David R. Cox. Regression models and life-tables. *Journal of the Royal Statistical Society: Series B*, 34(2):87–22, 1972.
- Dorota M. Dabrowska. Uniform consistency of the kernel conditional Kaplan-Meier estimate. *The Annals of Statistics*, pages 1157–1167, 1989.

- Vin De Silva and Joshua B. Tenenbaum. Global versus local methods in nonlinear dimensionality reduction. In *Advances in Neural Information Processing Systems*, pages 721–728, 2002.
- Martin Ester, Hans-Peter Kriegel, Jörg Sander, and Xiaowei Xu. A density-based algorithm for discovering clusters in large spatial databases with noise. In *International Conference on Knowledge Discovery and Data Mining*, pages 226–231, 1996.
- Stephane Fotso. Deep neural networks for survival analysis based on a multi-task framework. *arXiv preprint arXiv:1801.05512*, 2018.
- Pasi Fränti and Sami Sieranoja. How much can k-means be improved by using better initialization and repeats? *Pattern Recognition*, 93:95–112, 2019.
- Eleonora Giunchiglia, Anton Nemchenko, and Mihaela van der Schaar. RNN-SURV: A deep recurrent model for survival analysis. In *International Conference on Artificial Neural Networks*, pages 23–32. Springer, 2018.
- Mark Goldstein, Xintian Han, Aahlad Puli, Adler Perotte, and Rajesh Ranganath. X-CAL: Explicit calibration for survival analysis. *Advances in neural information processing systems*, 33:18296–18307, 2020.
- Humza Haider, Bret Hoehn, Sarah Davis, and Russell Greiner. Effective ways to build and evaluate individual survival distributions. *Journal of Machine Learning Research*, 21(85):1–63, 2020.
- Steve Hanneke, Aryeh Kontorovich, Sivan Sabato, and Roi Weiss. Universal Bayes consistency in metric spaces. *The Annals of Statistics*, 49(4):2129–2150, 2021.
- Trevor Hastie, Robert Tibshirani, and Jerome H. Friedman. *The Elements of Statistical Learning: Data Mining, Inference, and Prediction (2nd ed.)*. Springer, 2009.
- Kaiming He, Xiangyu Zhang, Shaoqing Ren, and Jian Sun. Delving deep into rectifiers: Surpassing human-level performance on ImageNet classification. In *IEEE International Conference on Computer Vision*, pages 1026–1034, 2015.
- John D. Kalbfleisch and Ross L. Prentice. *The Statistical Analysis of Failure Time Data*. Wiley, 1980.
- Edward L. Kaplan and Paul Meier. Nonparametric estimation from incomplete observations. *Journal of the American Statistical Association*, 53(282):457–481, 1958.
- Jared L. Katzman, Uri Shaham, Alexander Cloninger, Jonathan Bates, Tingting Jiang, and Yuval Kluger. DeepSurv: personalized treatment recommender system using a Cox proportional hazards deep neural network. *BMC Medical Research Methodology*, 18(1):24, 2018.
- Diederik P. Kingma and Jimmy Ba. Adam: A method for stochastic optimization. *arXiv preprint arXiv:1412.6980*, 2014.
- William A. Knaus, Frank E. Harrell, Joanne Lynn, Lee Goldman, Russell S. Phillips, Alfred F. Connors, Neal V. Dawson, William J. Fulkerson, Robert M. Califf, and Norman Desbiens. The SUPPORT prognostic model: Objective estimates of survival for seriously ill hospitalized adults. *Annals of Internal Medicine*, 122(3):191–203, 1995.
- Aryeh Kontorovich, Sivan Sabato, and Roi Weiss. Nearest-neighbor sample compression: Efficiency, consistency, infinite dimensions. In *Advances in Neural Information Processing Systems*, 2017.
- Samory Kpotufe and Nakul Verma. Time-accuracy tradeoffs in kernel prediction: controlling prediction quality. *Journal of Machine Learning Research*, 18(1):1443–1471, 2017.
- Amit Kumar and Ravindran Kannan. Clustering with spectral norm and the k-means algorithm. In *2010 IEEE 51st Annual Symposium on Foundations of Computer Science*, pages 299–308. IEEE, 2010.

- Håvard Kvamme and Ørnulf Borgan. Continuous and discrete-time survival prediction with neural networks. *Lifetime Data Analysis*, 27(4):710–736, 2021.
- Håvard Kvamme, Ørnulf Borgan, and Ida Scheel. Time-to-event prediction with neural networks and Cox regression. *Journal of Machine Learning Research*, 20(129):1–30, 2019.
- Changhee Lee, William R. Zame, Jinsung Yoon, and Mihaela van der Schaar. DeepHit: A deep learning approach to survival analysis with competing risks. In *AAAI Conference on Artificial Intelligence*, 2018.
- Weiyang Liu, Rongmei Lin, Zhen Liu, Li Xiong, Bernhard Schölkopf, and Adrian Weller. Learning with hyperspherical uniformity. In *International Conference On Artificial Intelligence and Statistics*, pages 1180–1188. PMLR, 2021.
- Yu A. Malkov and Dmitry A. Yashunin. Efficient and robust approximate nearest neighbor search using hierarchical navigable small world graphs. *IEEE Transactions on Pattern Analysis and Machine Intelligence*, 42(4):824–836, 2018.
- Chirag Nagpal, Xinyu Rachel Li, and Artur Dubrawski. Deep survival machines: Fully parametric survival regression and representation learning for censored data with competing risks. *IEEE Journal of Biomedical and Health Informatics*, 2021.
- Adam Paszke, Sam Gross, Francisco Massa, Adam Lerer, James Bradbury, Gregory Chanan, Trevor Killeen, Zeming Lin, Natalia Gimelshein, Luca Antiga, Alban Desmaison, Andreas Kopf, Edward Yang, Zachary DeVito, Martin Raison, Alykhan Tejani, Sasank Chilamkurthy, Benoit Steiner, Lu Fang, Junjie Bai, and Soumith Chintala. PyTorch: An imperative style, high-performance deep learning library. In *Advances in Neural Information Processing Systems*, pages 8024–8035, 2019.
- Liudmila Prokhorenkova and Aleksandr Shekhovtsov. Graph-based nearest neighbor search: From practice to theory. In *International Conference on Machine Learning*, pages 7803–7813, 2020.
- Alexander Rakhlin and Andrea Caponnetto. Stability of k-means clustering. In *Advances in Neural Information Processing Systems*, volume 19, page 1121, 2006.
- Rajesh Ranganath, Adler Perotte, Noémie Elhadad, and David Blei. Deep survival analysis. In *Machine Learning for Healthcare*, 2016.
- Mark J. Russo, Jonathan M. Chen, Robert A. Sorabella, Timothy P. Martens, Mauricio Garrido, Ryan R. Davies, Isaac George, Faisal H. Cheema, Ralph S. Mosca, and Seema Mital. The effect of ischemic time on survival after heart transplantation varies by donor age: an analysis of the United Network for Organ Sharing database. *Journal of Thoracic and Cardiovascular Surgery*, 133(2):554–559, 2007.
- M. Schumacher, G. Bastert, H. Bojar, K. Huebner, M. Olschewski, W. Sauerbrei, C. Schmoor, C. Beyerle, R. L. Neumann, and H. F. Rauschecker. Randomized 2 x 2 trial evaluating hormonal treatment and the duration of chemotherapy in node-positive breast cancer patients. german breast cancer study group. *Journal of Clinical Oncology*, 12(10):2086–2093, 1994.
- Roman Vershynin. *High-Dimensional Probability: An Introduction with Applications in Data Science*, volume 47. Cambridge University Press, 2018.
- Ulrike von Luxburg. Clustering stability: An overview. *Foundations and Trends® in Machine Learning*, 2(3):235–274, 2010.
- Tongzhou Wang and Phillip Isola. Understanding contrastive representation learning through alignment and uniformity on the hypersphere. In *International Conference on Machine Learning*, 2020.

- Zhiliang Wu, Yinchong Yang, Peter A. Fasching, and Volker Tresp. Uncertainty-aware time-to-event prediction using deep kernel accelerated failure time models. In *Machine Learning for Healthcare*, 2021.
- Jinsung Yoon, William R. Zame, Amitava Banerjee, Martin Cadeiras, Ahmed M. Alaa, and Mihaela van der Schaar. Personalized survival predictions via trees of predictors: An application to cardiac transplantation. *PloS one*, 13(3):e0194985, 2018.
- Qixian Zhong, Jonas W. Mueller, and Jane-Ling Wang. Deep extended hazard models for survival analysis. *Advances in Neural Information Processing Systems*, 34, 2021.
- Qixian Zhong, Jonas Mueller, and Jane-Ling Wang. Deep learning for the partially linear cox model. *The Annals of Statistics*, 50(3):1348–1375, 2022.